Controlling Surface-Induced Platelet Activation by Modulation of Contacting Interfaces

Zur Erlangung des akademischen Grades eines

DOKTORS DER NATURWISSENSCHAFTEN

(Dr. rer. nat.)

von der KIT-Fakultät für Chemie und Biowissenschaften

des Karlsruher Instituts für Technologie (KIT)

genehmigte

DISSERTATION

von

M.Eng. Gurunath Prasad Apte

Dekan: Prof. Dr. Hans-Achim Wagenknecht
Referent: PD Dr. Dr. Michael Hirtz
Korreferentin: Prof. Dr. Annie Powell

Tag der mündlichen Prüfung:19.07.2023

Kurzzusammenfassung / Abstract in German

Blutplättchen, auch Thrombozyten genannt, sind ein wesentlicher Bestandteil des menschlichen Blutgerinnungssystems. Die Hauptaufgabe der Thrombozyten innerhalb des Körpers besteht in der Blutstillung. Außerhalb des Körpers neigen Thrombozyten jedoch dazu, nach kurzem Kontakt mit synthetischen, nicht physiologischen Oberflächen zu aktivieren, was für viele Anwendungen unerwünscht sein kann, einschließlich der Lagerung von Thrombozyten und der Erforschung der Wechselwirkungen zwischen Thrombozyten und Arzneimitteln. Normalerweise werden Thrombozyten-Konzentrate in handelsüblichen Plastikbeuteln aufbewahrt, die eine große Menge an Weichmachern enthalten, um die Flexibilität des Beutels zu erhöhen und die Möglichkeit eines Bruchs während der Handhabung und des Transports zu vermeiden. Bei längerer Exposition können die giftigen Weichmacher in das Thrombozyten-Konzentrat entweichen.

Aktivierte Thrombozyten setzen eine Vielzahl von Proteinen frei, die den Prozess der oberflächeninduzierten Thrombozytenaktivierung (SIPA) weiter unterstützen. SIPA ist eines der Hauptprobleme von Medizinprodukten mit Blutkontakt und Transfusionsgeräten, und ein entscheidender Faktor für die verkürzte Haltbarkeit gelagerter Thrombozyten. Um SIPA zu vermeiden, werden den Thrombozyten-Konzentraten Antikoagulantien zugesetzt, so dass sie bis zu 5 Tage gelagert werden können. Diese Antikoagulantien greifen in die Aktivierungswege der Thrombozyten ein und beeinträchtigen so ihre Funktionalität. Das häufigste Problem bei der Lagerung von Thrombozyten ist schließlich die Gefahr einer bakteriellen Kontamination. Um dieses Problem zu lösen, werden verschiedene UV-Behandlungen eingesetzt, um das Risiko einer Kontamination mit Krankheitserregern zu minimieren. Studien zeigen jedoch, dass diese Strahlung mit kurzer Wellenlänge die Bestandteile der Thrombozytenmembran zerstören und zu einer Aktivierung der Thrombozyten führen kann. Diese zahlreichen, oft miteinander verknüpften Probleme verdeutlichen den dringenden Bedarf an einer effizienten Lösung zur Optimierung der Lagerungsbedingungen für Thrombozyten und zur Maximierung ihrer Lagerfähigkeit.

Ziel dieser Doktorarbeit ist es, Oberflächen zu entwickeln, die die Adhäsion von Thrombozyten hemmen und somit ihre Aktivierung und Aggregation verhindern - ohne dass der Zusatz von Antikoagulantien erforderlich ist. Für die Veränderung der Oberflächeneigenschaften stehen drei verschiedene Ansätze zur Verfügung: Biophysikalische, physikochemische oder biochemische Strategien können Verwendet werden, um eine plättchenfreundliche Oberfläche zu gestalten. In der ersten Phase dieses Projekts wurde eine Kombination aus

physikochemischen und biophysikalischen Ansätzen angewandt, um Hydrogele aus Gelatine und Agarose herzustellen, die anschließend durch Integration von Eisennanopartikeln zu Nanokompositen verarbeitet wurden. Agarose-basierte Hydrogel-Filme erwiesen sich dabei durch die Kombination von Oberflächenbenetzbarkeit und besseren mechanischen Eigenschaften als ideale Oberflächen. Mikroskopaufnahmen zeigten, dass die Anzahl der Blutplättchen, die an solchen Oberflächen adhärieren, deutlich reduziert und die Ausbreitung der Blutplättchen verhindert wurde. Hergestellte Agarose-Filme und ihre Nanokomposite konnten darüber hinaus bakterielles Wachstum erfolgreich hemmen: Von allen getesteten Proben wurde der höchste Prozentsatz an toten Bakterien auf den Nanokomposit-Filmen gemessen.

Die Topographie des Substrats spielt eine entscheidende Rolle für das Verhalten der Zellen und die Kontrolle ihrer Physiologie und Morphologie. Für die Veränderung der Oberflächentopografie stehen zahlreiche komplexe Techniken zur Verfügung. In dieser Arbeit wurden zwei Techniken mit individuellen Vorteilen zur Herstellung von Nanostrukturen eingesetzt.

Bei der ersten handelt es sich um ein auf der Rasterkraftmikroskopie (AFM) basierendes Fluidiksystem namens FluidFM, bei dem eine Monomere enthaltende Tinte aus der Öffnung des Cantilever Spitze auf die Oberfläche extrudiert wird. Nach dem Druckvorgang wird die Tinte polymerisiert, um 3D-Strukturen zu erhalten. Mit Hilfe von kontinuierlichen und diskontinuierlichen Topografien wurden hexagonale Bienenstock- bzw. halbkugelförmige Gitterstrukturen hergestellt. Dabei zeigte sich, dass die Thrombozyten diese Strukturierung mechanisch wahrnehmen und ihr Zytoskelett umorganisieren, was zu einer geringeren Ausbreitung der Blutplättchen führt. Darüber hinaus wurde die Technik zum Drucken einer modifizierten biofunktionalisierten Tinte verwendet, die so modifiziert wurde, dass Moleküle mit unterschiedlichen funktionellen Gruppen in die Basistinte integriert wurden. Diese Modifikation führte nur zu einer geringfügigen Veränderung der mechanischen Eigenschaften der gedruckten Strukturen, während ihre Funktionalität erhalten blieb. Die Möglichkeit, Bindungsmotive für spezifische Wechselwirkungen zu integrieren, demonstriert die Vielseitigkeit der FluidFM und ebnet den Weg für die weitere Erforschung des biochemischen/topographischen Ansatzes im Bereich der Entwicklung plättchenfreundlicher Oberflächen. Das Drucken von Mikro- und Nanostrukturen stellt eine schnelle, kostengünstige und effiziente Methode zur Herstellung verschiedener geometrischer Prototypen dar und kann

nicht nur zur Untersuchung verschiedener Strukturformen, sondern auch ihrer Größe und anderer topografischer Parameter eingesetzt werden.

Die zweite verwendete Technik war die thermische Nanoimprint-Lithografie (T-NIL), mit der ein breiteres Spektrum an Oberflächentopologien untersucht werden konnte, einschließlich Punkt, Kette, Pille und Quadrat-förmiger. Diese Nanomuster wurden auf Siliziumscheiben geätzt und auf einen PDMS-basierten Stempel übertragen, der so zum Prägen von Hydrogelen verwendet werden konnte. Verschiedene Topologien wurden auf die Oberfläche von Agarosegelen geprägt, um ihre zuvor beobachtete, hemmende Wirkung auf die Thrombozytenadhäsion zu verbessern. Das pillenförmige Nanomuster war dabei am besten geeignet, um die Thrombozytenadhäsion zu hemmen, was auf die Höhe der Struktur zurückgeführt werden kann.

Zusammenfassend lässt sich festhalten, dass in diesem Projekt Hydrogelfilme auf Agarosebasis, insbesondere in Form von Nanokompositen mit integrierten antibakteriellen Eisennanopartikeln, entwickelt wurden, die Lagerungsbedingungen für Thrombozyten deutlich verbessern, indem sie die SIPA und das Risiko einer bakteriellen Kontamination verringern. UV-Behandlungen von Thrombozyten-Konzentraten werden dadurch überflüssig. Durch die Einführung verschiedener Oberflächentopologien kann die Adhäsion von Thrombozyten gehemmt werden: Das FluidFM-basierte vielseitig einsetybare Nanodrucksystem wurde für die Erforschung und Entwicklung von Prototypen effektiver Geometrien eingesetzt, während T-NIL für die Prägung ausgewählter Strukturen auf die Oberfläche von Agarose-Filmen verwendet werden kann, um eine einheitliche Oberflächentopographie zu schaffen.

Abstract

Platelets, also known as thrombocytes, are an essential component of the human blood coagulation system. Inside the body, the primary role of platelets is hemostasis. However, platelets have a tendency to activate immediately after brief contact with synthetic, non-physiological surfaces, which can be undesirable for many applications, including platelet storage and research of platelet-drug interactions. Usually, platelet concentrates are stored in commercial plastic bags, which use an excessive amount of plasticizers to increase the flexibility of the bag and avoid any possibility of breakage during its handling and transport. Long term exposure can lead to leaching of the toxic plasticizers into the platelet concentrates.

A plethora of proteins are released by activated platelets, which further assist in the process known as surface-induced platelet activation (SIPA). SIPA is a major concern when dealing with blood-contact medical devices and transfusion apparatus. It is also one of the key factors responsible for the reduced shelf life of stored platelets. To avoid SIPA, anticoagulants are added to the stored platelet concentrates, allowing them to be stored for a maximum of 5 days. These anticoagulants interfere with the activation pathways of the platelets, thereby affecting their functionality. Lastly, the most common problem with platelet storage is the possibility of bacterial contamination. To address the problem, a number of UV treatments are employed to minimize the risk associated with pathogen contamination. However, studies show that exposure to this low wavelength radiation can disrupt the components of the platelet membrane and result in platelet activation. These numerous, oftentimes interconnected problems illustrate the pressing need for an effective solution to optimize platelet storage conditions and maximize their shelf life.

The aim of this work was to engineer surfaces that inhibit platelet adhesion and therefore prevent their activation and aggregation – without the need for anticoagulants. For the modification of surface properties, three different approaches can be employed: Biophysical, physicochemical, or biochemical strategies are availabe to design a platelet friendly surface. In the first phase of this project, a combination of physicochemical and biophysical approaches was applied to prepare hydrogels from gelatin and agarose, which were subsequently fabricated into nanocomposites by integrating iron nanoparticles. Agarose-based hydrogel films are thereby convinced by the combination of favourable surface wettability and mechanical properties. Microscopic images revealed that the number of platelets adhering to such surfaces was significantly reduced and platelet spreading was prevented. The fabricated agarose and its

nanocomposites furthermore were found to successfully inhibit bacterial fouling. In addition, the highest percentage of dead bacteria was quantified over the nanocomposite films.

The topography of the substrate plays a crucial role in dictating the cell's behavior and controlling their physiology and morphology. Numerous sophisticated techniques are available to tune the topology of a surface in order to enhance the desired cellular functions. In this work, two techniques with individual advantages were applied to fabricate nanopatterns. The first was an atomic force microscopy (AFM)-based fluidic system called FluidFM, where a liquid-phase monomer based ink is extruded out from a cantilever with an aperture on the tip. Post-printing, the ink is polymerized to obtain 3D structures. Continuous and discontinuous topographies were employed to fabricate hexagonal hive and hemispherical grid structures, respectively, which revealed that the platelets mechanosense these physical cues and reorganize their cytoskeleton, resulting in lower spreading of platelets on the patterned surfaces as compared to the non patterned. Further, the technique was applied to print a modified biofunctional ink customized to integrate molecules with different functional groups into the base ink. This modification caused only a minor change in the mechanical properties of the printed structures while retaining their functionality. The ability to incorporate binding motifs to achieve specific interactions demonstrated FluidFM's versatility, which further paves the way to explore the biochemical/topographical approach in the domain of engineering platelet friendly surfaces. The printing device serves as a fast, cheap, and effective way to produce different geometrical prototypes of nanostructures and can be employed to survey not only distinct shapes but also their size and other topographical parameters.

The second technique used was thermal nanoimprint lithography(T-NIL), where a broader range of surface topologies could be investigated, including dot, chain, pill, and square. These nanopatterns were etched on silicon wafers and transferred to a PDMS-based stamp, which was then used to imprint hydrogels. Agarose gels were used to improve the observed inhibitory effect on platelet adhesion by integrating different topologys on the surface via imprinting The pill-shaped nanopattern demonstrated its superior ability to inihibit platelet adhesion, which can be attributed to the structure's height.

To conclude, in this project, agarose-based hydrogel films, especially in the form of nanocomposites with antibacterial iron nanoparticles, were found to significantly improve platelet storage conditions by reducing SIPA and the risk of bacterial contamination. UV treatments of platelet concentrates are thereby rendered unnecessary. By introducing different surface topologies, platelet adhesion can be inhibited: The FluidFM based multifaceted

nanoprinting system was employed to explore and develop prototypes of effective geometries, while T-NIL demonstrated how a distinct patterns can be transferred onto the malleable agarose based gel surfaces to create a uniform surface topographies.

.

Table of Contents

Chapter 1: Introduction

1.1 Platelet Physiology

1.1.1 Introduction to platelets

Platelets are the smallest type of cells found in the blood. Platelets are discoid-shaped, nucleus-free fragments of cells that originate from a type of mature cell called a megakaryocyte that is found in the bone marrow. Platelets constitute less than 1% of the total blood. Platelets are produced by a process called thrombopoiesis.[1] The hormone thrombopoietin simulates and regulates the thrombopoiesis, also called platelet production.[2] A single megakaryocyte can produce over 1,000 platelets, of which one-third is retained in the spleen while the rest circulate in the blood. A healthy person's blood contains between 150,000 and 350,000 platelets per microliter.[3] A platelet is around 1.5–3.0 µm in diameter.[4] It is important to understand the structure and physiology of the platelets, as they play a vital role in hemostasis. Hemostasis can be defined as the process that stops blood loss from a damaged vessel.[5]

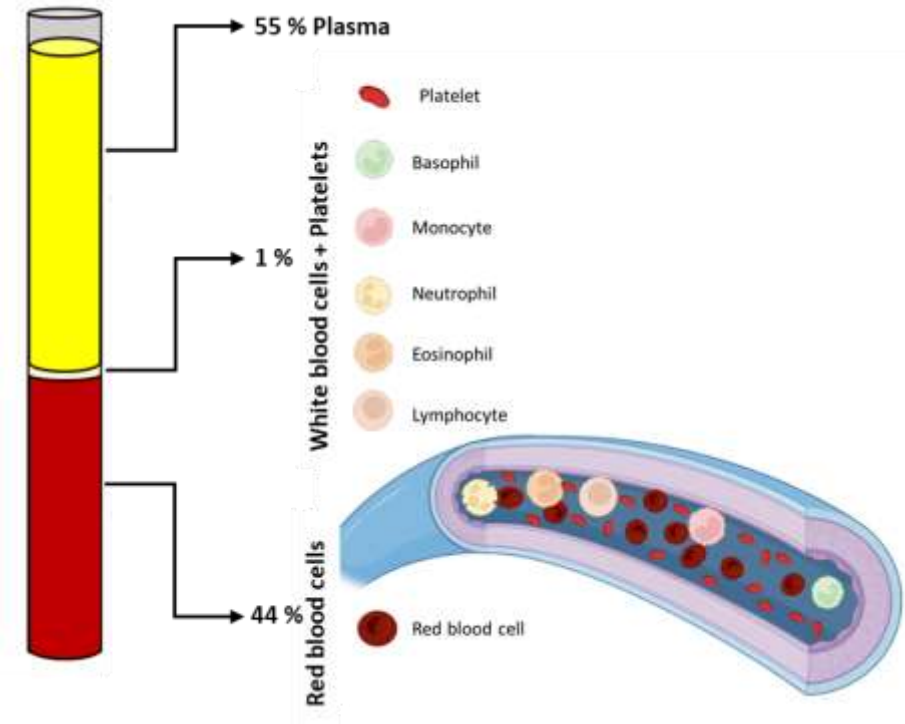

Figure 1: The composition of the human blood and the important cell types found in blood. Created with BioRender.com

Parts of the this chapter were already published in ACS Appl. Bio Mater. 2020, 3, 9, 5574–5589

1.1.2 Structure and Organelle

The platelet structure is divided into three zones **Figure 2**. The outermost is called the "peripheral zone." which consists of glycocalyx, which, apart from being a physical barrier, is also covered with several glycoprotein receptors that are involved in platelet adhesion.[6] Another component is the OCS, or open canalicular system, which comprises a network of channels connected to the surface and is known to facilitate the uptake and release of platelet contents.[7] The next important structure, classified in the peripheral zone, is the dense tubular system (DTS). The DTS controls platelet behavior by sequestering or releasing calcium, and thus plays an important role in platelet activation.[8] The DTS is expressed in resting platelets as narrow, elongated membranes.[8]

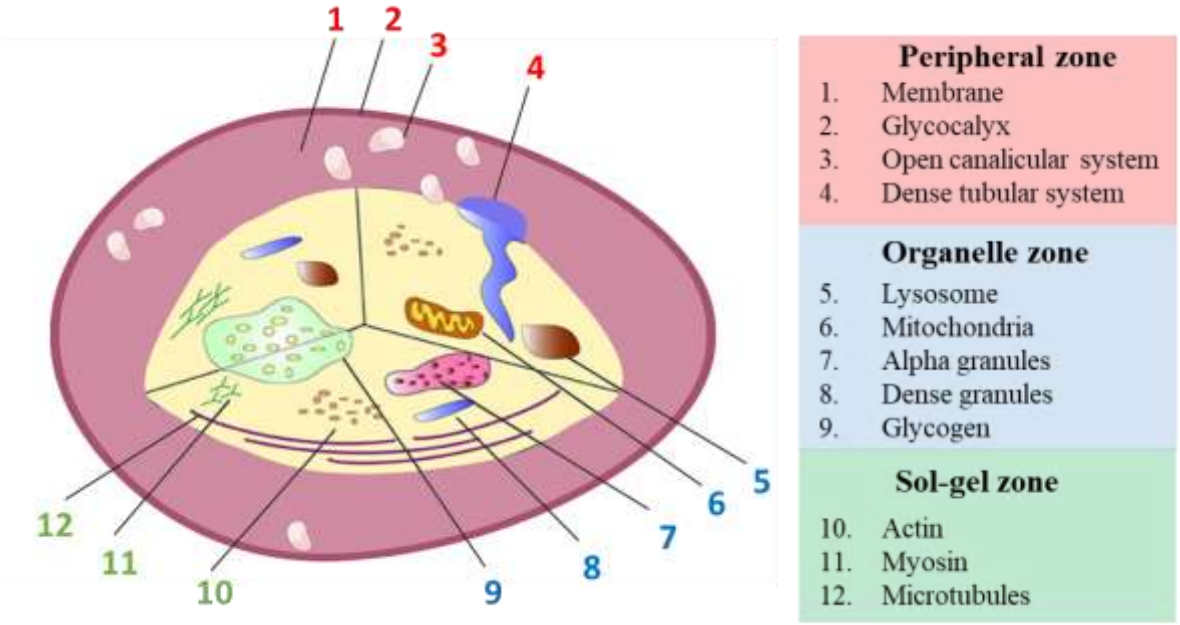

Figure 2: A schematic representation of the platelet structure with its components classified into three zones. Adapted from [9]

The next zone is the organelle zone. Platelets contain three main types of organelles with secretory functions: alpha granules, dense granules, and lysosomes. Platelet granules are formed when the platelet is still part of the megakaryocyte, but they mature inside a circulating platelet.[10] Platelets have alpha and dense granules in their cytoplasmic structure, which play a vital role in shape change after surface attachment, which is related to increased platelet cytoskeleton dynamics.[4] The most frequent platelet organelle, having a diameter of 200–500 nm, is called an alpha granule.[11] The quantity is determined by the platelet's size and the existence of other structures that take up space, like masses of glycogen. The average number of alpha granules found in a platelet is 50 to 80, while large ones can contain well over 100.[12]

Parts of the this chapter were already published in ACS Appl. Bio Mater. 2020, 3, 9, 5574–5589

Proteomic investigations have revealed over 300 soluble proteins involved in a wide range of processes, including hemostasis (von Willebrand factor [VWF] and factor V), inflammation (chemokines such as CXCL1 and interleukin-8), and wound healing (vascular endothelial growth factor [VEGF] and fibroblast growth factor [FGF]).[11] A comprehensive summary of the contents of alpha and dense granules has been tabulated by Reed et al.[13]

Compared to the alpha granules, dense granules are smaller (approximately 150 nm in diameter), fewer in number, and have a wide range of morphologies. Dense granules are mostly made up of bioactive amines (like serotonin and histamine), adenine nucleotides, polyphosphates, and pyrophosphates, as well as large amounts of cations, especially calcium.[14] Every platelet consists of 1–3 lysosomes. The role of lysosomes in hemostasis physiology is unknown. However, their contents are released together with the contents of alpha and dense granules on platelet activation. Apart from these, there are also glycosomes, tubular inclusions, and mitochondria, which play a role in the metabolism of the platelets. Although there is some evidence for residual protein synthesis capacity from messenger RNA (mRNA) brought over from megakaryocytes, platelets, unlike the vast majority of cells, lack a nucleus and so cannot adapt to new environments through de novo protein synthesis.[15,16] As a result, platelets require a variety of molecules that have already been created and are prepared to perform diverse physiological tasks and respond in the case of pathological events.[17]

The last of the three zones is the sol gel zone, which is located beneath the peripheral zone. It is made up of a transparent and viscous gel-like matrix.[10] It consists of an actin cytoskeleton (responsible for platelet shape change following activation) and microtubules (necessary to maintain the discoid shape).[18] As a result, the sol gel zone plays an important role in regulating the signaling processes necessary for platelet activation.[10] On activation, platelets undergo changes in their morphology. The actin found in the sol gel zone is responsible for such structural changes.[19] The spread platelet has four different actin structures that are distinctly composed and have different functions: filopodia, lamellipodia, stress fibers, and the contractile ring.[19] A micrograph of an activated platelet on glass depicts the platelet in **Figure 3** with filopodia—the thin projections of bundles of actin filament—and lamelliopodia—lateral extensions of a network of cross-linked actin filaments.

Parts of this chapter were already published in ACS Appl. Bio Mater. 2020, 3, 9, 5574–5589

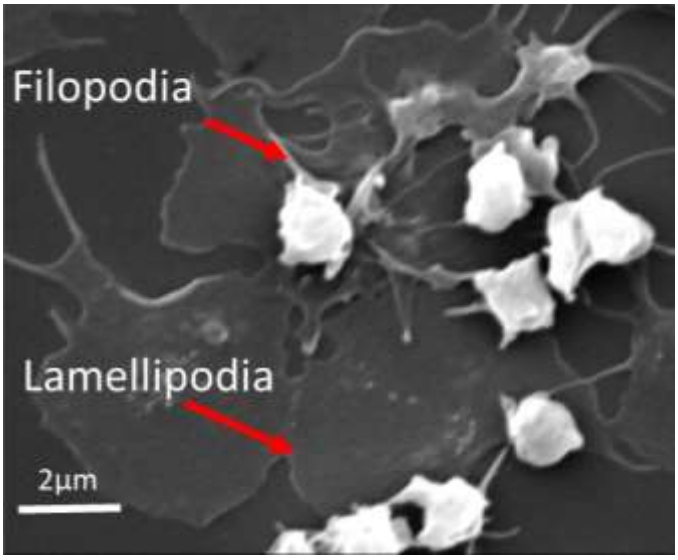

Figure 3: A scanning electron micrograph of activated platelets on the glass surface. The red arrows indicate the outgrowths of filopodia and lamelliopodia, respectively.

1.1.3 Surface Receptors

The major function of the platelets is to detect and seal any damage to the blood vessels, and this can be accomplished with the surface receptors on the platelet cytoskeleton. Platelet receptors act as the points of contact between platelets and their surroundings and determine platelet reactivity to a wide range of agonists and adhesive proteins.[20] The surface receptors on platelets, along with their granules, determine the specific cellular distinctiveness of platelets to a large extent. The disruption of the inner lining of the endothelial cells is sensed by these surface receptors, which initiate platelet activation. On activation of the platelet, several mechanisms are simultaneously realized.[21] To begin, activation leads to the secretion of agonist compounds to attract and activate other platelets. Besides, it activates the biochemical synthetic pathway that synthesizes other platelet agonists like thromboxane. Lastly, it alters the conformation of surface integrin αIIbβ3, which acts as a receptor for fibrinogen and VWF. Because platelets' primary task is hemostasis, it is not surprising that their major receptors have a direct part in this process, activating fellow platelets, interacting with damaged cell walls, or contributing to thrombus formation.[17]

Parts of this chapter were already published in ACS Appl. Bio Mater. 2020, 3, 9, 5574–5589

1.2 Platelet Activation

1.2.1 Physiological Platelet Activation

Platelet activation is a complex process that involves multiple steps that eventually lead to the formation of a thrombus. Platelets end up forming aggregates in this process to produce a hemostatic plug at the site of vascular damage **Figure 4.** Endothelial cells suppress thrombus development via a variety of methods under normal physiological circumstances. They reveal a negatively charged (anionic) saccharide-containing layer on the cell surface known as the glycocalyx. The hydrophilic proteoglycans and glycoproteins have a hydrated surface. As a result, water molecules form a protective layer that inhibits platelet adhesion by disabling the binding of coagulation proteins.[22] Furthermore, the release of nitric oxide, prostaglandin I2 (prostacyclin), tissue factor pathway inhibitor (TFPI), thrombomodulin, and heparin-like proteoglycans is employed to actively modify blood coagulation.[23,24] Platelets are triggered upon interaction with exposed collagen and vWF via cell membrane receptors when vascular injury and endothelial tissue damage occur.

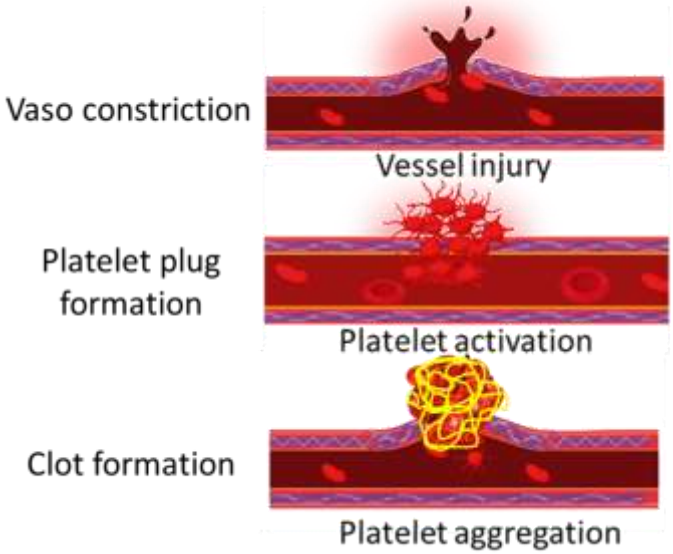

Figure 4: Schematic representation of hemostasis. Created with BioRender.com

Platelet activation is mediated by a number of adhesion receptors and ligands.[25] Further platelet-platelet interactions are regulated by ligands such as vWF, fibronectin, and fibrinogen. Platelet receptors such as glycoprotein Ib (GPIb)/V/IX have binding sites in the vWF, while fibrinogen can bridge integrin IIb3 receptors on platelet surfaces.[26] Integrin or glycoprotein VI (GPVI) receptors are responsible for the initial platelet attachment. The intracellular granules, namely the dense granules, include substances like adenosine diphosphate (ADP), adenosine

Parts of this chapter were already published in ACS Appl. Bio Mater. 2020, 3, 9, 5574–5589

triphosphate (ATP), guanosine 5′-[thio]diphosphate (GDP), and 5-hydroxytryptamine (5-HT), while the granules contain vWF and fibronectin.[27] These bioactive elements derived and released from the granular secretion further activate platelets by signaling positive feedback. Additionally, they cause the activation of integrin Iib3 and fibrin, both of which contribute to the6ormationn of a thrombus or a platelet plug.[27]

1.2.2 Surface Induced Platelet Activation

When blood platelets are exposed to non-physiological or artificial surfaces, their physical appearance changes dramatically, and they transition from a non-sticky to an adhesive state. The term "surface-induced platelet activation" can be traced back to 1990, when Park et al. characterized the morphological changes of platelets on different surfaces. It is well known that different proteins in the blood circulation can activate platelets. On non-physiological surfaces, they can nevertheless adhere strongly and swiftly activate.[28,29] Studies in the past have shown how modifications to surfaces can have a direct impact on the spreading of platelets and the rate of their activation.[30] The transformation of contact-adherent platelets into fully spread form on biomaterials is the first step in the formation of a mural thrombus.[31] Platelets spread to increase the surface area of the adhesive junctions, and hence, the extent of spreading is expected to influence the overall adhesive interactions.[32] Multiple interactions occurring between the platelet and the surface can result in the generation of signals for platelet activation.[32] Membrane glycoproteins and cytoskeletal assembly are critical components in such interactions.[33] An interesting study undertaken by Yoshimoto et al. revealed the intrinsic mechanism that occurs during surface-induced platelet activation.[34] Their observations state that there is movement and centralization of platelet granules along the vertical axis toward the adherent surface.

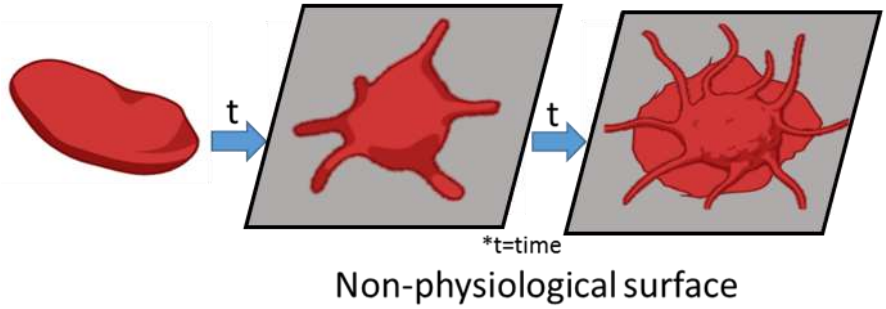

Figure 5: The behavior of platelets over a nonphysiological surface. Early attachment of the adhering platelet is followed by the development of elongated fillopodia and, eventually, the extension of the lamellipodium.

Parts of this chapter were already published in ACS Appl. Bio Mater. 2020, 3, 9, 5574–5589

After coming into contact with the surface, granules gather in the center of the platelet and tighten the ring of microtubules and microfilaments.[33] The organelles, too, are concentrated and form a hump in the center.[34] As platelet activation progresses, the centralized granules spread centripetally before being completely spread across the platelet.[35] Platelet granules are the most prominent structural features, and upon platelet activation, they coalesce in the center of the platelet to fuse with the open cannicular system (OCS).[36] The OCS is a membrane reservoir that is evaginated onto the platelet surface when the platelet comes into contact with nonphysiological surfaces.[36] Simultaneously, the platelet activation induced by the adhesion of platelets to the surface causes the actin present on the basal surface of the platelet to rapidly polymerize into filaments to form the platelet cytoskeleton.[35,37] This eventually culminates with the development of filopodia and lamellopodia **Figure 5**.[35] Surface-induced platelet activation is especially problematic during platelet storage because it causes platelet aggregation and can cause platelet concentrates to deteriorate.

1.3 Challenges in Platelet Storage

1.3.1 General Overview

Platelet concentrates have been transfused into critically ill oncology and hematology patients for the past half-century.[38] Platelet transfusions are commonly used in a variety of situations, including:

1. Bleeding disorders such as thrombocytopenia (low platelet count), von Willebrand disease, and idiopathic thrombocytopenic purpura (ITP).[39]
2. Cancer treatments, such as chemotherapy and radiation therapy, can reduce platelet count and increase the risk of bleeding.[38]
3. Bone marrow transplant: Because bone marrow transplantation can reduce platelet count, platelet transfusions are used to prevent or treat bleeding in these patients.[40]
4. Major surgery: Platelet transfusions are frequently used to prevent or treat bleeding in patients undergoing major surgery, such as heart surgery, liver transplantation, or spinal surgery.[41]
5. Trauma: Platelet transfusions are used to prevent or treat bleeding in patients who have suffered severe trauma from an accident.[42]

Parts of this chapter were already published in ACS Appl. Bio Mater. 2020, 3, 9, 5574–5589

6. Platelet dysfunction: Even if the platelet count is normal, platelets may not function properly in some cases. In these cases, platelet transfusions may be required to ensure normal bleeding and clotting.[38]

Platelet availability may be jeopardized due to rising platelet demand and their relatively short shelf life. One way to deal with rising demand and make more platelets available is to increase the length of time they can be stored.

According to US Food and Drug Administration (FDA) regulations on empty containers for the collection and processing of blood and blood components in reference to the biocompatibility of materials "the materials used in the construction of the device should not, either directly or indirectly through the release of their material constituents, produce an unreasonable risk of adverse local or systemic effects; be carcinogenic; or cause adverse reproductive and developmental effects."[43] Platelets are considered fresh if they have been stored for less than three days.[44] It has been divided into two categories: transfusion of "old" platelets (those that have been stored for more than three days) and transfusion of "young" platelets (those that have been stored for less than three days). It should be noted that platelet activation causes changes in the storage medium as well as the accumulation of bioactive substances. Transfusion of "old" platelets may expose patients to a variety of risks, including a decrease in platelet transfusion efficacy, an increase in adverse events in addition to transfusion-associated sepsis, and immune-mediated events.[45]

Before transfusion, fresh platelets isolated from healthy donors are usually concentrated and stored in a plastic bag. The material commonly used for storage bags should be able to withstand high steam sterilization and plasma freezing. Platelets metabolize glucose and oxygen to produce lactic acid and CO_2, resulting in a pH drop.[46] To address this issue, the storage material must be gas permeable.[47] The main problem with the current platelet storage protocol is that platelets have a short life span as they are activated and, in some cases, contaminated by bacteria over time.[48] Platelets are typically stored for no more than 5 days prior to transfusion. When bacterial contamination is controlled or pathogen reduction technologies are used, the storage period in some blood services is extended up to 7 days.[49,50] Changes in both platelets and storage medium occur during platelet storage, which results in platelet activation and dysfunction. However, the clinical significance of this is still unknown.[45] There is a high demand for transfusing platelets, but the short storage duration makes meeting that demand difficult. Extending the duration of platelet storage may expose patients to a potential decrease in platelet transfusion efficacy as well as potential increases in adverse

Parts of this chapter were already published in ACS Appl. Bio Mater. 2020, 3, 9, 5574–5589

events such as inflammation and/or immune-mediated events. Following hematology and oncology patients, post-cardiac surgery patients are the second largest group to receive platelets. Because of their pre-transfusion inflammatory state, these patients are especially vulnerable to platelet adverse events.[51,52]

In the following section, an attempt has been made to summarize all the factors that are responsible for the limited time of platelet storage.

1.3.2 Material

Many studies have recently focused on the advancement of platelet storage.[53,54] Prowse et al. summarized a total of 26 commercially available platelet storage bags, which are available in seven types of plastic foils, including polyvinyl chloride (PVC) with four plasticizers, various geometries, and thicknesses that range from 0.28 to 0.5 mm.[53] There are so many different combinations because, over the past few decades, there have been significant changes in the ways that platelets are collected, processed, and stored for transfusion. PVC and polyolefin are the most commonly used materials.[53] Plasticizers such as n-butyryl-tri-n-hexyl citrate (BTHC), di(2-ethylhexyl) phthalate (DEHP), trioctyltrimellitate (TOTM), and diisononyl ester of 1,2-cyclohexanedicarboxylic acid (DINCH) are commonly used.[53] A comprehensive summary has been presented in **Table 1**. However, there has not yet been a fixed standard regarding which material works best.

Table 1 Different combinations of plastic and plasticizer used in the manufacturing of the platelet bags, along with their advantages and disadvantages.[53]

Plastic	**Plasticizer**	**Advantages**	**Disadvantages**
PVC	BTHC	Superior gas exchange properties, maintains higher oxygen level	Expensive, High leachability, allergic, mildly toxic
PVC	DEHP	High Flexibility, resistance to breakage	High leachability, Decreased activity of phospholipase A2
PVC	TOTM	Gas permeability, less hepatotoxicity, Slower leaching, longer half life, better recovery	Estrogenic activity, poor pH maintainance
PVC	DINCH	Non-phthalate plasticizer	Higher hemolysis
Polyolefin	None	No plasticizer, better pH maintainance, higher recovery	Lower oxygen levels, high breakage rate

Parts of this chapter were already published in ACS Appl. Bio Mater. 2020, 3, 9, 5574–5589

1.3.3 Temperature

The same holds true for temperature as it does for storage material. Over the history of platelet storage, the focus has alternated between cryopreserved (−80°C), cold stored (4°C), and room temperature (20–24°C). Yet the question of the best temperature to store the platelets remains unanswered. Currently, platelets are stored at 22±2 °C because this temperature range allows for the platelets to maintain their functionality and quality for a longer period of time.[55] It has been observed that higher temperatures can cause the platelets to become more susceptible to activation.[56] Though the platelets are typically stored at 22 °C to preserve their functionality, this temperature promotes bacterial growth.[45]

1.3.3.1 Cryopreservation

In 1972, Dr. Valeri was the first to publish a method describing the cryopreservation of platelets.[57] DMSO is used to store the platelets at –80 °C, where platelet concentrates can be preserved for several years.[58] However, Raynel et al. studied the microparticles formed during platelet cryopreservation and discovered that, when compared to fresh platelets, microparticles formed during freeze and thawing expressed more GPIV, GPIIb, and the GPIb-V-IX complex, and constituted more cytoskeletal proteins like actin or filamin A.[59] In addition, Johnson et al. discovered that the peak of thrombin synthesis in the supernatant of cryopreserved platelets could increase approximately tenfold when compared to levels obtained before freezing.[60] Some studies also suggest that cryopreserved platelets have a number of morphological and functional defects, but when infused in vivo, they appear to function hemostatically.[61,62] In practice, it has likely been limited by the technical problems associated with its freezing and thawing, along with the impact the technique has on the platelets.[63] Having said that, when it comes to a longer duration of storage, the only option approved by the EU is to add a cryoprotectant and freeze them at temperatures of –80 °C.[63]

1.3.3.2 Cold

Cold storage of platelets is thought to reduce bacterial contamination and platelet metabolism, thereby extending storage time and reducing waste.[64] In vitro, cold storage has been shown to reduce lactate accumulation and preserve platelet aggregation response better than RT storage.[64] Thus, before the late 1960s, platelets were stored in the cold. However, because it was discovered in the late 1960s that chilled platelets are rapidly cleared from circulation after transfusion, platelets were not stored in the cold after that. Still, some current research suggests

that using platelets maintained at 4 °C rather than at room temperature, or 22 °C , may be more successful at forming clots and reducing excessive bleeding.[65]

1.3.4 pH

Platelets are extremely metabolically active cells at room temperature. As they metabolize glucose and consume oxygen, they create significant amounts of lactic acid and CO2, which causes the pH to fall.[66] A low pH eventually cause a "platelet storage lesion": pH values below 6.8 result in increased platelet activation and the expression of apoptotic markers in vitro, and pH values below 6 result in low recoveries in vivo.[53,67,68]

1.3.5 Gas Permeability

Due to changes in platelet isolation methods that resulted in an increase in the number of platelets per bag, containers with higher gas permeability are now required. Higher gas permeability allows O_2 to enter and CO_2 to exit, thereby correcting the pH of the storage medium.[69] Gas permeability can be increased by using larger containers and/or varying the type of material and thickness of foils used to make containers.[70] The improved gas permeability of the storage containers can extend the storage time from 3 to 5, and later to 7 days.[54,69]

1.3.6 Bacterial Contamination

Transfusion medicine still struggles with bacterial contamination. Platelets are vulnerable to bacterial development due to their room-temperature storage and biological nature.[45] There exist various mechanisms that can result in platelet contamination, with the primary cause being the infiltration of skin flora at the puncture site. The pathogens in question primarily consist of gram-positive bacteria, including Staphylococcus aureus, coagulase-negative Staphylococci, viridans group Streptococci, Bacillus spp., Corynebacteria, and anaerobic diphteroid gram-positive bacilli such as Propionibacterium acnes.[71] Bacteria can attach to platelets through hemostasis receptors and eventually lead to platelet aggregation. *Streptococcus sanguinis, S. epidermidis, and C. pneumoniae* have all been shown to undergo such mechanism to bind to platelets.[72] Platelets express a variety of pattern recognition receptor families, including Toll-like receptors, C-type lectin receptors, and nucleotide-binding oligomerization domain-like receptors, as well as integrins commonly associated with the hemostatic response, such as GPIIb-IIIa or GPIb.[73] The first complement protein C1q, the von Willebrand factor, fibrinogen, fibronectin, and other proteins are used by bacteria to directly or indirectly bind these receptors.[72]

Parts of this chapter were already published in ACS Appl. Bio Mater. 2020, 3, 9, 5574–5589

Pathogen reduction technologies like UV[74] and gamma[75] irradiation have been used to deactivate a wide range of organisms (viruses, fungi, bacteria, and parasites) and are one of the most convenient ways to deal with the fast changing epidemiological environment and the constant emergence of new diseases. However, even with the current techniques, further in vivo studies are recommended to answer questions about the quality, safety, and efficacy of transfused platelets.[74,76] Because of all these issues, the current shelf-life of platelet products is only 5 days, and bacterial contamination testing is mandatory.[77] Some hospitals even have stricter criteria and will not use platelets that have been stored for more than three days. The shelf life is significantly shorter than that of red blood cells, which can be kept in the refrigerator for 42 days.[78] Because of the short storage time and bacterial contamination, a significant amount of the platelet products are discarded, resulting in high monetary losses and a global shortage of platelet products in blood transfusion services.[79] Some of the above mentioned factors are even interdependent, so any research related to this domain requires a holistic approach.

1.4 Engineering platelet friendly Surfaces

Platelets have an 8-12-day lifetime when in circulation but only a 3-5-day shelf life when stored outside of the body. Having discussed the challenges of platelet storage in the previous section, it is important to resolve the long pending issue of the ideal platelet storage technique. One way to deal with this is to tailor the surface properties of the material used in storage. Surface engineering can be achieved by modifying the surface using three strategies: physicochemical, biophysical, and biochemical modification **(Figure 6)**. These strategies are widely applied while tuning the properties of the biomaterial in order to dictate the response of cells. It has been observed on numerous occasions how a peculiar cellular response can be invoked by tweaking a single property of the surface. To achieve the goal of creating an ideal surface for platelets, a similar idea can be applied.

Parts of this chapter were already published in ACS Appl. Bio Mater. 2020, 3, 9, 5574–5589

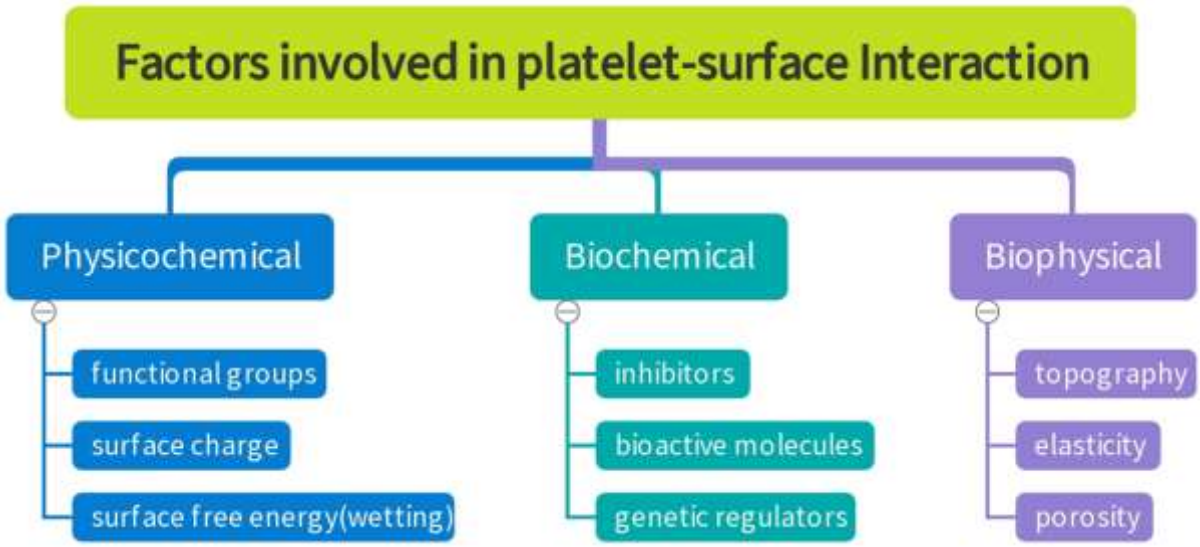

Figure 6: Different factors influencing the interaction of platelets with the surface are categorized into three groups: physicochemical, biochemical, and biophysical.

1.4.1 Physicochemical Modification

The earliest contact between blood and materials is known to occur through the multitude of proteins originating from the blood proteome. So, when platelets come in contact with a material, they actually do not come in direct contact with the surface, but rather with a protein layer that has been adsorbed on it.[80] Platelets can adhere to the adsorbed proteins vWF, fibronectin, and vitronectin on artificial surfaces via the integrin receptor αIIbβ3.[81]

The primary goal of developing bio- and biocompatible materials for many years was to change the chemical properties of artificial surfaces. As a result, it should come as no surprise that changing the surface properties of biomaterials frequently improves the biological performance of any artificial material surface. Platelets adhere to and activate on surface-bound plasma proteins, implying that protein-repelling surfaces may have the ability to reduce platelet activation. Several anti-fouling surface methods have been developed over the past decades to reduce protein adsorption.[80] In this strategy, surface properties like wetting, energy, charge, and chemistry are modulated. Wetting plays an important role in determining the primary steps of protein interaction and binding on any surface. Meanwhile, it is widely accepted that a surface's wetting behavior, or hydrophilicity, plays an active and decisive role in protein adsorption and thereby in platelet adhesion.[82] A film of water molecules covers hydrophilic

Parts of this chapter were already published in ACS Appl. Bio Mater. 2020, 3, 9, 5574–5589

surfaces. To adsorb to such materials, a protein must first conquer the adjacent water molecules.[83,84] The more hydrophilic a surface is, the more energy is required to replace a water molecule. As a result, hydrophilic surfaces are less likely than hydrophobic surfaces to be covered with proteins. Therefore, one of the most popular approaches to make anti-fouling materials is the development of hydrophilic surfaces **(Figure 7)**.[85] Further physicochemical surface features are considered to improve water molecule adsorption and reduce unspecific protein adsorption. A material must also be electrically neutral, contain hydrogen bond acceptors, and not contain hydrogen bond donators.[85,86] According to studies, the conformation of an adsorbed protein may be more significant than the protein amount itself.[87–89] Consequently, the surface chemistry must regulate not the protein adsorption itself but rather the protein conformation.

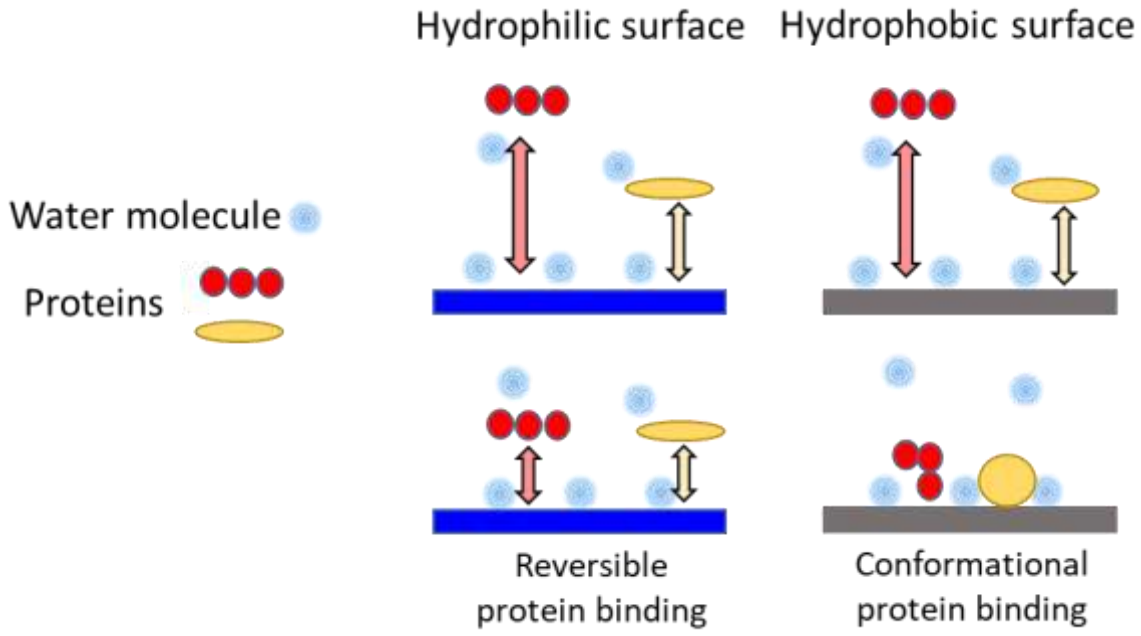

Figure 7: Differential protein binding characteristics are expressed on hydrophilic and hydrophobic surfaces.

With regards to surface charge, there are several examples that prove that a positively charged surface tends to promote adhesion and proliferation of certain cells, which then also translates to a similar behavior in platelet adhesion. Yang et al. (2019) studied the protein-repelling properties of a copolymer composed of 3,4-ethylene dioxythiophene and negatively charged graphene oxide.[90] The copolymer composed of 3,4-ethylene dioxythiophene and negatively charged graphene oxide[91] decreases human serum albumin protein adsorption by 40% and platelet coverage by more than 90% due to the repulsive negative charges between the surface

Parts of this chapter were already published in ACS Appl. Bio Mater. 2020, 3, 9, 5574–5589

and proteins or cells.[91] In another study, Corum et al. observed an increase in adhesion as the negative charge density of the surface went down.[92]

Surface chemistry also plays an important role in platelet adhesion. Park et al. explain in detail how platelets show less affinity for binding when exposed to the same polyurethane surface with different PEG-modified terminal groups such as OH- or NH_2-, which show a greater reduction in platelet adhesion than the SO_3 group, pointing to ionic interactions between the platelet membrane and different terminal groups.[93]

1.4.2 Biophysical Modification

The primary goal of developing bio- and biocompatible materials for many years was to change the chemical properties of artificial surfaces. As a result, it should come as no surprise that changing the surface properties of biomaterials frequently improves the biological performance of any artificial material surface.

Topography

All mammalian cells are highly sensitive to surface topography.[94] The creation of nanoscopic topographies using various techniques has been identified as a useful approach to controlling cellular response to surfaces and is thus increasingly used in tissue engineering and biomedicine in recent decades. Researchers all over the world are now controlling cell behavior, for example, by using nanopatterning and nanostructuring techniques to create 3D anti-thrombogenic interphases with varying topographies. In the design and fabrication of these 3D anti-thrombogenic interphases and their associated functional surfaces, patterning techniques such as 3D printing, lithography, electrospinning, and two-photon polymerization (2PP) are used.[95] At the nanoscale, there is a complex interaction of cells with extracellular matrix-mimetic surfaces, as well as chemical and mechanical cell signaling that controls cell behavior inside the body.[96] Because protein adsorption from blood on an implant surface is an initial cellular response, surface protein assembly is critical in understanding the biocompatibility of the surface or implant.[97] Firkowaska-Boden et al. reviewed protein adsorption on polymeric surfaces and concluded that polymers can be nanostructured to mimic the length scale of protein molecules. The nanoconfinement properties of nanostructured surfaces can be used to modulate the distribution, orientation, and conformation of protein molecules when designing the implant surface.[97] Furthermore, Wang et al. investigated the effects of protein adsorption on different zinc oxide nanotopographies (nanoparticles, nanorods, nanosheets, and nanobeams). They discovered that the amount of fibrinogen

Parts of this chapter were already published in ACS Appl. Bio Mater. 2020, 3, 9, 5574–5589

adsorbed varied depending on the topography.[98] As a result, proteins are important mediators in the nanotopographical control of cell behavior. Numerous studies are being conducted to investigate a cell's response to surface topography.[99–102] In most mammalian cells, nanotopography has an effect on cell function.[103] The substrate is not only responsible for cell support but also for cellular processes such as adhesion, proliferation, growth, and spreading.[104] Nanoscale surface modification has been used to elicit specific cell responses.[105,106] The adhesion of bovine platelets was reduced at low shear stresses on submicron structured (array of pillars) polyether(urethane urea) compared to smooth control.[107] Because platelets were found to be localized in the inter-pillar spaces, optimizing the pillar geometries could further reduce platelet adhesion.[107] Another example of nanotopographical influence on platelet response comes from Bui et al. who created nanoscale groove arrays and discovered that platelet activation was significantly lower on groove sizes of 100 nm compared to 500 nm.[81] Mao et al. created a polystyrene film with a lotus leaf structure and hair-like nanotubes to mimic the lotus leaf's superhydrophobic surface. Surprisingly, these nanotube-structured films demonstrated excellent anti-platelet adhesion and anticoagulation properties.[108] Simon-Walker et al. conducted an important study in which they used nitric oxide to send an antithrombotic signal from a modified heparin-chitosan polyelectrolyte multilayer coated on titanium nanotubes.[109] The platelets' morphology on the titanium surface undergoes aggregation and activation, while the nanotubes from titanium oxide inhibit platelet activation to some extent; however, aggregation persists. Additional coating with polyelectrolyte multilayers significantly improved platelet aggregation inhibition, but when this surface was nitrosated, the results looked far better. This is a very promising approach that combines nanotopography and chemical surface modification to reduce platelet-surface adhesion and activation. The strategy was inspired by endothelial glycocalyx.[109]

Koh et al. conducted a comparative study on platelet response to different topographies.[110] The experiments were carried out by varying the pillars' interspacing, width, and height. Although no significant differences in platelet adhesion were found, the effect of variable interspacing was seen in the platelet activation mechanism. When the inter-pillar spacing was reduced to 1 µm, the platelet surface interaction was low, or the platelets had less contact with the surface, inhibiting activation.[110] Similar findings were made when investigating the impact of width on platelet activation, with a reduction in pillar width from 500 nm to 250 nm showing significant differences in platelet adhesion.[110] An interesting observation was made regarding the impact of the pillar topography's height/aspect ratio, where tall flexible pillars limit platelet interaction

Parts of this chapter were already published in ACS Appl. Bio Mater. 2020, 3, 9, 5574–5589

to the tips only, whereas short ones remain stiff and allow platelet attachment. Hulander et al. prepared a nanoparticle surface gradient by synthesizing gold nanoparticles with diameters ranging from 36 to 56 nm and immobilizing them on a smooth gold substrate in another example of nanotopography influencing platelet adhesion and activation.[111] They discovered that the cells perceived smooth surfaces with 36 nm nanoparticles and structured surfaces with 56 nm nanoparticles.[111] The larger particle size reduces the cell's contact area between particles, inhibiting platelet activation.

In comparison to bacterial adhesion, research on platelet adhesion on surfaces with varying topography has been limited. Milner and colleagues demonstrated that molding submicron pillars (with heights and separations ranging from 400 to 900 nm) on polyurethane surfaces could reduce platelet adhesion.[107] They hypothesized that higher roughness reduced the contact area between the platelet and polyurethane by limiting the contact points to the tops of the pillars. They anticipated that this would reduce the possibility of interactions between adsorbed fibrinogen and platelets.[107] Fibrinogen is important in platelet adhesion to biomaterials with different topographies, and less fibrinogen-PLT interaction results in less adhesion or weak attachments that can be released by lower shear forces.[112,113]

Surface Stiffness

Anucleate platelets perceive substrate stiffness and convert it into biological signals. As platelets mechanosense the substrate stiffness, increasing substrate stiffness increases platelet adherence and spreading.[114] Importantly, adhesion to stiffer substrates also leads to higher levels of platelet activation that can be measured by integrin αIIbβ3 activation, granule secretion, and procoagulant activity. Mechanistically, Rac1 and actomyosin activity mediate substrate-dependent platelet adhesion, spreading, and activation to various degrees. This ability of platelets to mechanosense microenvironmental signals in building a thrombus or hemostatic plug and mechanotransduce them into differential adhesion, spreading, and activation provides biophysical insight into platelet aggregation-activation heterogeneity during thrombus formation. Glycoproteins IIb-IIIa or αIIbβ3 integrins are platelet adhesion receptors that are responsible for platelet aggregation on the harder surface.[115] The mechanism of how platelets take cues about substrate stiffness and switch their activation response was previously understood.[114] Qui et al. observed platelets' ability to mechanosense surfaces of varying stiffness and that they undergo cytoskeletal reorganization on harder surfaces. [114] While much research has been done to establish the theory of how substrate stiffness influences platelet

Parts of this chapter were already published in ACS Appl. Bio Mater. 2020, 3, 9, 5574–5589

adhesion, activation, and spreading, the idea of tuning the substrate stiffness to mediate these platelet processes remains unexplored.[114,116,117]

1.4.3 Biochemical Modification

In order to improve the hemocompatibility capabilities of surfaces, they can be modified utilizing bioactive molecules or biopolymers such as polysaccharides, peptides, and antibodies. Heparin, chitosan, and certain zwitterionic polymers are examples of biopolymers that have already been widely employed to stop platelet and protein attachments. The most commonly used antithrombogenic agent is heparin, which is a naturally occurring polysaccharide.[118] Its structure is extremely similar to that of heparan sulfate, a proteoglycan found on the surface of endothelial cells that gives those cells their inherently anticoagulant capabilities.[119] The antithrombin-binding properties of heparin prevent the production of fibrin mesh. Heparin is a molecule that is strongly negatively charged, so to prevent a decrease in its biological activity, it is typically integrated onto titanium surfaces through electrostatic interactions with positively charged polymers.[120] Using the layer-by-layer (LbL) self-assembly method, heparin has been mixed with other polycations, including chitosan, tanfloc, and collagen, to coat titanium implants.[120]

Dipyridamole, a small molecule antiplatelet medication, was used to surface-modify PU membranes to show its ability to inhibit platelet adherence. Dipyridamole was employed in a study to modify the surface of PU membranes by attaching it directly to PU membranes. The platelet adhesion density of the dipyridamole-linked PU membranes fell by 72%, 35%, and 52%, respectively, after 15, 30, and 60 minutes of incubation in human platelet rich plasma. Another study observed that the surface grafting sites of primary amine (NH_2) are improved in PU membranes by including polyethylenimine (PEI). The adherence of platelets to PEI-PU membranes was reduced by the tethering of heparin and phosphorylcholine (PC) groups[91]. Heparin and fibronectin films were created by co-immobilization on aminosilanized titanium surfaces by Li et al.[121] This method combines co-immobilization with electrostatic interaction, and the co-immobilized films remained stable after five days of immersion in phosphate-buffered saline (PBS). This improved the hemocompatibility of titanium surfaces. Yang et al. treated the surface of TiO2 nanotube arrays with the anticoagulant medication bivalirudin before adding a 5-layer polydopamine coating.[122] Bivalirudin's release kinetics were controlled by the polydopamine coating, and its activity was detectable for more than 300 days as opposed to 40 days in TiO2 nanotubes loaded with the bivalirudin substrate.[122 123] Ex vivo and in vitro studies revealed improved hemocompatibility for such coatings.

Parts of this chapter were already published in ACS Appl. Bio Mater. 2020, 3, 9, 5574–5589

Nitric oxide (NO) release and heparan sulfate recruitment are two ways that the endothelial cells that line the inside surface of healthy blood arteries prevent blood clotting. [124] A layer known as the glycocalyx, which is abundant in proteoglycans containing glycosaminoglycan (GAG), makes up the endothelium´s inner lining. The development of multifunctional surfaces that can resemble the endothelial environment has been the focus of recent studies. To achieve glycosaminoglycan functionalization, Simon-Walker et al. coated TiO_2 nanotubes (TiO_2NT) with heparin-chitosan polyelectrolyte multilayers (PEM).[109] After that, NO-donor chemistry was applied to these surfaces to create a significant antithrombotic signal. Comparing modified TiO_2 surfaces to those with other control groups, GAG-based surfaces, and NO-donor chemistry revealed a significant decrease in platelet adhesion and activation. Concerning the anti-fouling and antibacterial properties of NO, a comprehensive review involving NO-based biomaterials for the development of multifunctional antibacterial biomedical devices was recently published.[125]

Parts of this chapter were already published in ACS Appl. Bio Mater. 2020, 3, 9, 5574–5589

Chapter 2: Motivation and Thesis Overview

Motivation

Platelet-surface activation is a problem encountered during platelet storage that ultimately leads to platelet aggregation and, consequently, the degradation of platelet concentrates. Current storage techniques do not provide complete solutions to the platelet activation problem. Platelets can be stored for a maximum of 5 days prior to transfusion. The average number of platelet concentrates transfused every day in Germany alone is around 1300 units. Platelets are one of the most utilized and expensive of all the other blood components that are transfused. Several surveys conducted around the world report platelet concentrate waste ranging from 10% to 20%. At the same time, it is also revealed that there are significant shortages. This condition can be attributed to the short shelf life of platelets.

The platelet storage bags available on the market are available in two variations: textured and smooth. However, on careful examination, one can clearly spot that the patterned or imprinted structures on the interior layer of the bag are larger than 100µm in size. The average size of platelets is only about 3µm and hence it is unclear if such large patterns have any significant impact on a comparatively small platelet (**Figure 8**). The next challenge with the current commercial technique of platelet storage is the materials used in manufacturing the bags. To make it flexible and avoid breakage during transportation, the majority of them use PVC or polyolefin with a significant amount of plasticizers. Another difficulty in storing platelets is the reliance on anticoagulants to prevent platelet aggregation. Studies have shown that this can, in turn, partially alter the functionality of the platelets.

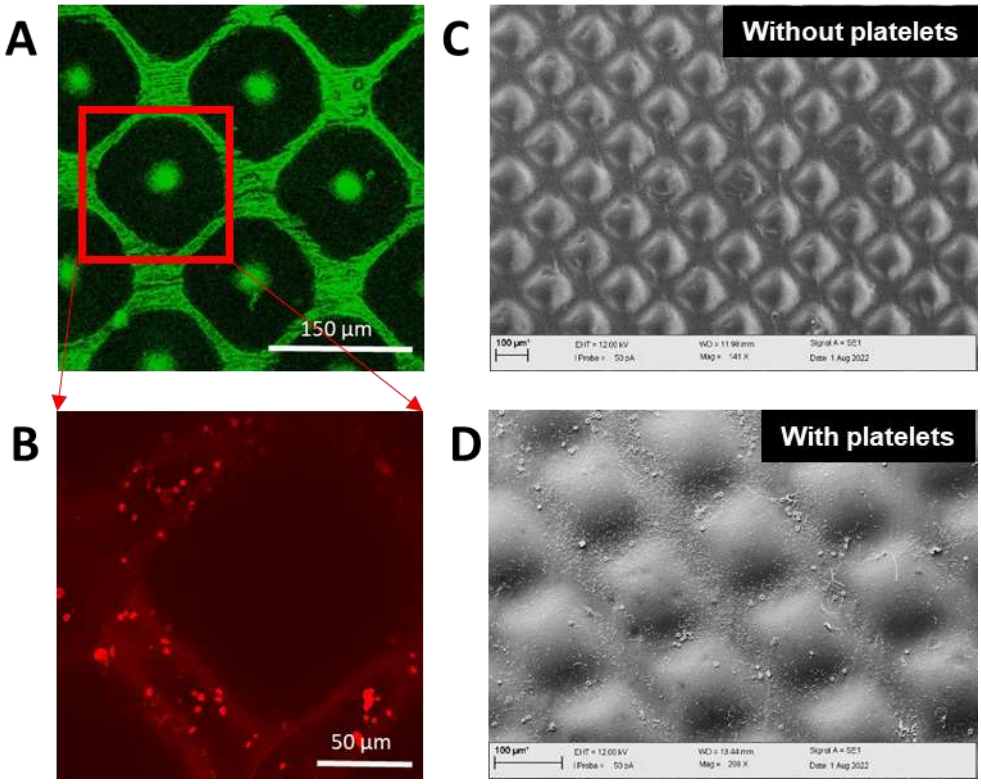

Figure 8: Platelet adhesion on commercial platelet storage bags.(A)CLSM image of platelet bag. (B) platelets adhering on the platelet surface imaged by CLSM. SEM micrographs of platelet bag surface (C) without and (D)with platelets.

However, the biggest challenge for platelet storage is bacterial contamination. Bacterial contamination and septic transfusion reactions are key contributors to morbidity and mortality. Statistics report that between 1:1000 and 1:2500 platelet units are bacterially contaminated, with the skin's bacterial microflora being the primary source. Various pathogen inactivation technologies that employ UV irradiation techniques are utilized to mitigate the problem. However, several molecular analyses have identified that the signaling pathways linked to platelet function and normal physiological processes are altered.

As a start and acute measure, an impactful sub-micron or nano-topography that can be translated into the existing platelet bags could address a part of the larger problem. However, in order to solve the platelet storage conundrum, an alternate bio-thrombo-compatible material with built-in antibacterial properties must be developed in the future.

Thesis Overview

An attempt to address the fundamental problem of surface-induced platelet activation was undertaken in the thesis. As explained in the introduction, this challenge can be addressed by tuning the properties of the surface (**Figure 9**). This can be done by employing three different approaches individually or in combination: physicochemical, biophysical, and biochemical.

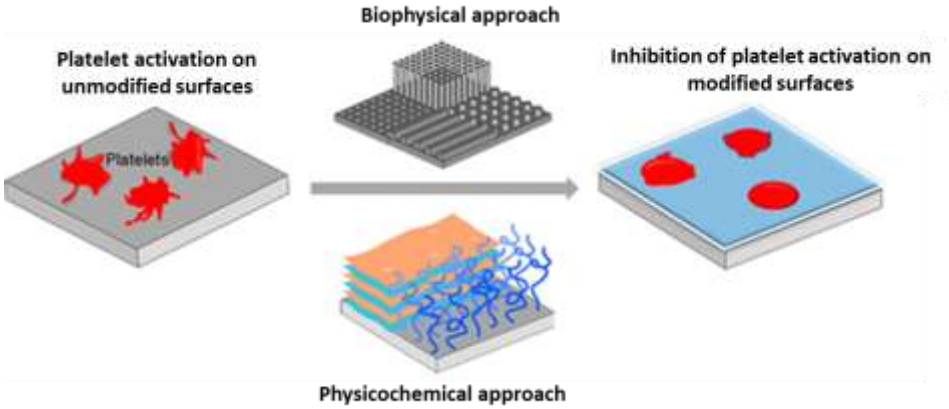

Figure 9: Schematic representation of modulating surface induced platelet activation by employing different approaches. Adapted from[80].

In chapter 4, platelet-compatible surfaces that can inhibit the adhesion and spread of human platelets were fabricated using hydrogel films made of gelatin and agarose along with their respective nanocomposites, which were formed by incorporating magnetite (Fe_3O_4) nanoparticles (**Figure 10**). The results from the characterization data showed that the agarose films, when compared to gelatin, had higher surface wettability, better controlled-swelling capabilities, and more stiffness, which significantly reduced platelet adherence. The role of the nanoparticles was to enhance the physical and chemical properties of the hydrogel films. While all of the films inhibited platelets from spreading, agarose and its nanocomposite films repulsed platelets and inhibited platelet adhesion and activation more effectively than gelatin-based films did. The results showed that the surface activation of platelets can be changed by altering the properties of the films underneath and that bioinert agarose could be a potential candidate as a material for storing platelets and can even be used in medical applications.

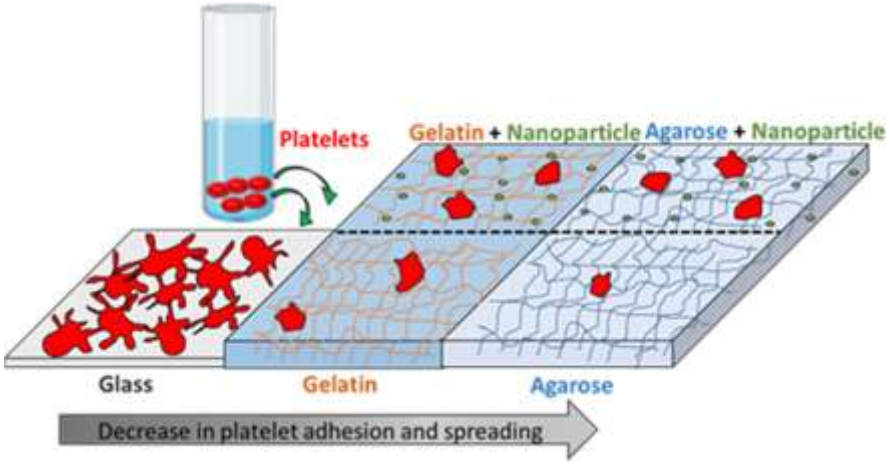

Figure 10: A representation of the differential response of platelets to soft, hydrophilic hydrogel and nanocomposite films. Adapted from[117].

In chapter 5, the use of AFM-assisted fluidFM in nanopatterning is demonstrated by printing various geometries with a commercial acrylate-based UV curable ink (Loctite AA3491). Different printing parameters, like pressure, speed, and force, which impact the printing process of the structures, were optimized. Two selected geometries—the multiplexed hemispheres (Grid) and hexagonal tiles (Hive)—were fabricated and investigated to study the response of platelets to their respective topologies (**Figure 11**). It was found that the grid and hive structures made the surface less stiff and provided the platelets with physical cues, which impeded the platelets from adhering to the surface. The findings indicate that nanopatterns limit platelet activation on surfaces, suggesting that nanotexturing of storage bags can extend the shelf life of platelet concentrates.

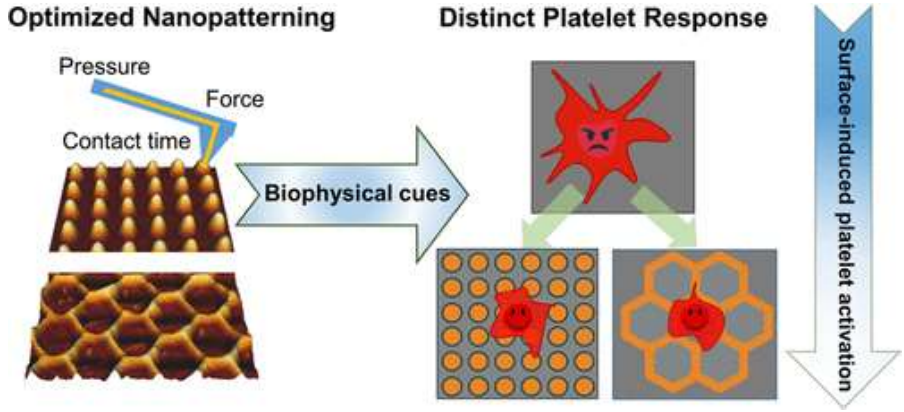

Figure 11: Implementing FluidFM to fabricate nanopatterns to evoke an intended platelet response. Adapted from[126].

After the successful demonstration of implementing the FluidFM system to fabricate grid and hive shaped nanostructures in the previous chapter, further effort was made in Chapter 6 to explore the potential of FluidFM-based nanoprinting by probing different avenues of printing. In a study undertaken in collaboration with colleagues from KIT INT, FluidFM was used to integrate biofunctional molecules into the ink, followed by printing in the shape of hemispherical features (**Figure 12**). In another work, it was demonstrated that the functionality was retained after the curing process without compromising the mechanical properties of the native ink, and to explore the FluidFM system's capabilities, similar patterns with varying interspacing and height were created. The rationale behind the experiments is to examine the distinct response that such modulation can generate within the platelets in order to gain more insights into the biophysical cues platelets can process. In another set of experiments, the effect of distinct curing times on feature stiffness was analyzed. It was discovered that the nanofeatures formed by extruding attoliters of ink did not differ significantly in stiffness.

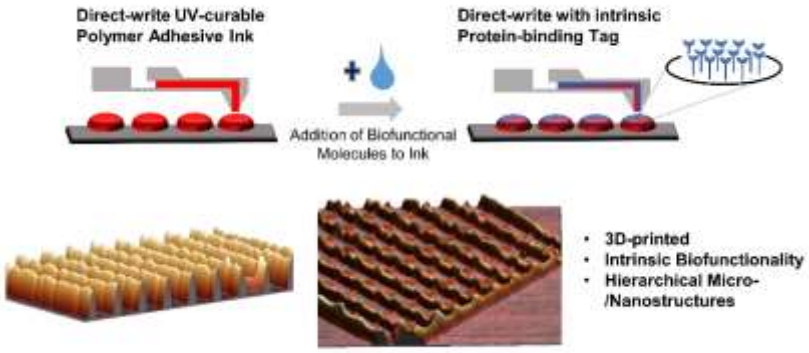

Figure 12: A graphical representation of FluidFM-based printing used to incorporate biofunctionality into printed structures. Adapted from[127].

Given the findings in chapters 4 and 5 that platelet adhesion to the surface can be modulated by changing both the physicochemical and biophysical properties of the surface, both approaches were combined in Chapter 7 to achieve better results. Following the promising results from the agarose films in Chapter 4, it was selected as the substrate. The nanoimprinting technique was applied to imbibe different topological patterns, namely, squares, dots, pills, and chains (**Figure 13**). Fe_3O_4 nanoparticles were incorporated to induce antibacterial properties within the agarose films. The films were then characterized, followed by an evaluation of the adhesion of platelets and bacteria. The results showed an overall reduction in the number of

platelets on all the agarose surfaces, both patterned and non-patterned. The antibacterial effect of particles within the gels showed promising results.

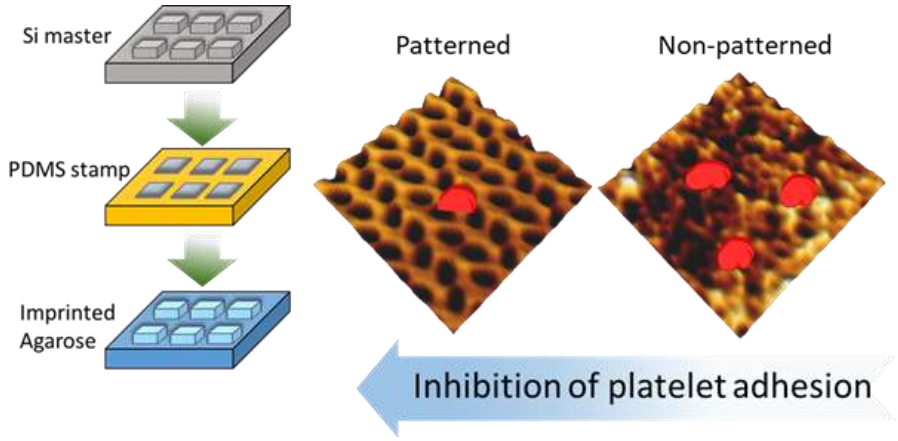

Figure 13: The process of imprinting agarose gels is illustrated together with the differences in platelet adhesion over a structured and non-structured surface.

Schematic overview of the thesis

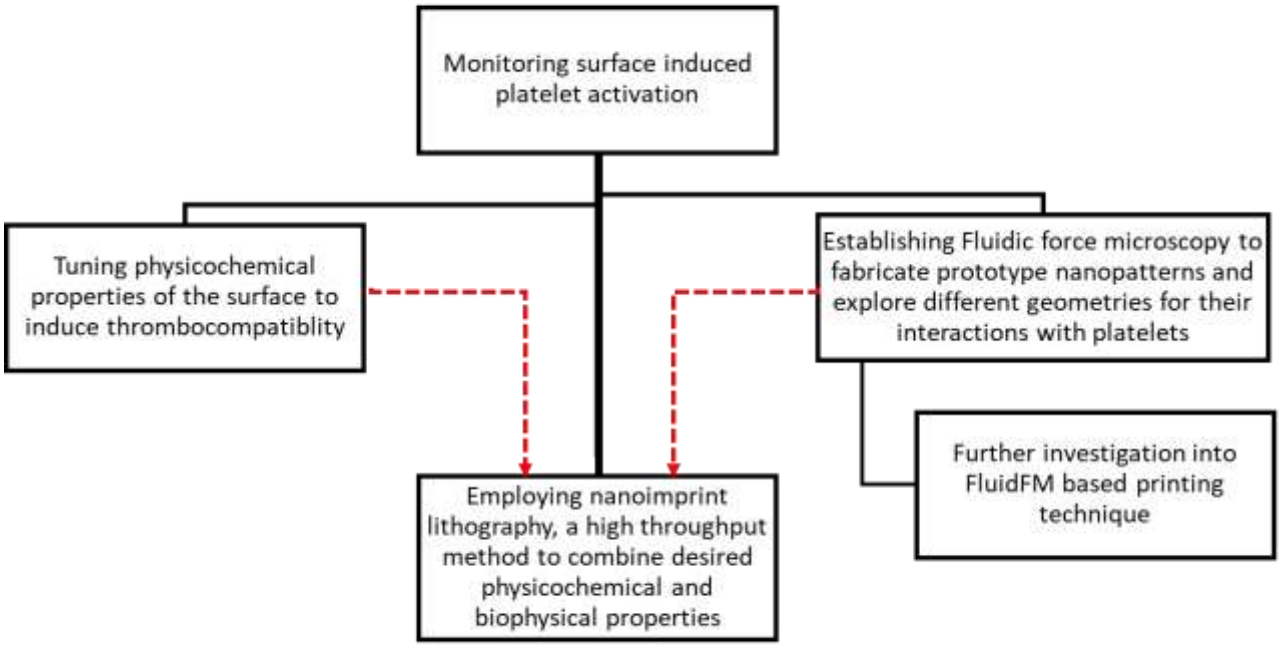

Figure 14: Flowchart explaining the work carried out in this thesis

Chapter 3: Background of Methods and Materials

This chapter provides a brief overview of the important and frequently used material and technique throughout this thesis.

3.1 Agarose and its Applications

3.1.1 General introduction

Agarose is a biocompatible polysaccharide extracted from marine red algae that contains agarobiose (a disaccharide of D-galactose and 3,6-anhydro-L-galactopyranose) repetitions (**Figure 15**).[128] Agar is derived from the Rhodophyceae family of red seaweeds, of which Gracilaria and Gelidium are commercially important genera.[129] Araki and colleagues discovered the primary characteristics of primary structure and separated the fraction with the best gelling properties, naming it agarose.[130] Agarose, the main component of agar, has the formula $[C_{12}H_{14}O_5(OH)_4]n$, whereas agaropectin is a more complex polysaccharide with sulfuric and uronic acid residues.[130] Agaropectin is seperated from of agar to make agarose.[131] The remaining fractions were termed as agaropectin. Agarose gelation and melting points vary from 30–40 °C and 80–90 °C respectively, depending on its molecular weight, concentration, and number of side groups.[132] Furthermore, this natural carbohydrate polymer is able to self-gel because it has oxygen and hydrogen in its side groups. The intra- and intermolecular hydrogen bonding of agarose molecules causes gelation at high temperatures (60 °C).[133] Agarose gelation occurs in three steps: induction, gelation, and pseudoequilibrium, in which hydrogen bonding and electrostatic intraction result in the helical structure of the agarose molecule, which then forms gel.[132] The need for a biocompatible material in the development of storage options for blood products has been a longstanding challenge for the researchers.[80] Natural carbohydrate polymers play an important role in this regard due to their non-toxicity and good compatibility with various tissues and organs.[134] The similarity of agarose, a natural carbohydrate polymer, to the extracellular matrix results in appealing properties that pique the interest of researchers.[135] Literature reveals that the potential of agarose, unlike that of other polysaccharides like chitosan and alginate, has not yet been fully explored.[132] The structure and morphology of the agarose polymer can be customized by adjusting its concentration.

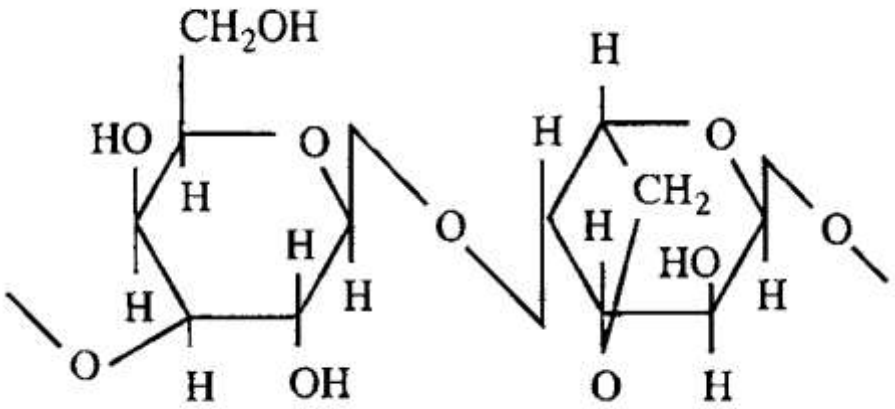

Figure 15: The repeating unit of agarose consists of D-galactose and 3,6-anhydroL-galactose. Adapted from[128].

3.1.2 Agarose Gelation

The OH-4 of the D-galactopyranosyl and the adjacent hemiacetal oxygen atom of the anhydro-L-galactopyranosyl residues form intramolecular hydrogen bonds.[136] The anhydro-L-galactopyranosyl residue is a cage-like sugar that helps stabilize the proposed intramolecular hydrogen bonding at high temperatures. Intermolecular hydrogen bonding occurs between the ring O-3,6-atom and the OH-2, which are oriented axially on different molecules of anhydro-L-galactopyranosyl residues (**Figure 16)**.[133] The association causes the cage effect, which results in the lowest energy state of electrons on the anhydro-L-galactopuranosyl residues' lone pairs of ring oxygen atoms.[137] Because the conformation has a tetrahedral distribution, it attracts not only other molecules but also water molecules via hydrogen bonding.[137] Agarose molecules' intra- and intermolecular hydrogen bonding results in gelation up to high temperatures, and their periphery is surrounded by hydrophobic carbon and hydrogen atoms, both of which are required to contribute to the hydrophobic effect.[133] Because of the decrease in entropy, this hydrophobic effect promotes hydrogen bonding within water molecules. As a result, hydrogen bonding occurs easily with water molecules on the outside of the polymer helices.[133]

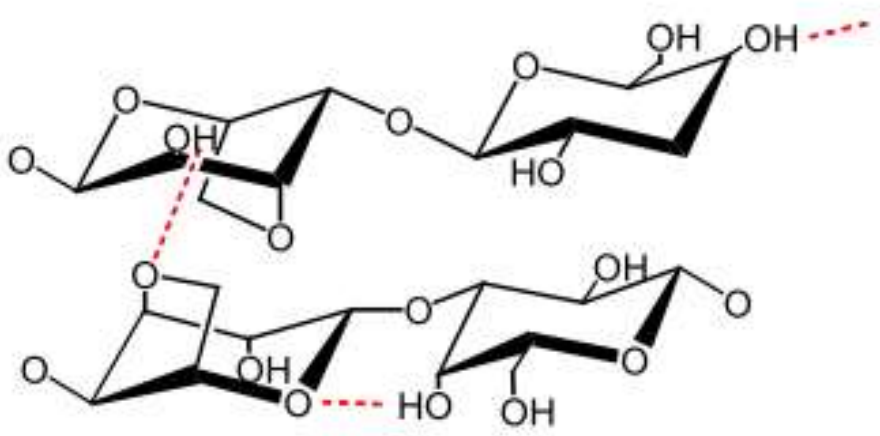

Figure 16: The gelation mechanism of agarose. Hydrogen bonding is represented by red dotted lines. Adapted from[133].

3.1.3 Application

Agarose has been previously employed in the areas of tissue engineering to construct scaffolds and in regenerative medicine to reconstruct impaired tissues.[134] The agarose gel mimics the extra cellular matrix and tissues and can be further coupled with other proteins and polymers to tune the required properties.[138] Agarose has been previously used in the domain of drug delivery.[132] The majority of polysaccharides have a high surface charge. This phenomenon occurs when the drug carrier comes into contact with an impediment during its circulation within the body, such as protein corona formation. While agarose has a neutral surface charge at different pH levels, this property allows agarose to transport drugs with a low amount of protein corona formation and improve delivery efficiency.[139] Agarose has been used in multiple independent studies for cartilage regeneration, nervous system regeneration, cardiac regeneration, bone regeneration, skin regeneration, and corneal regeneration.[134] Agarose can be used in many different ways because its mechanical properties can be changed by changing its concentration. It has been used as a microfluidic platform for cellular applications and has even been seen as an alternative to PDMS.[140141] Zarrintaj et al. used agarose to create a tissue-like phantom model. It has proven to be hemocompatible and noncytotoxic.[132]

The application of agarose in the electrophoresis of biomolecules is well known. Agarose hydrogel forms a stable, three-dimensional network of pores that can trap and separate these molecules based on their sizes. The pore size of agarose gels can range from a couple of micrometers down to a few hundred nanometers, depending on the concentration of the

agarose. thus making the expelled proteins from platelets difficult to adsorb on the surface of the agarose.[142] The higher the concentration, smaller is the pore size. Since these proteins play a crucial role in platelet adhesion by mediating the complex interactions between them and the substrate and by regulating signaling pathways that control platelet behavior, this results in difficulties for platelets during initial docking.

3.2 Fluidic Force Microscopy (FluidFM)

A general introduction to the most practiced method during the course of this thesis is outlined in this section.

3.2.1 General Introduction

Atomic force microscopy (AFM) is widely used in the field of material and life science research. After becoming a typical surface-imaging technology, AFM was employed in biological research to explore cell adhesion and electromechanical properties.[143] FluidFM combines a conventional AFM with microchanneled cantilevers tightly connected to an external reservoir.[144] The dispensing liquid can be filled in the reservoir and released out at a controlled pressure. The microfabrication of microchanneled cantilevers is based on the thermal fusion of two silicon wafers to form cavities lined with silicon dioxide within the silicon body. The cantilever microchannel then enters the silicon chip and exits through an open reservoir.[144] Finally, focused ion beam milling is used to create an aperture at the cantilever tip's apex (**Figure 17)**.[144] As a result, the tips obtained combine fluidic versatility with AFM force control accuracy. The latter enables gentle manipulation and isolation of single cells,[145] quantification of cell-substrate[146] and cell-cell interaction,[147] and reversible immobilization of cells at the aperture edge, whereas pressure control enables quantitative manipulation of liquids and reversible immobilization of cells at the aperture edge.

Researchers need precise instruments to manipulate, produce, and prototype on the nano- and microscale in the pursuit of technological miniaturization. Microfluidic probes in FluidFM technology give remarkable flexibility and control for printing patterns and exploring nanostructure formation. This technique is also being expanded in the areas of protein arrays for sensing applications[148], chemical gradients for cell migration research[149], the comprehension of chemical processes in femtoliter droplets[144], and nano-fabrication processes[150]. FluidFM's unique combination enables it to push the boundaries of single cell research, nanotechnology, and biophysics. In this work, FluidFM was particularly used for two applications, namely, single platelet force spectroscopy and nanoprinting.

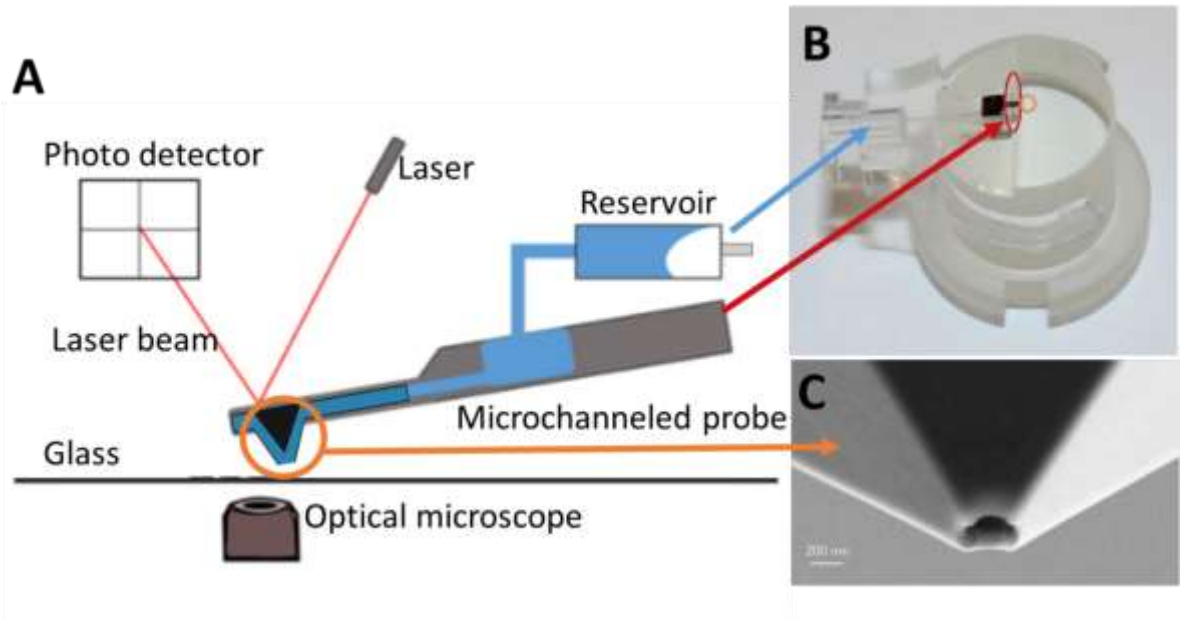

Figure 17: A schematic representation of the FluidFM setup and its important components (A) The FluidFM consists of a hollow microchannel with a reservoir at one end to store the fluid and a nano- or micro-aperture at the other end to control the flow of the fluid inward or outward. (B) A microchanneled probe mounted on a probe holder, with a blue arrow pointing to the reservoir and a red arrow pointing at the probe. (C) A scanning electron micrograph of the FluidFM cantilever with a nanoaperture. Image courtesy of Cytosurge AG.

3.2.2 Single Platelet Force Spectroscopy (SPFS)

Platelet adhesion, just like cellular adhesion, involves highly regulated interactions in which platelets interact with one another following a physiological process or with different non-physiological substrates (**Figure 18**). In mammalian cells, adhesion is involved in controlling many functions, including differentiation, tissue development, and inflammation.[151]

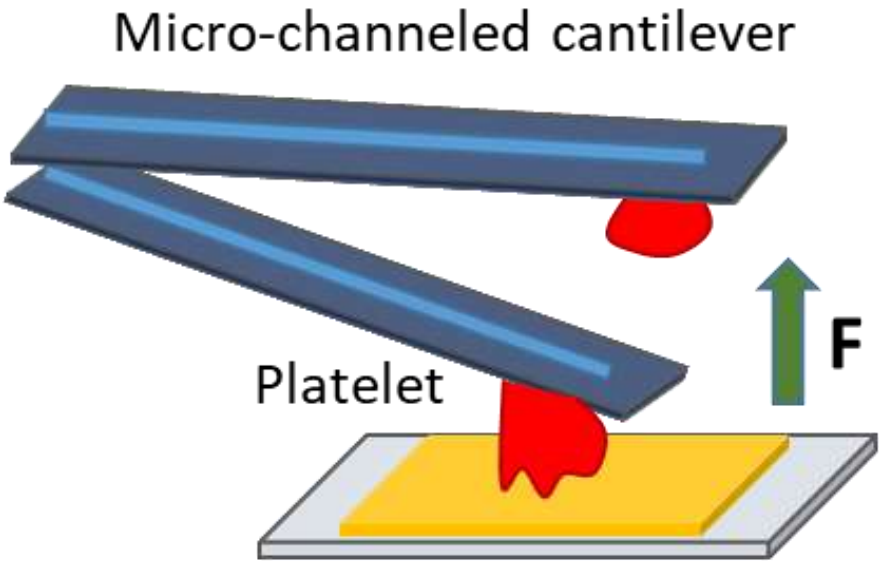

Figure 18: Illustration of single platelet force spectroscopy with a platelet on the cantilever at the substrate's surface, indicating the de-adhesive force experienced by the platelet before moving to its home position.

Previously, Bui et al. performed SPFS in a traditional way by immobilizing the platelet on the tip of the cantilever that was coated with collagen G.[81] The cantilever, together with the adhered platelet, was then used to measure the adhesion force between the platelet and different nanostructured surfaces. This is an effective way to gain insights into the interaction between the surface and the platelet. However, this method of performance requires additional effort and a lot of consumables, as each cantilever can only be used once. FluidFM can solve this issue due to its ability to pick up or release the platelets by applying negative or positive pressure, respectively.

FluidFM provides multiple options for studying adhesion at the single-cell level. Potthoff et al. developed FluidFM-based single-cell force spectroscopy (SCFS) by replacing the traditional cell trapping cantilever chemistry with negative pressure based cell immobilization.[147] The authors used this system to study yeast and mammalian cell adhesion by performing serial and dynamic long-term adhesion measurements. Cohen et al. used FluidFM-based SCFS to compare homotypic (between the MCF7 breast cancer cell line) and heterotypic adhesion forces (between MCF10A breast cancer cells and nontumorigenic HS5 cells).[152] Overall, all of the studies cited have demonstrated FluidFM's added value in the investigation of microbial adhesion, cell-substrate, and cell-cell interactions. Unlike conventional AFM, which requires the use of chemical treatments to immobilize the cells on the cantilever, FluidFM uses a physical process based on underpressure cell immobilization.

As a result, here the biases in adhesion force measurements caused by potential changes in cell physiology caused by chemical treatments are avoided. Furthermore, unlike irreversible chemical fixation, underpressure immobilization is a reversible process that allows multiple manipulations of the same cell.[153]

3.2.3 Nanoprinting

While techniques for fabricating microstructures are well established, the technology available for producing nanostructured surfaces is still limited. To achieve direct printing down to nanometer-sized objects, 3D printing at the nanoscale represents a new research and development challenge. The use of nanodispensing techniques, such as FluidFM, is a recent advancement in micro- and nanostructured 3D printing. FluidFM is a microfluidics-based atomic force microscopy (AFM) technique that uses a hollow cantilever with an aperture at the tip apex for precisely localized liquid dispensing(**Figure 19**).[154] Its use quickly expanded to nanolithography, for example, with the use of nanoparticles[155] and biomimetic membranes[156]. Micro- and nanostructures can be printed, depending on the size of the tip aperture. This technique could be used to create hierarchical structures at multidimensional scales using the commercially available UV-curable adhesive Loctite.[157,158] This is a highly viscous ink composed of various liquid methacrylate esters that undergo cross-linking polymerization when exposed to UV light.[159] As a direct-write technique, this method is incredibly versatile for pattern and structure formation, with excellent resolution down to the scale of tens of nanometers. FluidFM can thus be further used as a platform technology to generate polymer features by utilizing rapid surface-initiated crosslinking and versatile macrocrosslinkers.[127] A successful, robust nanoprinting platform must address several critical design parameters, including a high degree of control over material spatial deposition, continuous printing with minimal to no intermediate steps to stabilize printed layers without loss of feature registry between printing steps, and the deposition of solvent-free material to reduce or eliminate shrinkage from solvent loss and enable the creation of multilayered features.[160]

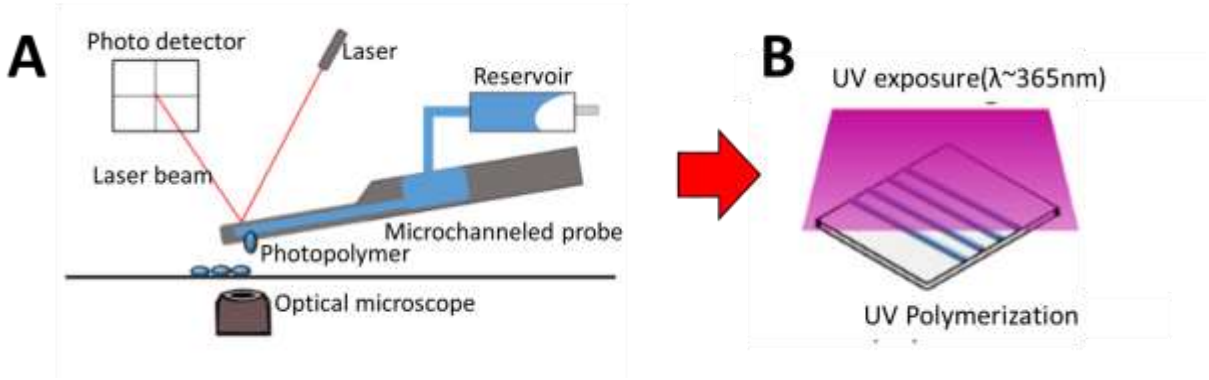

Figure 19: Nanoprinting Process Using FluidFM Technology (A) Schematic showing how a nanopipette works during nanoprinting, followed by (B) UV curing polymerization of the printed patterns. Adapted from[126]

Chapter 4: Controlling surface induced Platelet Activation by modifying Physicochemical Properties of the Surface

4.1 Chapter Overview

Biomaterials, particularly biopolymers, are widely used in the development of various cardiovascular valves,[161] artificial blood vessels,[162] dialyzers,[163] and implants[164]. When dealing with blood purification applications such as hemodialysis, plasmapheresis, or blood oxygenation, the aspect of coagulation that involves protein adsorption followed by platelet adhesion is especially important.[165] As a result, it is critical to control the biofouling of surfaces by plasma proteins, which can eventually lead to thrombosis.[166] Surface-related implant material complications can be reduced by developing effective surface coatings.[167] However, developing an antithrombotic surface for implants remains a challenge. Minimal platelet-surface activation has a significant impact on both implantation and platelet storage. Thus, the development of anti-thrombogenic surfaces with the goal of reducing anticoagulant administration is critical. However, more research is needed in the field of developing an antithrombotic surface, particularly for platelets. Furthermore, the lack of a hemocompatible bulk biomaterial has fueled the development of new surface coatings and surface engineering to combat thrombosis.[167]

As previously discussed, platelets tend to activate immediately after brief contact with artificial surfaces in vitro, which is a disadvantage in many applications such as platelet storage and platelet-drug studies.[168] Activated platelets expose glycoprotein IIb/IIIa, which initiates fibrinogen binding and promotes platelet aggregation.[81,169] In addition, their granules release prothrombotic substances.[169] The releasing proteins cross-link and activate the surrounding platelets while also increasing thrombin generation in conjunction with plasma clotting factors. During implantation, blood proteins adsorb on the surface of an implant, allowing platelets to adhere and form thrombuses, which can lead to stroke or extremity ischemia.[170,171] As a result, platelets play an important role in determining the fate of an implant in the early stages after implantation.[80] Platelet-surface interaction is critical in biomedical applications and in vitro studies. Controlling platelet-surface activation, on the other hand, is difficult and requires more effort because they activate immediately when they come into contact with any non-physiological surface.

The results presented in this chapter were already published in ACS Omega 2021, 6, 16, 10963–10974

Hydrogels are highly hydrated polymers with a polar polymer backbone and a large amount of bound water.[172] As a result, hydrogels are promising biomaterial candidates because they have the potential to mimic the native biological tissue microenvironment.[134] Because hydrogels exhibit antifouling activity, particularly in the presence of hydrophilic hydroxyl groups, they are promising candidates for developing blood-compatible materials.[173] The platelet density and degree of activation on the surface of synthetic hydrogel films have been reported to be controllable, taking them one step closer to being bioinert for platelet applications.[174] Agarose and gelatin hydrogels find a wide range of applications in tissue engineering and regenerative medicine.[175,176] Hydrogels have an advantage over other biomaterials due to their unique ability to hold large amounts of water molecules (up to 40 times their dry weight) while maintaining structural stability.[177] The surface of a biomaterial is critical in determining the material's hemocompatibility.[178] In hydrogels, the steric repulsion of hydrated chains contributes to their bioinertness.[174] Agarose, a natural polymer, contains hydroxyl groups that contribute to the hydrogel's overall antifouling properties.[138,179–181] On the other hand, gelatin is a biocompatible biopolymer with hydration properties and antimicrobial properties.[182] A reduced adhesion in pig platelets to agarose has been previously reported.[183] However, the response of human platelets to hydrogels, particularly those formed by agarose, has received insufficient attention. This gap was filled in this study by tracking the behavior of platelets on gels formed by agarose and gelatin. Hence, agarose and gelatin based hydrogel films were developed to inhibit platelet-surface adhesion.

Recently, a novel method for strengthening hydrogel networks by incorporating nanoparticles (NPs) has been described.[184–186] Some of the developed procedures for fabricating nanocomposite hybrids include mixing NPs into an existing polymer network or blending them with polymers to crosslink the polymer chains.[184] These hybrids are known as nanocomposite hydrogels. Nanocomposite hydrogels improve the hydrogels' existing physical, chemical, and biological properties.[177] NPs coated with carboxymethyl dextran (CMD) have a dextran backbone substituted with carboxymethyl groups, which gives the nanoparticle a polyanionic character. Furthermore, due to steric repulsions between particles, the soft polymer coat that surrounds the NPs makes these systems less likely to aggregate.[187] In this study, an attempt was made to study how Fe_3O_4 nanoparticles affected the properties of agarose and gelatin gels, as well as whether the nanocomposites reduced platelet-surface activation. Because of their superparamagnetic properties, Fe_3O_4 NPs are used for a variety of biomedical applications, ranging from MRI to MPI to drug delivery with specific coatings, and are thus considered

The results presented in this chapter were already published in ACS Omega 2021, 6, 16, 10963–10974

biocompatible.[188,189] They also have antibacterial properties[190,191] which could make them promising nanocomposites for bacterial contamination in platelet storage. It was hypothesized that nanocomposite hydrogels with defined properties could modulate platelet response to a nonphysiological surface.

In this study, agarose and gelatin hydrogels were created before progressing to make nanocomposite hydrogels by incorporating synthesized CMD-coated Fe_3O_4 NPs into the respective hydrogels. The effect of the gels' various physicochemical properties on platelet adhesion was investigated. To characterize the fabricated gels and study the response of platelets on them, multiple technologies were used, including dynamic light scattering (DLS) contact angle, nanoindentation, force spectroscopy, confocal laser scanning microscopy (CLSM), and scanning electron microscopy (SEM).

4.2 Results

4.2.1 Fabrication of Hydrogel and Nanocomposite Films

The effect of hydrogels and nanocomposite films on platelet-surface activation was studied by creating films from bio-inert materials such as gelatin and agarose, as well as their nanocomposite gels (**Figure 20**). The study of platelet response on gels formed by different polymer concentrations revealed that gelatin at 10% and agarose at 1% provided the best stability. Furthermore, the hydrogels were created in customized silicone molds and had to be removed before characterization. As a result, 10% gelatin, 1% agarose, and a film thickness of 2 mm were chosen for further investigation in this study. To make gels, gelatin and agarose were melted at 60 and 95 °C, respectively, before being left to physically crosslink at 35 and 40 °C, respectively (**Figure 20**). A cooling process allows the molecules to form stable networks of triple and double helix-coil polymer chain transition arrangements.[129,192]

The results presented in this chapter were already published in ACS Omega 2021, 6, 16, 10963–10974

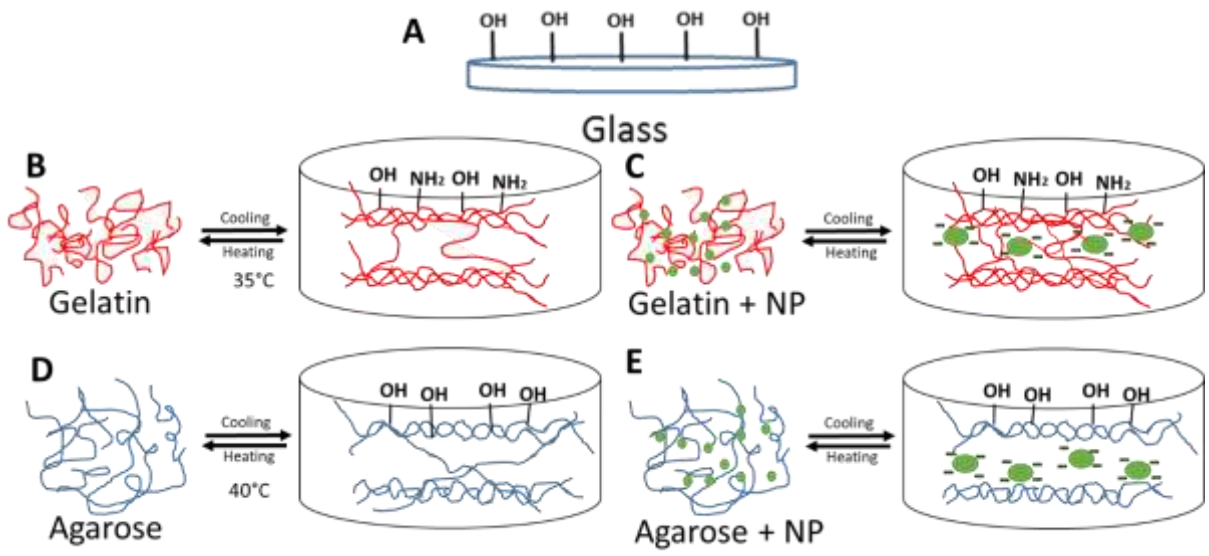

Figure 20: Schematic illustration of the hydrogel's polymer networks with and without NPs. (A) surface of bare glass containing numerous hydroxyl groups serves as a control. Hydrogen bonding enables gelatin hydrogels to create a triple helix-coil structure. (C) The addition of NPs (green) increases the cross-linking between the negatively charged carboxyl groups of CMD coated on the particle surface and the amino groups on gelatin chains. (D) The fibers of agarose hydrogels have a double helix-coil configuration. (E) The addition of NPs disrupts the gelation phase, resulting in weaker matrix formation in comparison to native agarose hydrogels. Adapted from[117]

Different concentrations of NPs in the films were tested to determine the threshold beyond which the particles caused platelet aggregation on the surface (**Figure 21**). It was observed platelets started forming aggregates at 3.2 mM concentration while no aggregation was observed at ≤2 mM concentration. A high possible concentration of nanoparticles should be added to the gels to achieve the best antibacterial effect without compromising platelet viability. As a result, 2 mM was identified as the optimal concentration for the formation of nanocomposites (**Figure 21**). Electrostatic interactions between carboxylic groups in CMD molecules coated on NPs and amine groups in gelatin crosslink and stabilize the nanocomposite gels.

The results presented in this chapter were already published in ACS Omega 2021, 6, 16, 10963–10974

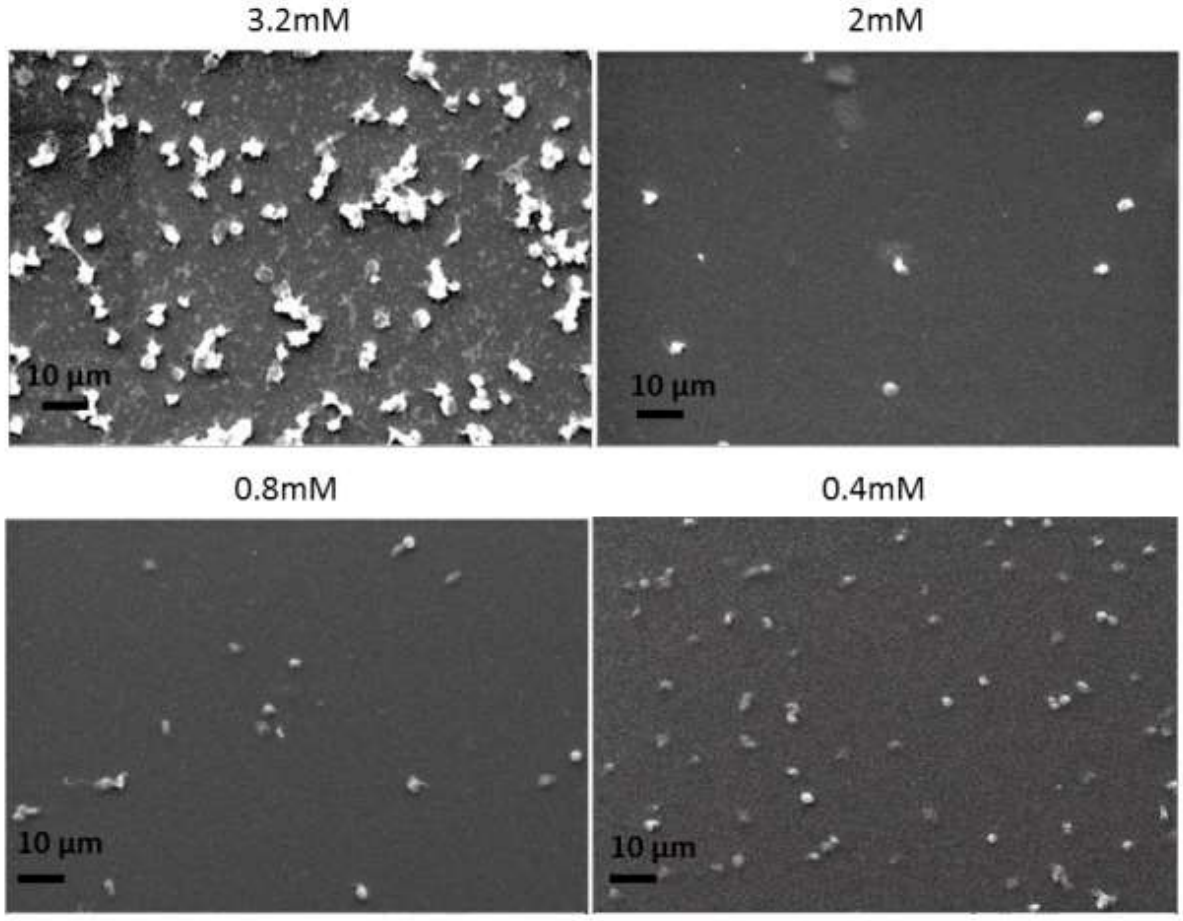

Figure 21: Platelet activation on gelatin nanocomposites fabricated with varying concentrations (3.2mM, 2mM, 0.8mM, and 0.4mM) of nanoparticles within the hydrogels, as depicted by scanning electron micrographs. Adapted from[117]

4.2.2 Characterization of Hydrogel and Nanocomposite Films

4.2.2.1 Surface Wettability

The surface wettability of the fabricated films was then assessed using the captive bubble method via static water contact angle measurements. Glass slides covered with a coating of hydrogel and hydrogel nanocomposites were inverted and immersed in distilled water for this purpose (**Figure 22**). The contact angle was measured using the ellipse fitting method after an air bubble was trapped. Lower contact angles indicate that the surface is more hydrophilic. The contact angle was greatest for the bare glass surface (51.1±4.2°), then gelatin (22.6±4.4°), and agarose (10.6±6.6°). However, nanocomposites influence surface wettability in a different way. The contact angle for gelatin-nanocomposites (46.1±12.5°) was greater than that of gelatin alone (22.6±4.4°), but reversed for agarose-nanocomposites (4.8±6.6°) versus agarose

The results presented in this chapter were already published in ACS Omega 2021, 6, 16, 10963–10974

(10.6±6.8°). However, agarose gels had substantially lower contact angles than gelatin gels, indicating that agarose gels are more hydrophilic.

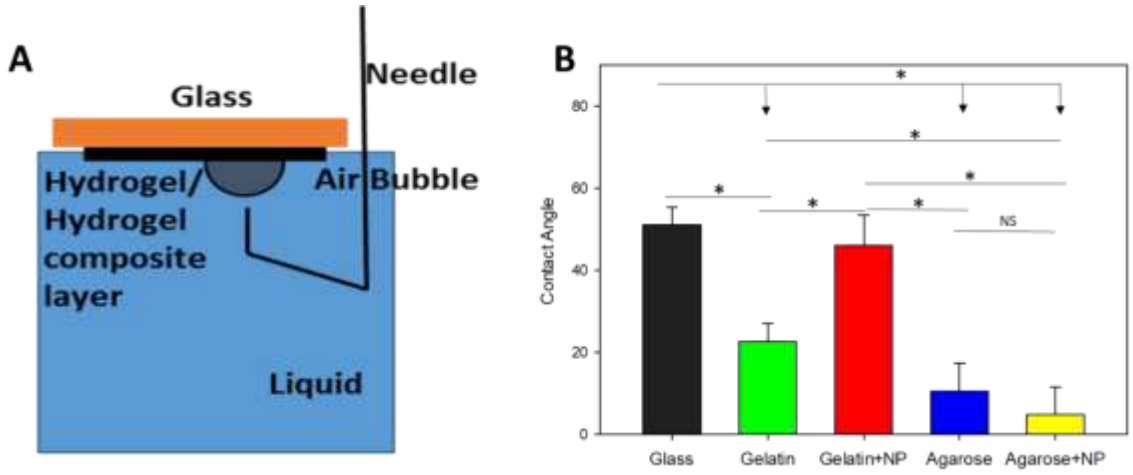

Figure 22: The captive bubble technique is used to measure contact angles. (A) Experimental setup diagram for taking measurements on gels and glass samples. (B) The graph depicts the recorded contact angle values on different samples, along with the standard deviation. * Statistically significant difference determined by the oneway ANOVA test ($P < 0.05$). Adapted from[117]

4.2.2.2 Water Retention Properties

At room temperature (RT), the hydrogels and nanocomposites' stability was investigated by assessing their swelling and water retention capabilities. The weights of the fabricated gel (W_X), the wet gel (W_{PBS}) immersed in PBS, and the gel stored in a dry environment (W_{AIR}) at various time points were measured. W_{PBS}/W_X or W_{AIR}/W_X were used to calculate the proportion of swelling or deterioration at each time point. In the event of hydrogel degradation, the degradation trends were nearly the same regardless of the polymer or the use of NPs (**Figure 23**). However, there was a clear distinction between the gelatin and agarose polymers during swelling. While gelatin films showed a higher elevation in weight gain, agarose films showed an almost negligible increase in weight.

The results presented in this chapter were already published in ACS Omega 2021, 6, 16, 10963–10974

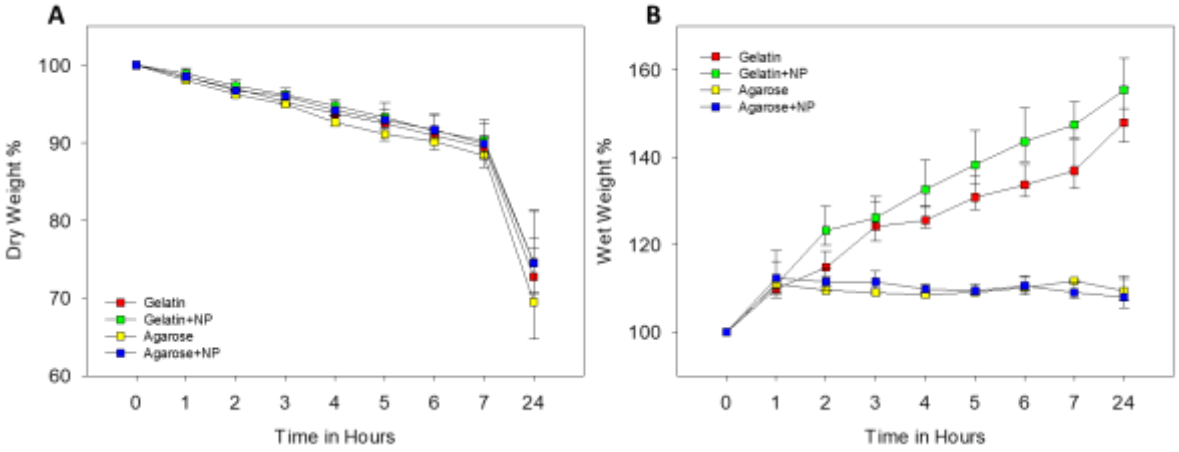

Figure 23: The degradation and swelling behavior of hydrogel and nanocomposite films. (A) There was no statistically significant difference in water retention between gelatin (green), gelatin nanocomposite (red), agarose (blue), and agarose nanocomposite (yellow). (B) Gelatin (green) and gelatin nanocomposite (red) showed a continuous increase in swelling behavior, whereas agarose (blue) and agarose nanocomposite (yellow) did not show a significant increase in gel swelling and reached equilibrium. n = 3 repetitions. Adapted from[117]

4.2.2.3 Gel Elasticity

The mechanical behavior of the fabricated films was then investigated using an AFM-based nanoindentation technique using a 3 µm colloidal probe (**Figure 24A**). The bead indents the underlying surface when an indentation force is applied, leading the cantilever to flex and the indentation of the gel to be recorded in the force-distance curve (**Figure 24B**). Typical approach curves revealed that gelatin had the greatest indentation depth, followed by gelatin-nanocomposites, agarose-nanocomposite had the lower, and agarose had the least indentation depth. The Young's modulus (E) of the films was determined by fitting the indentation curve induced by the deformation with the Hertz model. Data analysis of F-D curves obtained at separate points on each gel from two distinct gel preparation times revealed that the E value of the gelatin film (**Figure 24C**) was more than an order of magnitude less than that of agarose (**Figure 24D**). NPs, on the other hand, increased the E value of the gelatin film while lowering the E value of the agarose film.

The results presented in this chapter were already published in ACS Omega 2021, 6, 16, 10963–10974

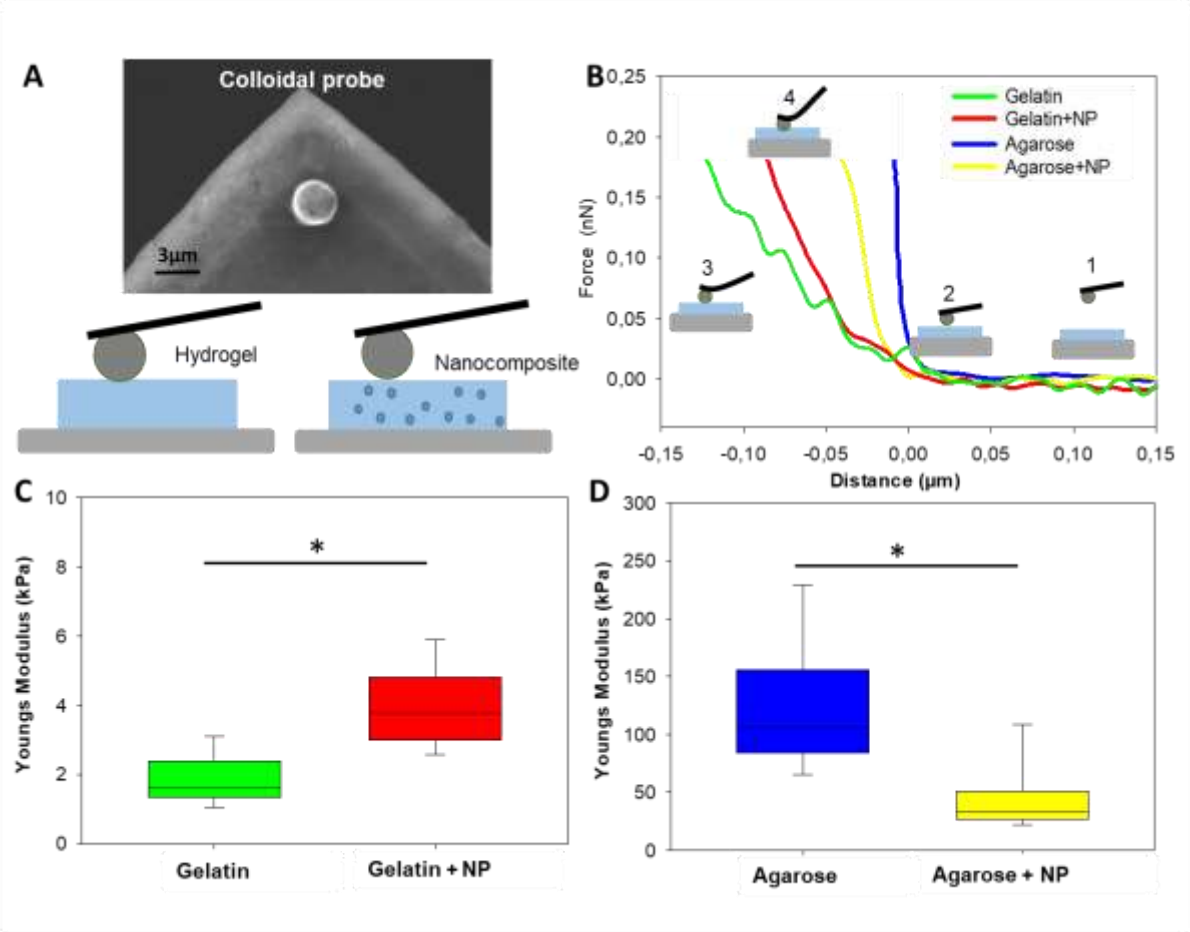

Figure 24: Nanoindentation was used to determine the stiffness of the fabricated films. (A) Diagram of a probe contacting the hydrogel and nanocomposite samples. Below: AFM cantilever SEM image with a gold colloidal particle attached. (B) Typical force-distance curves for the four different films. Young's modulus was measured on gelatin (green) and gelatin nanocomposites (red), and agarose (blue) and agarose nanocomposites (D) (yellow). * The one-way ANOVA test determined a significant difference (P 0.05). Note: the scale bar in the y-axis in (C) differs from (D). Adapted from[117]

4.2.3 Studying Platelet Behavior

The SEM images taken on the samples of agarose, gelatin, and glass as part of the preliminary investigation (**Figure 25**) clearly show the different binding behaviors of platelets on the surfaces. Most platelets adhered to the glass surface, where they were also most strongly activated, as shown by the growth of filopodia and lamellipodia extensions. After that, fewer platelets adhered to the gelatin surface, and the fewest adhered to the agarose surface.

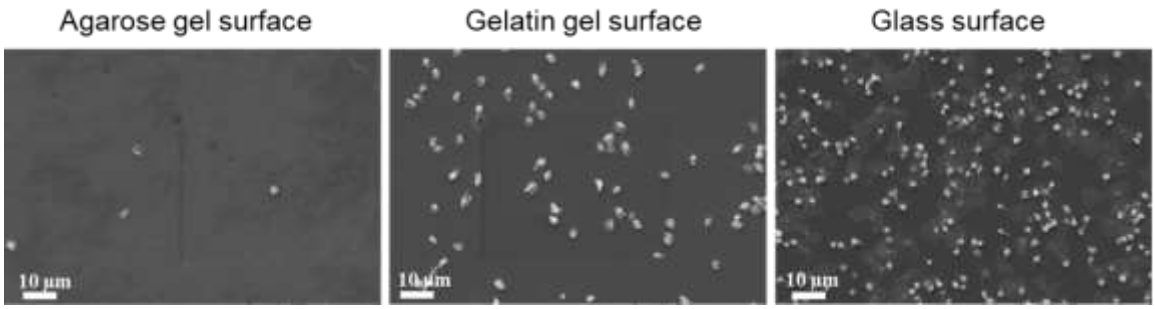

Figure 25: Platelets on agarose, gelatin, and glass surfaces displaying different degrees of platelet activation

4.2.3.1 Quantification of Adhered Platelets

Platelets were placed on the four investigated film types, and the response of the platelets on those surfaces was tracked using CLMS. The number of adhered platelets was greatest on bare glass, followed by gelatin, and finally agarose. On the glass surfaces, platelet morphology changed along with the development of filopodia and lamellipodia, whereas no significant platelet activation was observed on all other surfaces (**Figure 26**).

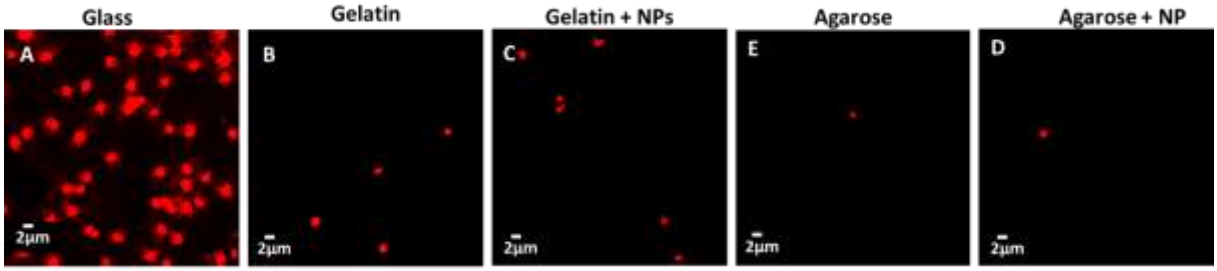

Figure 26: Confocal micrographs of platelets stained with anti-CD42a antibody dye on various surfaces after a 2-hour incubation period. (A) A higher density of platelets and a higher degree of platelet activation were observed on the glass when compared to (B) gelatin, (C) gelatin nanocomposites, (D) agarose nanocomposites, and (E) agarose.

Figure 27 displays the average spreading area of platelets on respective surfaces. The calculated platelet spreading area on bare glass (7.9±3.0 µm2) was significantly greater than on other surfaces. However, in both cases, in the absence and presence of nanoparticles, the size of platelets on gelatin (4.2±1.7 µm2) is slightly larger than that on agarose (3.4±1.6 µm2). Adding NPs had no effect on platelet spreading on gelatin (3.8±1.7 µm2) or agarose gels (3.5±1.5 µm2). According to the findings, agarose and its nanocomposite gels inhibited

The results presented in this chapter were already published in ACS Omega 2021, 6, 16, 10963–10974

platelet-surface adhesion and activation more effectively than gelatin and its nanocomposite gels.

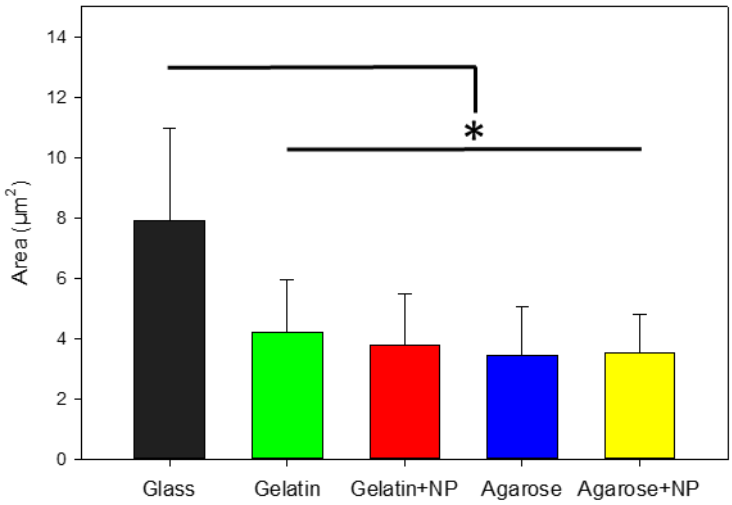

Figure 27: Average spreading area of the adhering platelets on the various substrates. *Statistically significant variation, as indicated by the one-way ANOVA test (P <0.05). Adapted from[117]

4.2.3.2 Optimization of Parameters for Single Platelet Force Spectroscopy

To obtain comparable results, the results' dependence on the chosen measurement parameters was first determined in order to find a parameter set suitable for comparative analysis. The parameters used to record the force-distance curves can have an effect on the final adhesion force values. The effect of measurement parameters such as contact time and an applied setpoint was also investigated on platelet adhesion forces, measured on glass surfaces (**Figure 28**). Higher setpoints produced stronger adhesion forces. In order to overcome electrostatic interaction between the platelet and the glass surface, a minimum setpoint of 5 nN must be used while performing the experiment. As a result, the effect of the setpoint on the adhesion force between platelets and bare glass in the range of 5 nN to 20 nN was investigated, and it was found that increasing the setpoint increased the final adhesion force. A 5 nN setpoint resulted in the lowest adhesion force. A fourfold increase in set point resulted in a nearly doubling of adhesion forces. It was assumed that a greater applied force (a higher setpoint) forced more platelets into adhesion contact with the glass surface, resulting in a greater adhesion force. At setpoints of 10 nN, the lowest variations and intermediate adhesion forces

The results presented in this chapter were already published in ACS Omega 2021, 6, 16, 10963–10974

were observed. As a result, the 10 nN setpoint was determined to be the best value for the following force spectroscopy measurements.

Longer contact times resulted in stronger adhesion forces in addition to higher set points. The contact time, which is the amount of time the platelet is in contact with the surface, was measured between 0 and 7.5 seconds. The adhesion force increased as the contact time increased. At 7.5s of contact time, the adhesion force increased to around 4 nN with a large variation, indicating a strong and complex response of platelets on the glass, as seen in the CLMS image (**Figure 26**). Because the variation in adhesion force between 2.5 s and 5 s contact time was small, indicating a stable range of measured adhesion force, 5 s of contact time was chosen for future experiments. The successful force curves obtained at 5 s of contact time yielded 91%, which is roughly equal to that obtained at 0 s contact time. Because of the strong adhesion of platelets on the glass, the yield of successful force curves was significantly reduced at too long contact times (7.5 s), as previously observed.[168] Adhesion force varies greatly due to different platelet donors and platelet heterogeneity.[193]

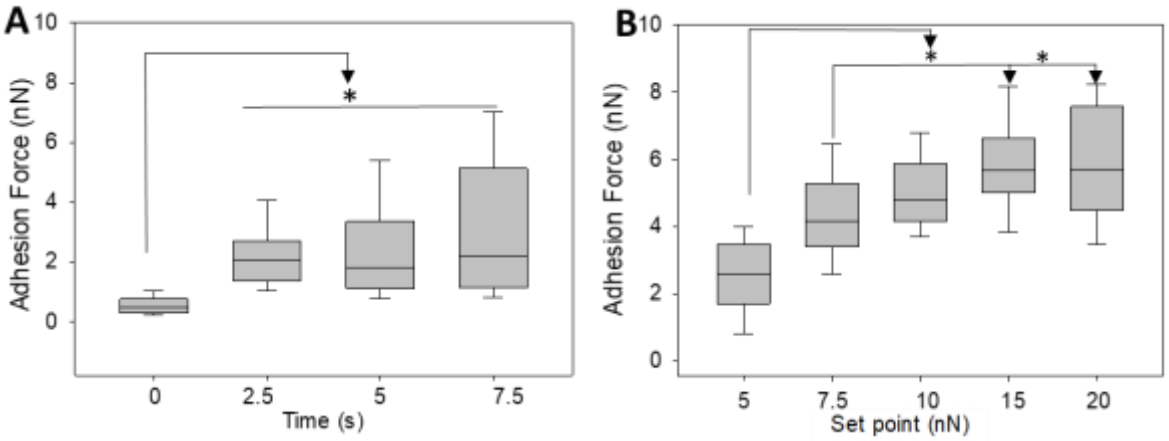

Figure 28: Impact of different AFM parameters on adhesion forces (A) A box plot comparing the variance in adhesion forces on glass surfaces for different contact times (with setpoint as 10nN). (B) A box plot comparing the variance in adhesion forces for different contact times on glass surfaces (with contact time as 0s). platelet donors for (A) and (B). Adapted from[117]

4.2.3.3 Adhesion Force between Platelets and Surfaces

The adhesion forces between platelets and gels were then measured using the above conditions (10 nN setpoint, 5 s contact time). There was a noticeable difference in adhesion forces between glass and hydrogels (**Figure 29**). The force values measured on the glass surface were up to five times higher than those measured on the gels. The adhesion forces measured on gelatin

The results presented in this chapter were already published in ACS Omega 2021, 6, 16, 10963–10974

were significantly higher than those measured on agarose, and gelatin nanocomposite demonstrated higher adhesion forces than agarose nanocomposite. However, no significant difference was observed between the nanocomposite gel and their respective native hydrogels.

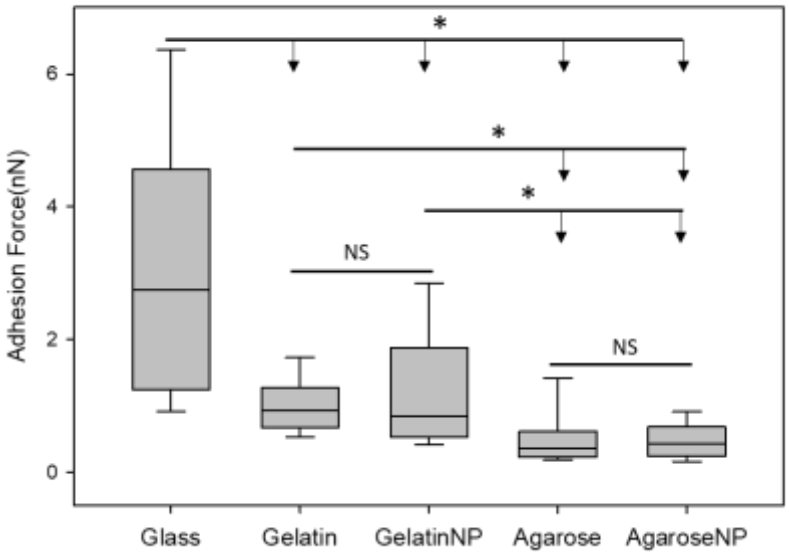

Figure 29: A typical box plot depicting adhesion forces between single platelets and various surfaces from n = 3 independent platelet donors/conditions. The one-way ANOVA test ($P < 0.05$) was used to determine the statistically significance. Adapted from[117]

4.3 Discussion

In this study, it was observed that agarose-based hydrogels and their nanocomposite counterparts are stable, inert, and can significantly reduce platelet adhesion and activation. Gelatin nanocomposites increase the gel's stiffness in comparison to the native gel, but their stability is inferior to that of agarose gel. Although gelatin film reduces platelet adhesion significantly compared to bare glass, the degree of platelet adhesion and activation is slightly greater than that of agarose film. Depending on multiple characteristics such as wettability, gel-stiffness, water retention, and chemical function, agarose and gelatin hydrogels as well as their nanocomposites have diverse impacts on platelet adhesion and activation. The most promising materials for inhibiting platelet-surface activation are agarose and its nanocomposite gels.

The wettability of biomaterials, also known as surface hydrophilicity or hydrophobicity, is crucial when the material will be in close contact with blood. The investigated agarose films here exhibit a high degree of hydrophilicity, indicating a surface with a high resistance to

The results presented in this chapter were already published in ACS Omega 2021, 6, 16, 10963–10974

unfavorable protein absorbance, which eventually results in a significant decrease in platelet adhesion. Consistently, it has been demonstrated that the level of platelet-surface activation decreases as the hydrophilicity of the surface increases[194,195], whereas a hydrophobic surface facilitates protein absorption and increases platelet-surface activation.[196] In addition, surface chemistry is known to influence surface wettability.[197] The presence of multiple hydroxyl groups in agarose molecules makes them highly hydrophilic (**Figure 20**). The degree of hydrophilicity is highest for agarose, followed by gelatin, and lowest for glass, indicating the possibility of tuning the surface property of glass or other hard metal surfaces by coating them with these polymers. The finding that agarose is more hydrophilic than gelatin is consistent with prior research.[141]

When NPs were added to gels, the wettability of agarose did not change significantly, whereas the wettability of gelatin nanocomposites declined significantly (**Figure 22**). This is due to the gelatin crosslinking with the CMD coating on the Fe_3O_4 nanoparticles. This reduces the number of free polar amino groups on the surface of the gelatin nanocomposite sample as compared to the case of native gelatin gel. In the case of agarose, the addition of -COOH groups to the existing -OH groups on NPs contributes to the gel surface becoming slightly more hydrophilic. Consistently, the contact angle on agarose decreased after the addition of NPs, whereas it increased in the case of gelatin nanocomposites. The degree of platelet adhesion and activation is most likely controlled by surface characteristics such as hydrophilicity among the investigated surfaces. The greatest contact angle (i.e., the least hydrophilicity) was observed on bare glass, followed by gelatin composites and gelatin, and finally the lowest for agarose composites and agarose. These result in the greatest density of platelet adhesion on the glass surface, followed by gelatin composite and gelatin, and the least on agarose composite and agarose. Recent studies have demonstrated that several types of nanoparticles could inhibit bacterial growth.[198–200] Current platelet storage is severely hindered by bacterial contamination; therefore, these nanocomposite gels may be a potent tool not only for stabilizing the gels but also for imparting antibacterial properties. However, this hypothesis requires additional study.

Water retention and swelling of hydrogels are critical for understanding hydrogel stability. The findings from this study showed that water molecule evaporation was minimal and unaffected by the hydrogel's chemical composition. Considering that platelet storage is also conducted at room temperature, the swelling studies for hydrogels conducted at RT are of particular importance for platelet storage.[201] In addition, it has been reported that the swelling behavior of hydrogels is also correlated with the cell adhesion properties of the hydrogels[202], and that

The results presented in this chapter were already published in ACS Omega 2021, 6, 16, 10963–10974

hydrogels with a lower swelling degree exhibit poor cell adhesion.[203] In agarose-based gels, the more controlled swelling behavior contributes to the restriction of platelet adhesion to the surface. In contrast, both gelatin composite and gelatin show a linear increase in water retention overtime that resulted in a slight increase in platelet response on these surfaces.

The stiffness of the surface is also an important mediator in controlling platelet adhesion, activation, and spreading on any surface.[114] It was found that agarose gels were stiffer than gelatin gels. Glycoproteins IIb-IIIa or IIb3 integrins are crucial adhesion receptors on the surface of platelets and are responsible for platelet aggregation.[115] It is known that a stiffer substrate induces higher resistance forces that result in stronger platelet adhesion and outside-in signaling of αIIbβ3, which in turn generates a greater actomyosin-mediated internal balancing force that causes platelets to spread more.[114] Nonetheless, both agarose and its nanocomposite gels inhibited platelet adhesion and activation significantly. A greater degree of platelet spreading on glass was observed, which is considerably more rigid (in the GPa range) than the soft hydrogels agarose (E = 181.2±158.5 kPa) and gelatin (E = 1.72±0.8 kPa). The combination of nanoparticles and agarose produced a softer film (E = 53.3±68.4 kPa). The extensive intermolecular hydrogen bonds that lead to the formation of a helix coil structure are responsible for the gelation of agarose.[133,204] It is possible that the presence of NPs during this transitional phase impeded the formation of bonds, thereby weakening the polymeric network. In the case of gelatin nanocomposites, the Youngs modulus value increased (E = 3.84±1.1 kPa) compared to gelatin alone (E = 1.72±0.8 kPa), indicating the formation of a more compact network. This is due to the electrostatic crosslinking between the amine groups of the gelatin and the carboxyl groups within the CMD molecule that is coated on the NPs. To simulate the traction forces generated by platelets on the surfaces, the applied force for indentation measurements was on the order of a few hundred piconewtons. In this study, the indentation measurements are crucial because the material's stiffness can play a decisive role in determining the outcome of cell adhesion.[104,205,206]

The confocal micrographs of the platelets on the various surfaces demonstrate once again that gel properties such as wettability and surface stiffness are critical in the development of biocompatible materials. The highly hydrophilic agarose-based surfaces significantly inhibited platelet adhesion and activation. Less hydrophilic gelatin-based surfaces followed, resulting in a weaker inhibition of platelet-surface activation. Even though the number of platelets that adhered to gelatin-based surfaces was marginally greater than that of agarose, it was significantly lower than that of the glass-control group. On gelatin-based surfaces, however,

The results presented in this chapter were already published in ACS Omega 2021, 6, 16, 10963–10974

platelet activation was observed, whereas it was completely absent on agarose surfaces. The presence of certain functional groups within the polymers, such as hydroxyl, has been previously observed to contribute to the antifouling properties of the hydrogels.[173] Platelet adhesion is the initial step that ultimately leads to platelet activation cascades and aggregation, so the micrographs demonstrate the significance of the antifouling properties of the surfaces.[207] Oss et al. consistently found that the surface exposed to air during the casting process had the lowest adhesion of platelets when compared to other casting techniques.[183] The study also indicates that agarose derived by removing the sulfate groups from agar retains the anticoagulant properties of its structurally similar heparin-like precursor.[183]

FluidFM force spectroscopy is a newly developed aspect incorporated into the conventional AFM system for assessing adhesion force between single cells and surfaces. This technique allows the capture of single cells by applying negative pressure to a hollow cantilever, thereby avoiding the immobilization of cells on a colloid probe through chemical bonds as described in traditional protocols, which might also induce platelet-surface activation.[168] There is currently no optimal protocol for measuring platelet adhesion with FluidFM. Before conducting force spectroscopy measurements between platelets and the investigated surfaces, the most significant parameters in force spectroscopy measurement, including the contact time and the setpoint, which directly affect the magnitude of the measured adhesion forces were optimized.[208] It was determined that a contact time of 5 s and a setpoint of 10 nN are optimal for measuring platelet-surface adhesion force. Other parameters such as applied pressure, z length, and z speed influence the value of the measured adhesion forces in FluidFM, as described previously.[146,208] However, for platelet adhesion measurements, these parameters were kept constant.

The results of FluidFM force spectroscopy revealed a distinct distinction between the control glass and other hydrogels or hydrogel-nanocomposite samples. Single platelet interactions with fabricated gels are up to five times weaker than those between single platelets and bare glass. Gelatin gel and its nanocomposite produced a greater adhesion force than agarose. These findings are consistent with CLMS images in which only the gelatin nanocomposite gel displayed a small amount of platelet activation, whereas the other gels did not. Thus, it is evident that there is a strong correlation between the degree of platelet-surface activation and the adhesion forces between platelets and surfaces. It is demonstrated that several hydrogels, each with their own set of properties such as wettability, stiffness, and water content, can significantly inhibit platelet activation. The agarose hydrogels were able to significantly inhibit

The results presented in this chapter were already published in ACS Omega 2021, 6, 16, 10963–10974

platelet adhesion. Platelet-surface activation was controlled by the adhesion forces between platelets and surfaces.

The fact that the addition of nanoparticles had no negative effect on platelet activation indicates that these nanocomposites are safe for platelet applications. Nanocomposites can be promising antibacterial application materials. Numerous attempts have been made to identify a material capable of inhibiting platelet-surface activation for both basic research and medical applications. However, a reliable, stable, and robust material remains to be discovered. With agarose, a very low density of adhered platelets was observed, and the surface morphology of platelets did not change after two hours of surface contact. Thus, this work clearly demonstrates a potential application of the potent agarose gel for inhibition of platelet-surface activation, as the agarose gel is simple to produce without the need for additional materials, extremely stable, and inert. Agarose could serve as a potential candidate for the enhancement of platelet storage bags and vascular implants. However, additional research is necessary to determine the stability of the gels in the presence of platelet concentrates and the storage buffer or condition over extended periods of time.

4.4 Limitations

The hydrogels and nanocomposites formed with gelatin had problems concerning the stability issue when conducting AFM-based indentation or imaging methods for longer durations. The temperature in the closed cabinet of an AFM can go beyond room temperature because of the heat generated by the AFM head and the overhead camera. Since the melting temperature of gelatin gels can vary from 25 to 40 °C, it was seen that the gelatin gel transformed into a semi-molten stage, which resulted in high adhesion of the cantilever to the surface, with occasions where the cantilever failed to come back and complete the retract phase, thereby interfering with and disrupting the measurements.

The results from the CLSM images were quantified to analyze the spreading of the platelets. However, it was also clear that there appeared to be a reduction in the quantity of platelets adhering to agarose and its nanocomposites. The number of platelets on gelatin surfaces was 2.9 times greater than on agarose surfaces, and the number of platelets on gelatin + NP surfaces was 1.38 times greater than on agarose + NP surfaces. However, this data is not included in the result section because this is only a rough quantification, as the number of platelets on surfaces was extremely low and therefore required locating the platelets first, followed by taking

The results presented in this chapter were already published in ACS Omega 2021, 6, 16, 10963–10974

micrographs at specific areas of interest on the films. Thus, in this case, counting the number of platelets in selected areas does not represent the overall adhesion of platelets on the films.

Although FluidFM can easily be used to determine the strength of interaction between a variety of cells and surfaces,[147] extending it to platelet measurements requires a lot more effort. Single platelet force spectroscopy (SPFS) using FluidFM to directly obtain the adhesion force between single platelets and surfaces remains difficult because the high negative pressure used to pick platelets can cause damage to the platelet membrane and even aspiration of platelets, thereby blocking the internal microchannel. Furthermore, platelet adhesion to the micro-channeled cantilever occasionally results in cantilever aperture blocking. Thus, future refinement of SPFS using FluidFM is required, particularly in cantilever functionalization to minimize platelet adhesion, spreading, and activation, as well as identification of the minimum applied pressure to platelets to reduce platelet damage.

4.5 Conclusion and Outlook

It was investigated how hydrogel nanocomposite films and hydrogel-fabricated hydrogels affected the suppression of platelet-surface activation. Agarose and agarose nanocomposite materials showed promising results for human blood platelet applications. The agarose hydrogel and its nanocomposites had higher surface wettability, better controlled-swelling capabilities, and higher stiffness than gelatin, resulting in a stronger inhibition of platelet adherence and spread. The way platelets behave on the fabricated gels demonstrates how biomimetic surfaces with antifouling properties regulate cellular responses. Agarose nanocomposite has a significant application in the fabrication of anti-bacterial platelet storage bags since a variety of NP types have anti-bacterial qualities.

The ultimate goal would be to include such antithrombotic surfaces in blood-contacting medical devices and procedures. These preliminary findings pave the way for the creation of anti-thrombosis materials based on agarose hydrogels, which could be used in implantations, platelet/blood storage bags, and in biotechnological and pharmacological trials. The promising effects of agarose can be enhanced by introducing a topological factor to increase the impact on platelet adhesion inhibition.

4.6 Experimental section

4.6.1 Fabrication of Hydrogel and Nanocomposite

The molds for fabricating the hydrogel and nanocomposite films were made by mixing equal amounts of silicone rubber compound and silicone duplicating compound for 3 minutes with a

The results presented in this chapter were already published in ACS Omega 2021, 6, 16, 10963–10974

wooden spatula, followed by tapping to get rid of any bubbles. Titanium stubs of diameter 14 mm and height 2 mm were then stuck on the bottom of a 3-compartment petri dish. The mixture was then poured into each compartment of the petri dish, followed by tapping. The petri dish was then placed in an oven at 60 °C for 1 hour. Post-solidifying the molds, they were then removed and cleaned with distilled water and subsequently with 70% ethano (**Figure 30A**).

At 95 °C and 60 °C, respectively, agarose 1% (Lonza, Cologne, Germany) and gelatin 10% (Sigma-Aldrich, Germany) were added to PBS solution (Thermofisher, Bremen, Germany) with magnetic stirring. Before nanocomposites could form stable gels, particles were added to the respective solutions. The hydrogel or nanocomposite samples were made by pouring the above solution into custom-made silicone molds. Gels with a height less than 2 mm were found to reduce the stability of films while extracting them from silicone molds. Samples with a diameter of 14 mm and a height of 2 mm were created (**Figure 30B and C**). All experiments were carried out on the surfaces exposed to air during casting. Within an hour of being made, the gels were put to use. Fe_3O_4 nanoparticles were obtained from BPT-IBA, the particles were synthesized under a microfluidic condition with continuous flow mode.

The results presented in this chapter were already published in ACS Omega 2021, 6, 16, 10963–10974

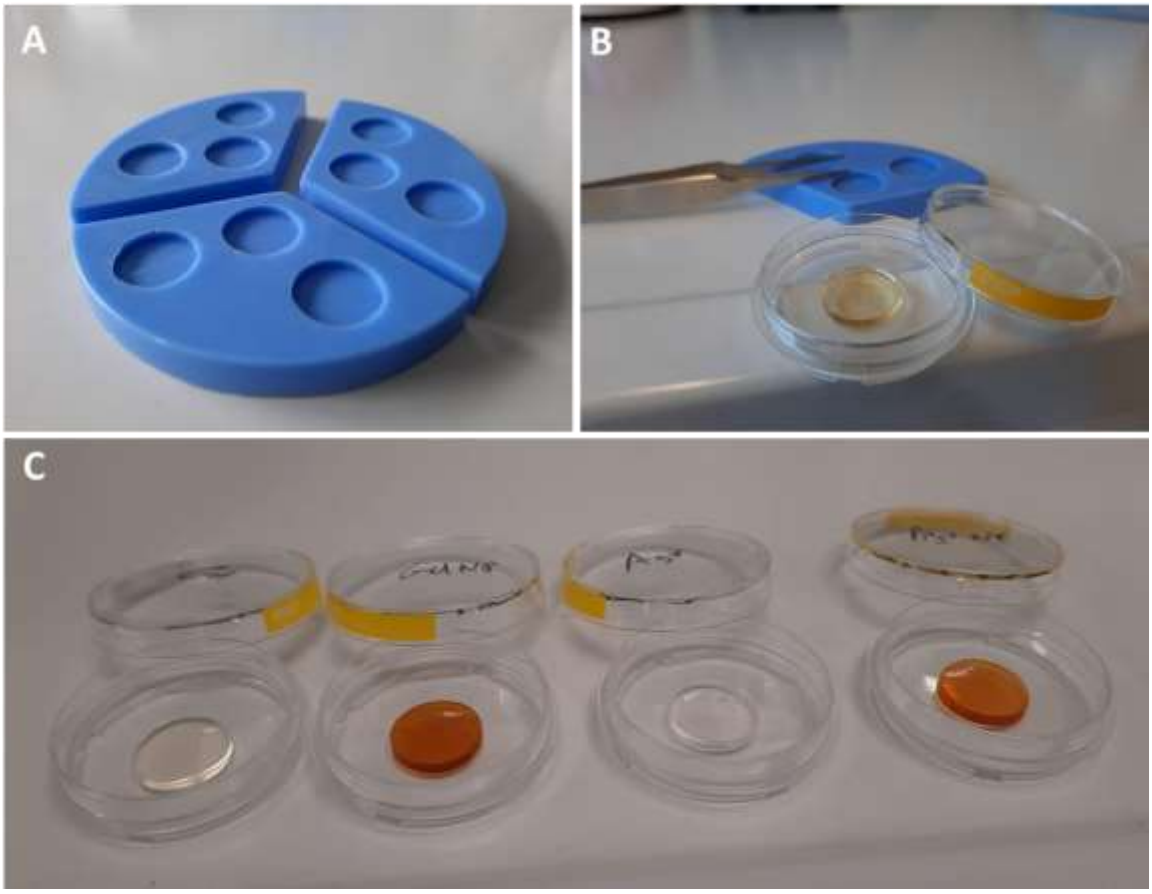

Figure 30: Fabrication of hydrogel and hydrogel nanocomposite films (A) The in-house produced silicone molds used in fabricating the gel films (B) A gelatin nanocomposite film taken out of the mold. (C) the four samples of hydrogel and nanocomposite films from gelatin and agarose, respectively (from left to right).

4.6.2 Characterization of Nanoparticles

The Zetasizer was used to determine the size and surface zeta potential of the synthesized NPs (Zetasizer Nano ZS, Malvern Instruments Ltd, Worcestershire, UK). The size of particles in water was determined using dynamic light scattering (DLS) within 30 minutes at 25°C using disposal cuvettes (Sigma-Aldrich, St. Louis, USA). The average hydrodynamic sizes measured and their standard deviation values were examined. Particles were diluted in water (pH 6.3, conductivity 0.25 mS/cm) to a concentration of 2 mM and measured in a folded capillary zeta cell at 25 °C with 10 repetitions, as previously described.[209] The particles have a zeta potential of -56 mV and a size of 255 nm (**Figure 31**). The concentration of 2 mM was chosen as the final concentration for nanocomposites. SigmaPlot was used to analyze the data (version 14.0).

The results presented in this chapter were already published in ACS Omega 2021, 6, 16, 10963–10974

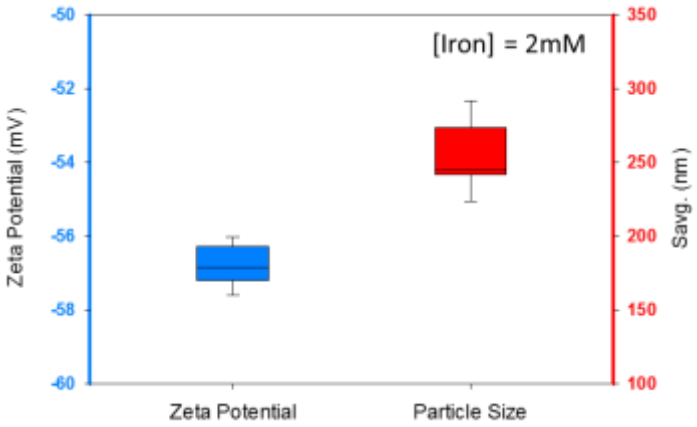

Figure 31: Characteristics of synthesized NPs. At 2 mM concentration, the zeta potential (blue) and average size of nanoparticles (red) were measured using dynamic light scattering. Adapted from[117]

4.6.3 Water Contact Angle

The water contact angle of the coatings was measured using the captive bubble method on the OCA 15+ system (DataPhysics Instruments GmbH, Filderstadt, Germany). This method is particularly useful when dealing with surfaces with high surface free energy and to avoid drying of hydrogels during measurement.bubble of air is injected beneath the sample, which is facing downward. The dosing volume was set to 3 µl, the dosing rate to 1 µl/s, and the contact angle was calculated using the ellipse fitting method. The drop phase was air, and the ambient phase was milliQ water (0.055 S/cm). Five air bubbles were placed at different locations on the coated surfaces to probe all of them. OCA 15+ software was used to calculate contact angles.

4.6.4 Swelling and Degradation Characterization

All gels were formed using the aforementioned molds, transferred to pre-weighed Petri dishes, and weighed (W_X) on a weighing scale (Sartorius, Germany). The gels were immersed in 2 ml PBS buffer to determine the wet weight (W_{PBS}), and measurements were taken every hour. Extra PBS was removed before weighing. To determine the weight in a dry environment (W_{AIR}), the fabricated gels were dried at room temperature (RT) with a relative humidity of 15-20%, and their weights were measured every hour. As previously described, swelling was calculated as W_{PBS}/W_X and degradation as W_{AIR}/W_X at each time point.[210,211]

The results presented in this chapter were already published in ACS Omega 2021, 6, 16, 10963–10974

4.6.5 Nanoindentation

The mechanical properties of the fabricated hydrogels and nanocomposites were measured using the AFM nanoindentation technique. A gold bead (CP-CONT-AU-A, Nanoandmore GmbH, Germany) attached to the end of a cantilever with a nominal bead diameter of 1.5-3 μm and a nominal spring constant of 0.02-0.77 N/m. This bead was used to generate force vs displacement (F-D) curves by contacting it with the gels. The F-D curves were obtained over the surface of a 10 × 10 μm^2 area by subdividing the area into equal-sized 8 x 8 pixels and acquiring 64 F-D curves at 3 μm/s tip velocity. After converting the force curve to the force-indentation curve, the elastic modulus of each sample was calculated by fitting the corresponding approach curve to the Hertz model,[212]

$$F = \frac{4E\sqrt{R}\delta^{\frac{3}{2}}}{3(1-v^2)}$$

After converting the force curve to the force-indentation curve, the elastic modulus of each sample was calculated by fitting the corresponding approach curve to the Hertz model,[212]

In this study, only one probe was used for nanoindentation experiments, and the bead diameter of 3 μm was precisely determined using SEM imaging. The force curves recorded from different locations on the hydrogels/nanocomposite surfaces were fitted to the Hertz model using a spherical tip shape model to obtain Young's modulus values. The total number of complete analyzable curves for gelatin was 449, for gelatin nanocomposite 239, for agarose 365, and for agarose nanocomposite 335. All calculated Young's modulus values from three repetitions for each gel were collected and analyzed using SigmaPlot (version 14.0).

4.6.6 Isolation of Platelets

Human blood was collected from healthy donors who had not used drugs in the previous 10 days and placed in an Anticoagulant Citrate Dextrose(ACD-A) 1.5 mL BD-Vacutainer tube (Heidelberg, Germany). The blood tube was covered in parafilm and allowed to rest at room temperature for 15 minutes. Platelet-rich plasma (PRP) was extracted from blood first by centrifugation at 120 g for 20 minutes at room temperature. Platelets were then isolated from PRP by centrifuging at 650 g for 7 minutes in the presence of 15% ACD-A, and 2.5 U/ml Apyrase (grade IV SIGMA, Munich, Germany). The platelet pellet was resuspended in 5 ml of pH 6.3 suspension buffer (137 mM NaCl, 2.7 mM KCl, 11.9 mM $NaHCO_3$, 0.4 mM Na_2HPO_4, 2.5 U/ml Hirudin) and incubated at 37° C for 15 minutes before again centrifuging at 650 g for 7 minutes. Platelet pellets were carefully resuspended in 2 ml of suspension buffer and counted

The results presented in this chapter were already published in ACS Omega 2021, 6, 16, 10963–10974

using a blood counter (pocH-100i, SYMEX, Germany). Following that, the platelets were incubated for 45 minutes at 37°C before being used.

4.6.7 Imaging of Platelets and Quantification

Platelets were stained for 30 minutes at room temperature in the dark with anti-CD42a FITC antibody dye (Dianova GmbH, Hamburg, Germany) at a final concentration of 0.1 g/ml. Platelets were then seeded on the gels at a concentration of $3x10^5$ cells/l and stored at room temperature for 2 hours. Rinsing with PBS removes unbound platelets. Following that, platelets were fixed in 4% paraformaldehyde for 30 minutes at room temperature. At RT in the dark, samples were examined using a confocal laser scanning microscope, the Zeiss LSM710 (Carl Zeiss, Gottingen, Germany). The red fluorescent signal was obtained by excitation at 488 nm (15 mW argon laser) with a 63x objective and detection in the 500–550 nm range. ImageJ software was used to further process the images and quantify the platelet spreading area.

4.6.8 Single Platelet Force Spectroscopy

Fluid force microscopy measurements were taken with a JPK Nanowizard 4 (Berlin, Germany) equipped with a FluidFM add-on (Cytosurge, Switzerland), placed under an acoustic hood, and mounted on an active vibration isolation system (Micro 40, Halcyconics, Germany) to reduce the effects of surrounding vibrations. To observe the platelets and approach the cantilever to the desired location, an inverted microscope (Axio Observer, Zeiss, Germany) was used from beneath. A FluidFM nanopipette (Cytosurge, Switzerland) with an aperture of 300 nm and a nominal spring constant of 2.09±0.15 N/m N/m was used for force spectroscopy. The reservoir was filled with suspension buffer before being calibrated using the contact-free thermal noise method. Before picking the platelet in the liquid environment, the calibrated spring constant of the nanopipette was 0.42±0.01 N/m. A single platelet was drawn to the aperture of the cantilever by applying a pressure of -800 mbar to it for 4-8 minutes. The pressure was reduced to -500 mbar for subsequent force measurements (**Figure 32**)

The results presented in this chapter were already published in ACS Omega 2021, 6, 16, 10963–10974

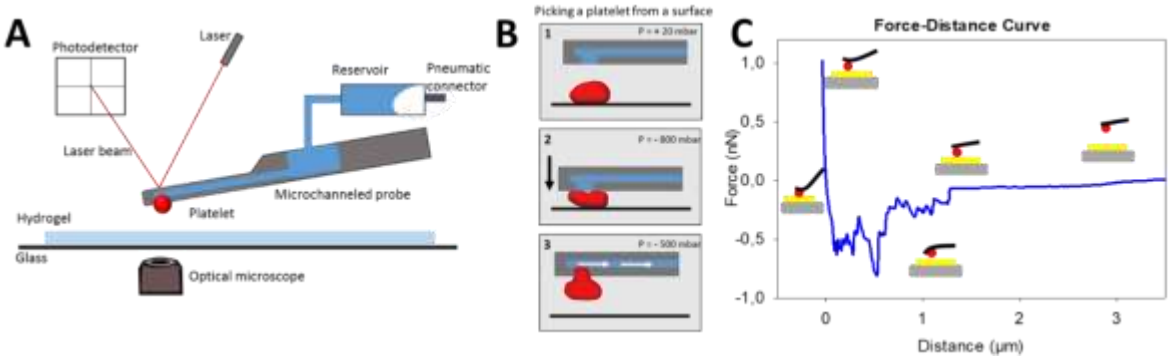

Figure 32: The basic principle of single platelet force spectroscopy (A) FluidFM's schematic representation for measuring platelet-gel adhesion forces (B) A simplified diagram of picking platelets from a surface (C) On the glass surface, a typical retraction curve was recorded, revealing rupture events that occurred while the adherent platelet was disrupted from the surface. Adapted from[117]

The cantilever with platelet was immersed in PBS liquid and a setpoint of 10 nN, a z-length of 3-5 µm, and a z-speed of 2.5 m/s were used to measure the force-distance curves. A platelet was chosen, and force map measurements were performed on each sample at three different locations, yielding 64 force-distance curves (10 × 10 μm^2). Three repetitions were performed for each gel type. The force maps obtained were then processed using the JPK data processing software (version 6.1.120).

The results presented in this chapter were already published in ACS Omega 2021, 6, 16, 10963–10974

Chapter 5: Customization of Biophysical Cues using FluidFM assisted Nanoprinting to restrict Platelet Spreading

5.1 Chapter Overview

Platelets are extremely sensitive and are quickly activated by non-physiological surfaces. The intrinsic mechanism of activated platelets allows them to release different proteins that take part in numerous pathways that initiate the platelet activation cascade. When activated by an external mechanical or chemical stimulus, platelets have an innate mechanism to produce a variety of chemokines and cytokines.[213] Surface-induced platelet activation is a problem faced during platelet storage, which eventually leads to platelet aggregation and, as a result, the deterioration of platelet concentrates.

Despite significant research being conducted to reduce current limitations, surface-induced platelet activation remains a relatively unaddressed issue. Surface-induced platelet activation can be reduced primarily through the use of two strategies: chemical and topographical modifications.[80] Agarose films presented in the last chapter belongs to the category of chemical modification group. In this chapter, I investigated topographical modifications. Implementing chemical modifications, particularly their transfer into a marketable product, is a time-consuming process fraught with regulatory pitfalls.[214] Topographical changes, on the other hand, can be relatively quick to translate into the market because they do not involve the regulatory hassle of introducing new materials.[215] Recent studies using topographical modifications for platelet research by various groups have revealed that topography influences platelet adhesion and activation trends.[81,110,216] Platelets are much smaller (only 1.5 to 3.5 μm^2) than most mammalian cells (with a size of several tens of micrometers) and thus only respond to nanostructured surfaces.

In the case of platelets, where the majority of the research has been done at the microscale,[107,108,217,218] several nanostructured surfaces,[219] including nanoparticles[111] and groove structures,[81] have also been studied. While substantial research has been conducted to establish the theory of how substrate stiffness governs platelet adhesion, activation, and spreading,[114,116,117] the concept of tuning substrate stiffness to in turn mediate these platelet processes has not yet been explored. In general, metals were used to build the discussed nanostructures, which were then coated with polymers or proteins to adjust their surface properties. These materials have low biocompatibility because metal can directly affect platelets and coating molecules can be released, altering the platelet storage buffer. As a result,

The results presented in this chapter were already published in ACS Appl. Mater. Interfaces 2022, 14, 21, 24133–24143

a reliable method based on stable nanostructures on such materials with high platelet compatibility is highly desirable.

The fluidic force microscope (FluidFM)[154], which is based on atomic force microscopy (AFM), was used to create hemispherical grid patterns and hexagonal tile nanostructures. Following which, the response of platelets on the fabricated structures was investigated. FluidFM has demonstrated versatility in the generation of functional and topographical features from synthetic[150,157] and biological materials.[156] The force mapping mode was used to print a hemispherical grid pattern, and the manipulation mode was used to print hexagonal tiles (honeycomb) using a commercial hybrid acrylate-based UV curable Loctite AA3491 (Henkel, Düsseldorf, Germany). The FluidFM parameters were optimized to dispense the appropriate amount of ink to print the structures on the glass in a reproducible manner. AFM and scanning electron microscopy (SEM) imaging were used to confirm the topography of structures. The effect of topography was then evaluated by measuring the adhesion and spread of human platelets on the fabricated surfaces. To determine the stiffness of the printed structures, nanoindentation measurements were performed.

5.2 Results

5.2.1 Optimization of FluidFM and Printing of Nanopatterns

5.2.1.1 Ink Selection and Optimization of Printing Parameters

Several inks were tested, including commercial UV-curable acrylate-based Loctite inks AA3494 and AA3491 and non-commercial in-house hydrogel inks obtained from BW-IBA like poly(2-ethyl-2-oxazoline) and lactide-ε-caprolactone methacrylate. However, after preliminary trials of reproducibility, feature stability, and ease of printing, the commercial Loctite AA3491 was selected for further use to prove as principle the role of nanostructures in inhibiting platelet-surface activation.

In FluidFM, the quality (desired characteristics and properties of the printed nanostructures) of the printed nanostructures is determined by parameters like setpoint, pressure, and contact time. To study the influence of these parameters on the printing process and determine the protocol that allows reproducible fabrication of the desired structures, The fabrication of the structures over a wide range of setpoint, pressure, and contact time, i.e., up to 22 nN, 800 mbar, and 20 s)

The results presented in this chapter were already published in ACS Appl. Mater. Interfaces 2022, 14, 21, 24133–24143

was realized. Parameters such as z-length and extended velocity were maintained at 5 µm and 2.5 m/s, respectively, throughout.

By comparing the change in the size of printed features, the effect of printing settings was determined. In the instance of force mapping mode, 10 hemispherical dots were printed for each measurement condition before being cured and gold-sputtered, followed by SEM imaging of the sample. ImageJ was used to transform the SEM pictures to a binary image for better display, after which the diameter of the dots was determined (**Figure 33**). In a similar fashion, for manipulation mode, a 30 µm line was printed, and then the width was averaged at five distinct positions to determine the mean width.

In the case of evaluating the effect of contact time (**Figure 33A**), the growth in hemisphere diameter with increasing time was apparent, with the hemisphere diameter nearly doubling from 1s to 20s. In the case of writing velocity, it was found that the line width declined after 1.0 m/s (**Figure 33B**). Intriguingly, the time the nanopipette is in contact with the surface appears to have the most effect on the printing process in both printing methods. To sum up, thicker features were produced via slower writing speed or longer contact time.

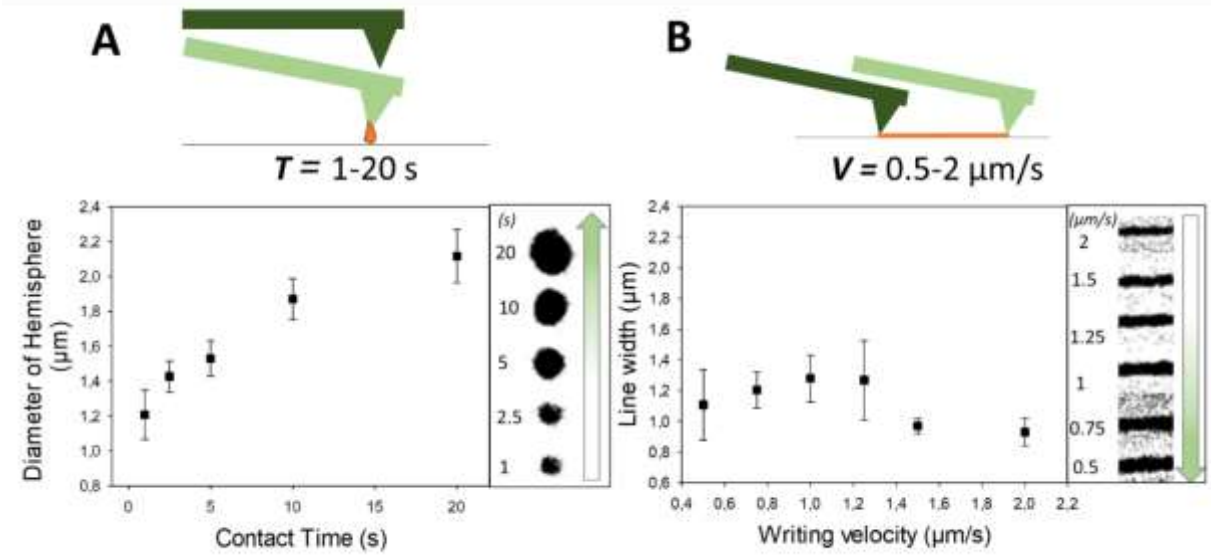

Figure 33: The optimization of printing parameters. The effect of contact time and writing speed as printing parameters on the extruded volume of ink and size of the printed structure in (A) force mapping mode to print dots and (B) manipulation mode to print lines. The SEM images of the corresponding dots and lines on the x-axis are displayed (on the right of each graph).

In the case of variation of other parameters in force mapping mode, it was observed that the setpoint (**Figure 34A**) has a small effect across a wide range, since no apparent trend was

The results presented in this chapter were already published in ACS Appl. Mater. Interfaces 2022, 14, 21, 24133–24143

observed between 2 and 20 nN. In the case of pressure (**Figure 34B**), the diameter of the features did not change until a pressure of >400 mbar was achieved, at which point the diameter increased.

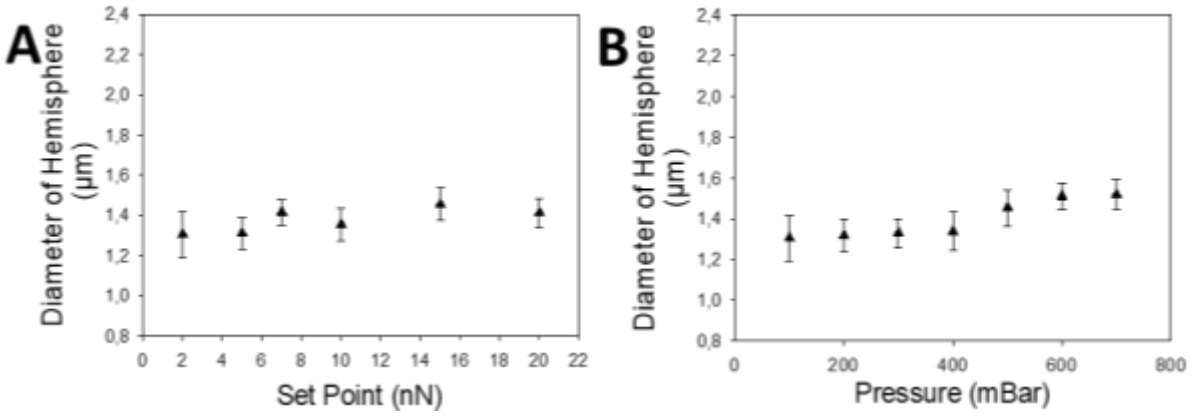

Figure 34: Optimization of (A)setpoint and (B)pressure as a printing parameters while using FluidFM in force mapping mode. Adapted from[126]

Concerning the parameters in manipulation mode, setpoint (**Figure 35A**) and pressure (**Figure 35B**) revealed no visible patterns, as seen by the overlapping of the high deviation bars. The most optimal settings for printing nanostructures are a setpoint of 10 nN and pressures in the range of 50-150 mbar.

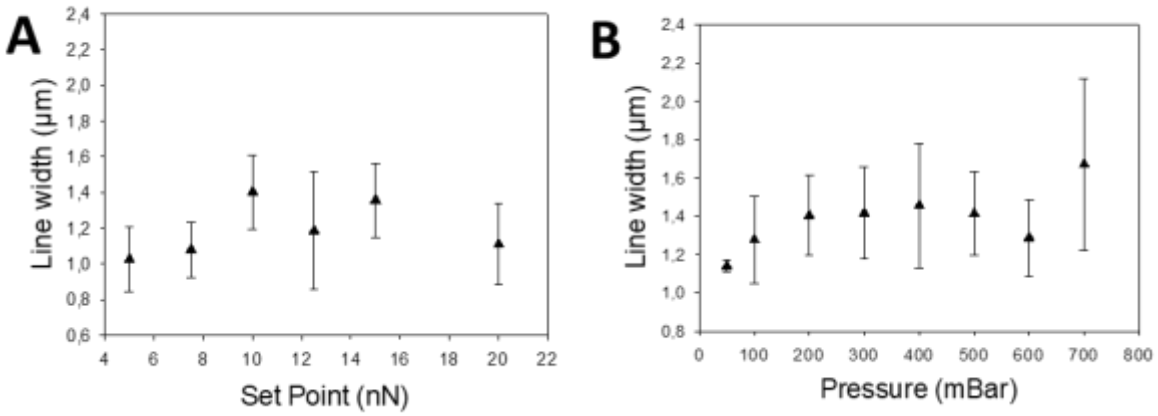

Figure 35: Optimization of (A) setpoint and (B) pressure as a printing parameters while using FluidFM in manipulation mode. Adapted from[126]

5.2.2 Characterization of Patterns

5.2.2.1 Topographical Characterization of Patterns

The FluidFM-based printing procedure is depicted schematically in **Figure 19**, which is followed by a UV exposure phase to stabilize the constructed structures. The hexagonal hive pattern and the hemispherical grid depicted in the cartoons were created using different printing techniques with the assistance of different AFM modes (**Figure 36A,C** (left)). Samples were scanned using AFM in force modulation mode, and the diameters and heights of the structured surfaces were measured in order to observe the fabricated patterns. **Figure 36A,C** (right) depict 3D topographies of grids and hives, with a red dashed line indicating the location from which the line profiles in **Figure 36B,D** were extracted.

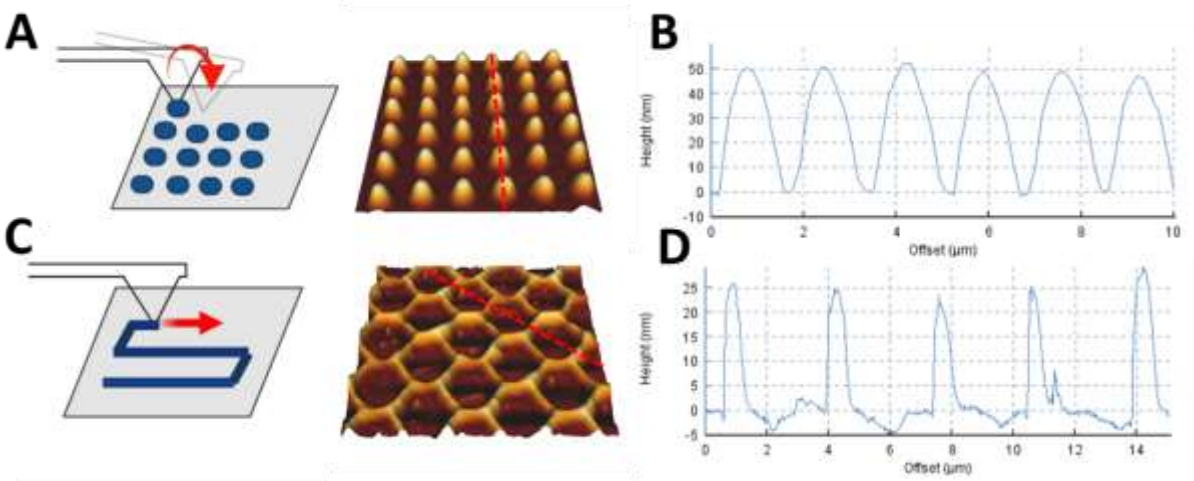

Figure 36: Diagrammatic representation of two AFM modes used for the process of printing: (A) force mapping mode to fabricate hemispherical grid structures and (C) manipulation mode to print the hive pattern enabled by free movement along the x- and y-axis; allowing fabrication of (right) the respective three-dimensional (3D) topographies of the printed structures with red-dashed lines showing (B, D) line profiles of the printed features. Adapted from[126]

In contrast to the nanopatterns, line profiles of glass and spin-coated polymer surfaces reveal that they are macroscopically smooth surfaces (**Figure 37**). The average diameter of the hemispheres in the grids created is 1000±80 nm, the average height is 48.0±1.4 nm, and the average distance between two features is 680±54 nm. In the case of hive patterns, the internal diagonal distance of the hexagons is on average 3.1±0.1 µm, whereas the height of the features is 26.4±3.3 nm.

The results presented in this chapter were already published in ACS Appl. Mater. Interfaces 2022, 14, 21, 24133–24143

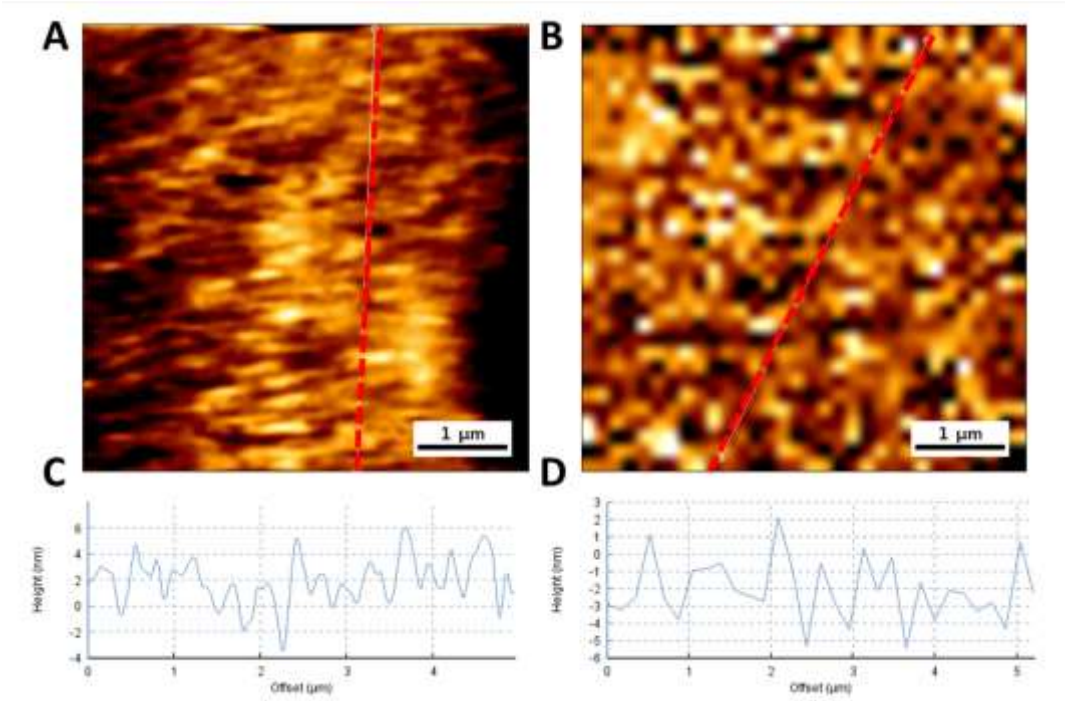

Figure 37: Surface topographs of non patterned surfaces. AFM image of (A) polymer-coated surface and (B) glass along with red dashed line showing their respective (C-D) line profiles. Adapted from[126]

5.2.2.2 Roughness

The roughness parameters on both the fabricated structures (grid and hive), glass, and spin-coated polymer were measured. The roughness specifications Ra and Rq indicate that nanopatterned surfaces have greater overall roughness than unpatterned controls (**Table 2**).

Table 2 Roughness parameters Ra and Rq were computed for all the surfaces

Roughness (nm)	**Glass**	**Grid**	**Hive**	**Polymer**
Average Roughness (Ra)	3.62	11.52	6.25	2.73
RMS Roughness (Rq)	4.62	13.93	7.62	3.39

5.2.2.3 Wetting

The contact angles of the uncoated glass surface and the spin coated polymer surface were measured using the sessile drop method. The spin coated polymeric surface was found to be less hydrophilic with contact angle of 77.9±5.0° as compared to the uncoated glass which was 43.0±1.9°.

The results presented in this chapter were already published in ACS Appl. Mater. Interfaces 2022, 14, 21, 24133–24143

5.2.2.4 Stiffness

Surface properties play an important role in controlling platelet-surface activation, and hence the stiffness of the structured samples was characterized. A colloidal probe with a 3 m diameter was used for the nanoindentation studies. A force-distance (F-D) curve is recorded after the probe makes an indentation on the structured surfaces, and this curve can be used to determine the stiffness of the surface. **Figure 38B** displays the map of Young's modulus values obtained by fitting the F-D curves using the Hertz model, whereas **Figure 38A** displays the topographic height map of the surfaces.

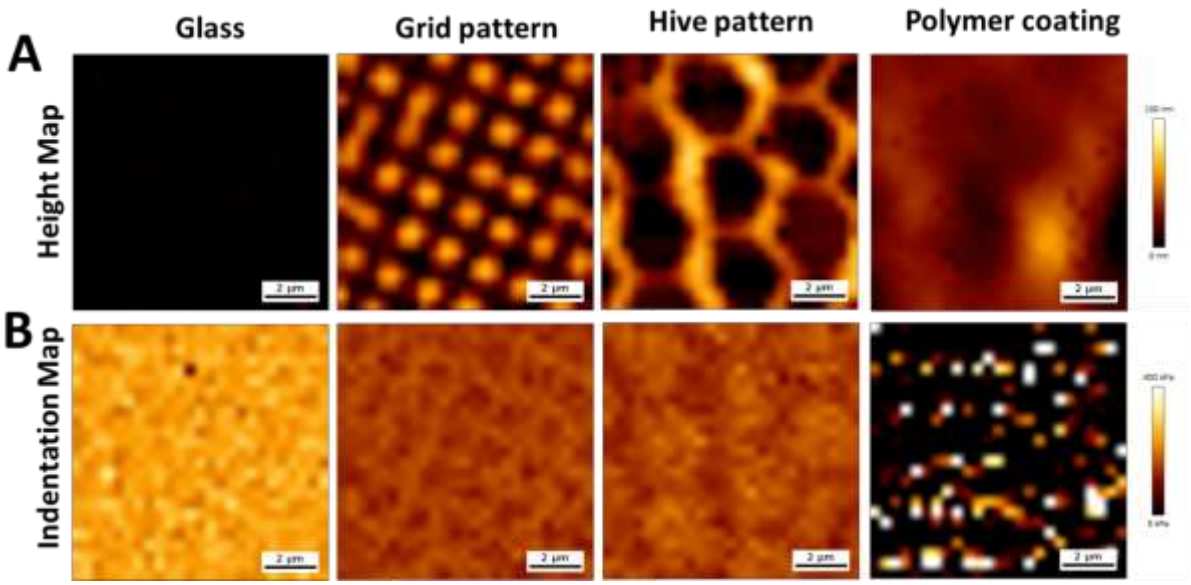

Figure 38: Determination of the stiffness of the patterns. (A) Height maps of bare glass, grid and hive patterns along with their respective (B)indentation maps. Adapted from[126]

To comprehend the stiffness felt by an object of a same size, it was decided to use a colloidal probe similar to platelet diameter (**Figure 39**).The distribution of the stiffness detected by the probe is shown by the histograms presented in **Figure 39B**. The median for the hive pattern is 253.3±18.9 kPa, whereas for the grid pattern is 244.9±14.98 kPa. Both printed structures overall appear to be softer on the probed length scale when compared to the glass with a median value of 338.5±21.9 kPa.

The results presented in this chapter were already published in ACS Appl. Mater. Interfaces 2022, 14, 21, 24133–24143

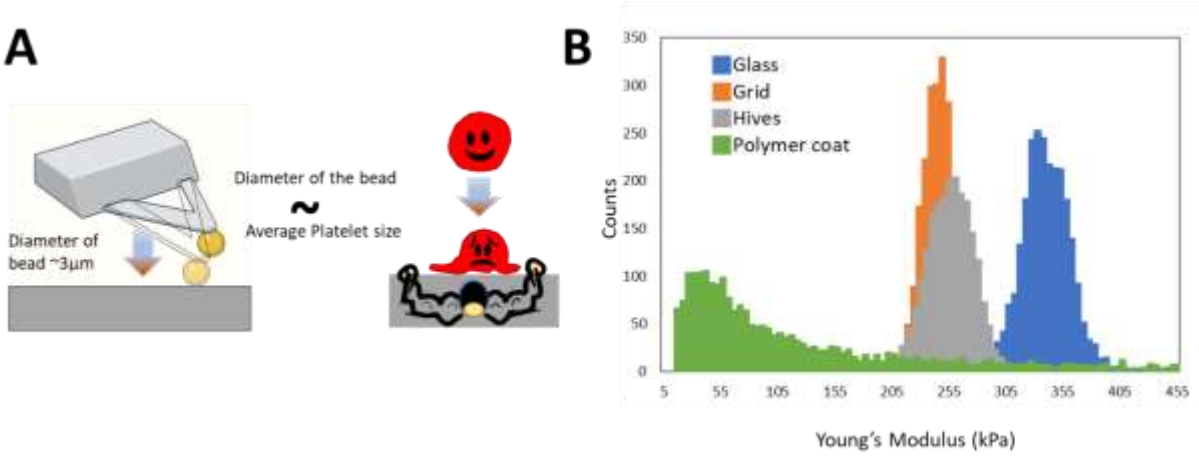

Figure 39: Schematic representation of (A) nanoindentation carried out using a cantilever with a bead to comprehend the stiffness experienced by a platelet on different surfaces and (B) distribution of E-modulus values on the different surfaces. Adapted from[126]

5.2.3 Behaviour of Platelets

5.2.3.1 Adhesion of Platelets

To determine how the platelets respond to the fabricated nanostructures, platelets were seeded on the samples for one hour, and the number of platelets adhering to the structured and non-structured regions of the same size was determined. The maximum number of platelets adhered to the spin-coated polymer, followed by bare glass, whereas the number of platelets adhered to the structured surfaces with grid and hive patterns was lower (**Figure 40**). In adhesion trials, the trend indicated greater platelet attachment on glass and polymer-coated surfaces, but the number of platelets on grid and hive patterned surfaces was substantially smaller, showing that the structured surfaces inhibited platelet adhesion.

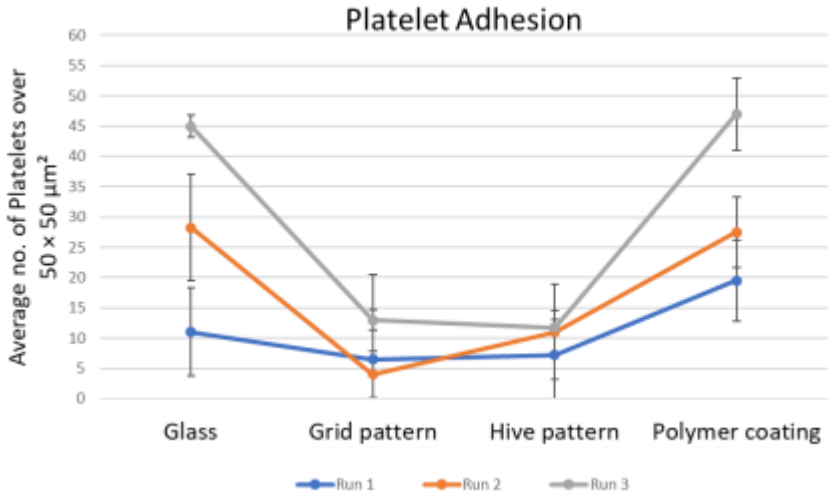

Figure 40: Graph representing the number of adhered platelets obtained from three independent experiments with platelets from three independent donors. Adapted from[126]

6.2.3.2 Spreading of Platelets

To gain a deeper understanding of platelet adherence on the patterns, the cellular adhesion and spreading capabilities were assessed using several platelet staining substances. Phalloidin, the first dye, labeled the actin filaments in the activated platelets, providing specific information about the filopodial and lamellipodial outgrowths (**Figure 41A-D**). The second dye is an anti-CD42a antibody coupled with FITC that serves as an identification for platelets, thereby confirming their presence (**Figure 41E-H**). The micrographs (**Figure 41I-L**) display confocal reflection microscopy pictures combined with fluorescence images of the phalloidin and FITC signals. In this mode, the structures beneath the platelets that are not visible in fluorescence can be distinguished. **Figure 42A** depicts the average platelet area in the two stainings, the difference between which can be interpreted as the spreading of activated platelets. On the spin-coated polymer, there was no noticeable spreading (the actin stain signal was equivalent to the CD42 signal), whereas the patterned samples had relatively higher spreading, However, it was highest on glass. The comparison of the total surface area covered by platelets (**Figure 42B**) suggests that there is a considerable difference between glass and other samples, but no significant difference was seen between the spin-coated polymer, grid, and hive patterned samples. When the strength of the signal from both dyes was compared, it was discovered that grid patterns were more effective at limiting platelet spreading as compared to the other geometry.

The results presented in this chapter were already published in ACS Appl. Mater. Interfaces 2022, 14, 21, 24133–24143

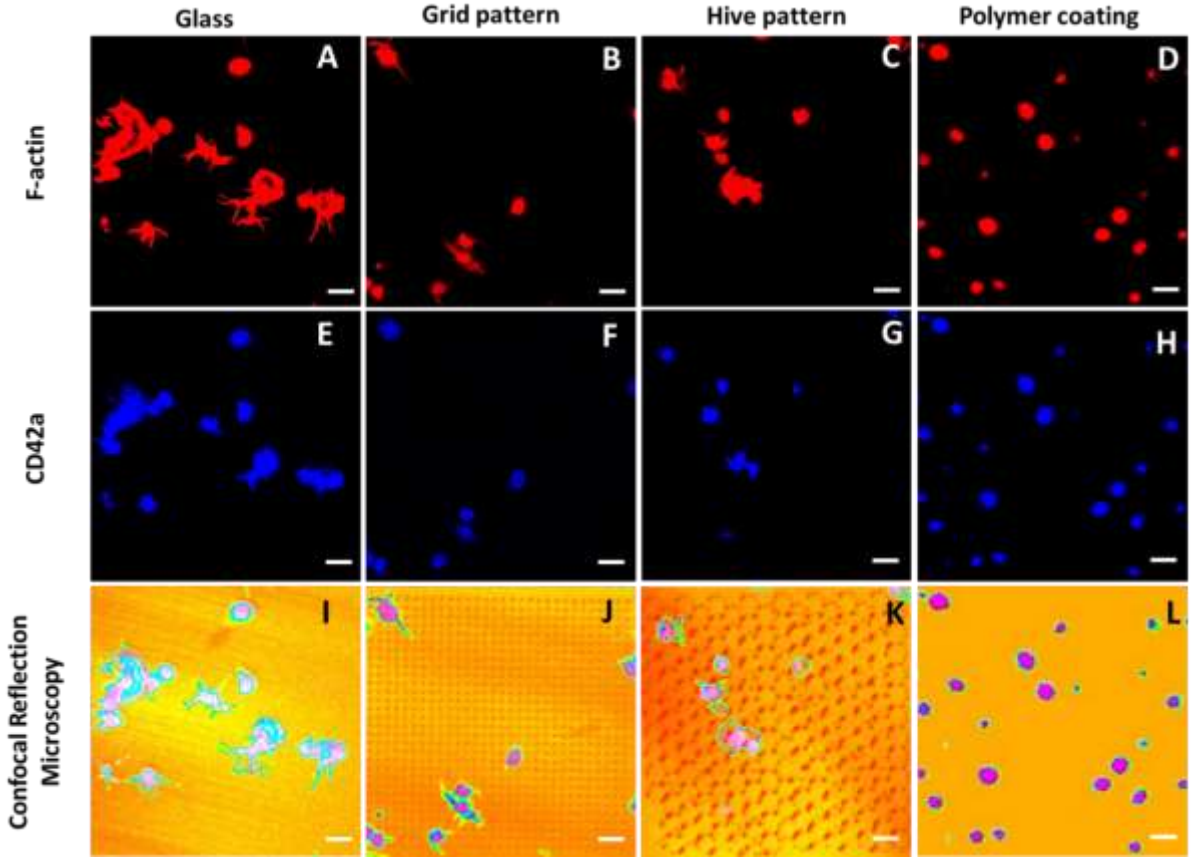

Figure 41: Response of platelets to nanostructured surfaces revealed through confocal reflection microscopy. (A) Platelet actin fibers were stained with DY590 phalloidin (red), and (E) platelet surface-expressed protein CD42a was stained with an anti-CD42a FITC-conjugated antibody (blue). Images were post-processed and merged with images taken by setting the filter T80/R20 for each sample to obtain a clear visualization of platelets along with unstained patterns (I-L). Adapted from[126]

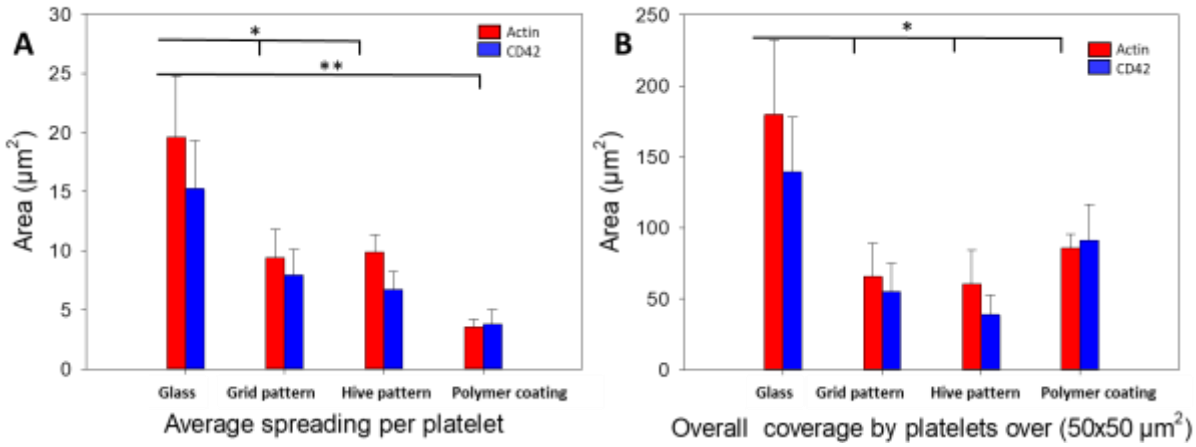

Figure 42: Quantification of the fluorescence signal from both stains to obtain the (M) average spreading area per platelet. Adapted from[126]

The results presented in this chapter were already published in ACS Appl. Mater. Interfaces 2022, 14, 21, 24133–24143

On comparing the ratio of the signals from CD42 and actin, it was seen that within the patterned surfaces, the least value was found on grid pattern **Figure 42A**. AFM imaging was further performed to visualize the difference in the spreading and activation of platelets on the grid pattern as compared to the glass control (**Figure 43**).

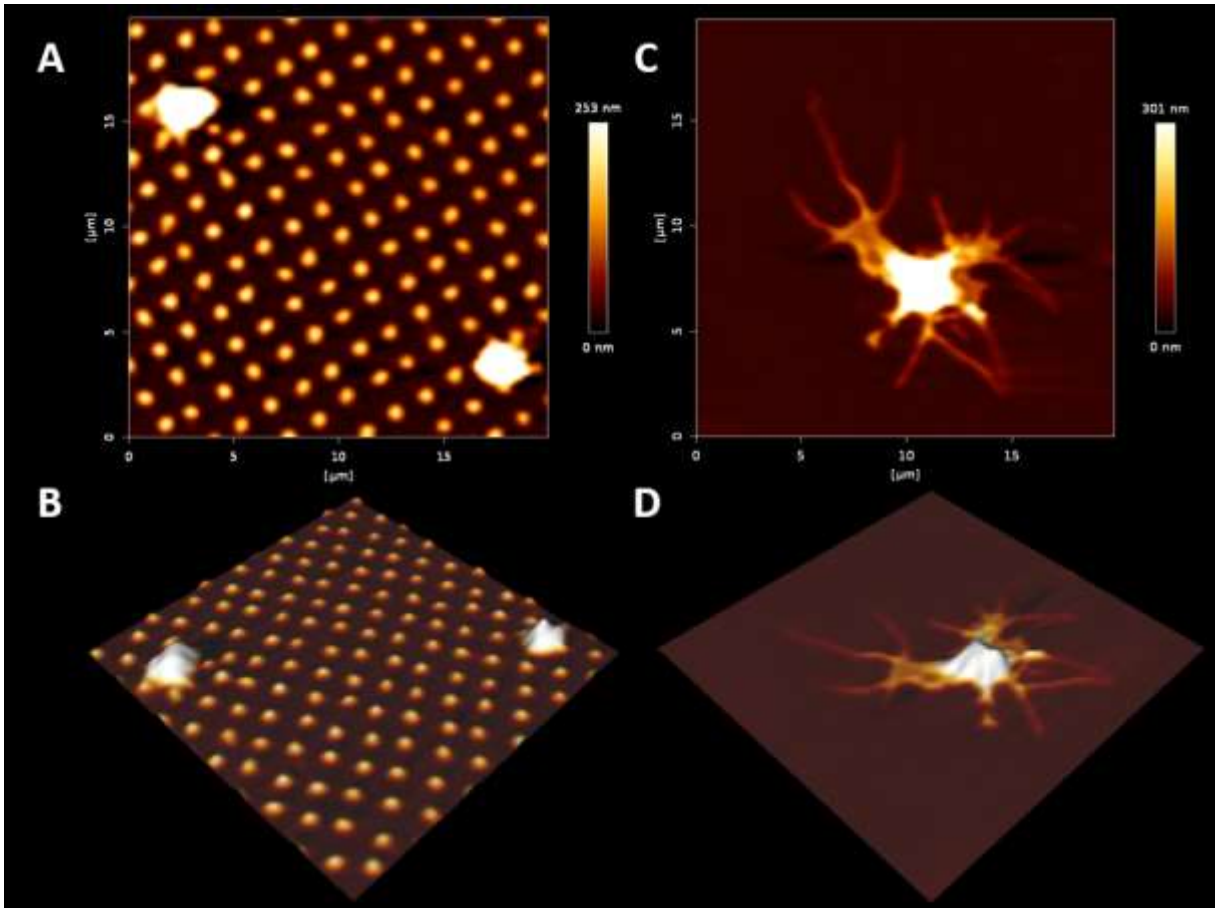

Figure 43: Behaviour of platelets on (A) a patterned grid surface and (B) glass, with their 3D AFM images in (B) and (D) respectively.

6.4.3 De adhesion Force between Platelet and Surfaces

The de adhesion experiment was carried out in order to gain some more insights into the interaction between the platelets and the different surfaces. The largest de-adhesion forces were seen when platelets interacted with polymer coatings, followed by nanostructured surfaces, and bare glass (**Figure 44**).

The results presented in this chapter were already published in ACS Appl. Mater. Interfaces 2022, 14, 21, 24133–24143

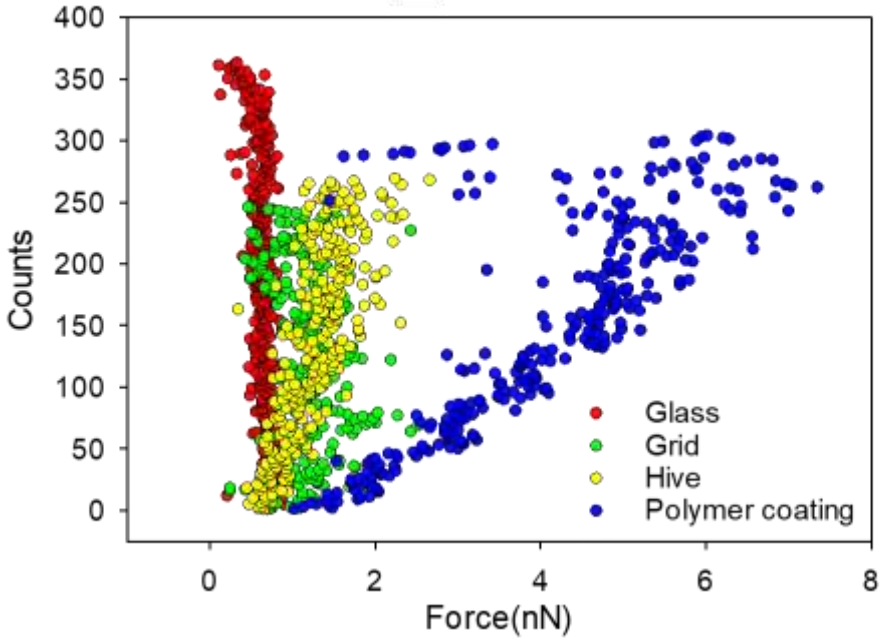

Figure 44: Single platelet force spectroscopy (SPFS) for the measurement of de-adhesion forces between platelets and surfaces. A scatter plot (left) represents the distribution of all the recorded maximum de-adhesion values. Adapted from[126]

5.3 Discussion

In this investigation, the different modes of FluidFM were demonstrated, which can be used to fabricate polymer nanostructures for platelet adhesion studies. By adjusting the physical printing parameters, the geometry and size of features can be altered. The optimal fabrication and replication parameters for stable hemispherical grid patterns and hexagonal hive nanostructures was determined. Both patterned surfaces inhibit platelet adhesion better than their control counterparts of bare glass or spin-coated polymer. The grid-patterned structures inhibited platelet adhesion slightly more (though not significantly) than the honeycomb structures. When compared to the plain glass surface, the patterns showed a significant decrease not only in the development of platelet lamellipodia but also in suppressing filopodia, or the outer protrusions.

The above findings support previous research that shows platelets sense underlying surface stiffness by reorganizing the cytoskeleton, increasing adhesion, and spreading on harder surfaces due to increased -granule secretion and αIIbβ3 integrin activation.[114] These procoagulant activities, which result in platelet activation, are a response to the mechanical

The results presented in this chapter were already published in ACS Appl. Mater. Interfaces 2022, 14, 21, 24133–24143

forces sensed at the adhesive junctions between the platelet and the platelet-surface interface.[220] As a result, in addition to receptor-ligand activation, which is usually responsible for platelet activation and aggregation, the biophysical interaction between the platelet and its contact surface also influences the fate of the platelet activation cascade. In this study it was found that the overall stiffness of uncoated glass differs significantly from that of the spin-coated sample, and that there is also a considerable difference between uncoated glass and nanopatterns. This stiffness trend is also reflected in the manner in which platelets spread on various surfaces (**Figure 42A**). Though the observations on platelet spreading are consistent with the aforementioned theory, the findings here regarding the spin-coated polymer appear to contradict the analogy between substrate stiffness and platelet adhesion. However, this seemingly counterintuitive result can be explained by the greater hydrophobicity of the polymer-coated surface (contact angle 77.9±5.0°) compared to that of uncoated glass (contact angle 44.0±1.9°). Increased hydrophobicity of the surface facilitates the adsorption of platelet-expelled proteins, thereby facilitating the initial docking of platelets to the surface. Spreading is kept to a minimum due to the low stiffness of the spin-coated polymer substrate. The polymer surface with the highest platelet adhesion was the one that was spin-coated. As platelet adhesion is the initial step in platelet activation[207,221] the spin-coated surface is unsuitable for platelet storage. The adhering platelet counts for the two fabricated nanopatterns revealed that the number of platelets on the grid pattern was only marginally lower than that on the hive pattern. The difference in the spreading areas shown in **Figure 42** also shows no significant difference. However, careful examination of the differences in the stained area from Actin and CD42a dye provides some insight into the behavior of platelets on the two different nanostructured samples. In comparison to CD42a, the expressed actin activity in the grid pattern is 1.19 times greater than in hives. This greater shift in F-actin to CD42a staining ratios for the hive patterns indicates a wider spread of actin filaments, implying a higher degree of platelet activation.

Though platelet spreading patterns on various surfaces could be quantified using confocal microscopy, a more interesting property for thorough characterization would be to study the extent of interaction between platelets and surfaces. Strong forces measured on the polymer coating explain why so many platelets adhere to its surface. Surprisingly, the glass had the lowest de-adhesion forces, but confocal micrographs revealed a high density and strong activation of platelets (**Figure 41**). Platelets are known to be activated by hard surfaces[114], and a sufficiently long seeding time of platelets also caused platelet activation on bare glass.

The results presented in this chapter were already published in ACS Appl. Mater. Interfaces 2022, 14, 21, 24133–24143

Furthermore, surface charge and surface energy influence platelet adhesion.[196] The weak adhesion forces on glass may be attributable to electrostatic repulsion between the negatively charged platelet membrane, which is composed of anionic glycocalyx, and the negatively charged glass surface. In addition, hydrophilicity may also play a role, given that the glass surface is more hydrophilic than the polymer coating. Hydrophilic surfaces are known to inhibit protein binding due to the presence of water molecules that are difficult to displace by the adsorbing proteins.[196,221] Consequently, the platelets may have experienced less adhesive force, and this may have contributed to the decrease in overall de-adhesion force measured during the brief contact time of platelets to the glass surface. Platelet interactions with nanostructures exhibited greater de-adhesion forces than on glass but significantly less than on the polymer coating. This reflects the combined behavior of both polymers (the patterns) and glass (the interface within the patterns). Taking into account the potential synergistic effects of adhesion and stiffness, the results make the low density of platelets adhering to the printed nanostructures plausible.

In addition to surface stiffness, chemistry, and wetting properties, surface roughness also contributes to the spreading of platelets. Surface roughness is generally essential for modulating cellular processes.[222] The roughness parameters Ra and Rq indicate that the overall roughness of nanopatterned surfaces is greater than that of unpatterned controls (**Table 2**). Numerous studies on the effect of topologies on the inhibition of platelet adhesion have been reviewed previously.[80] In some instances, topography either inhibited protein adsorption, thereby restricting platelet adhesion[110,223], or induced minimal platelet-surface contact area in others.[81] Nanotopology induces an increase in the overall surface's roughness (**Table 2**) and can therefore govern platelet spreading.

The results presented in this chapter were already published in ACS Appl. Mater. Interfaces 2022, 14, 21, 24133–24143

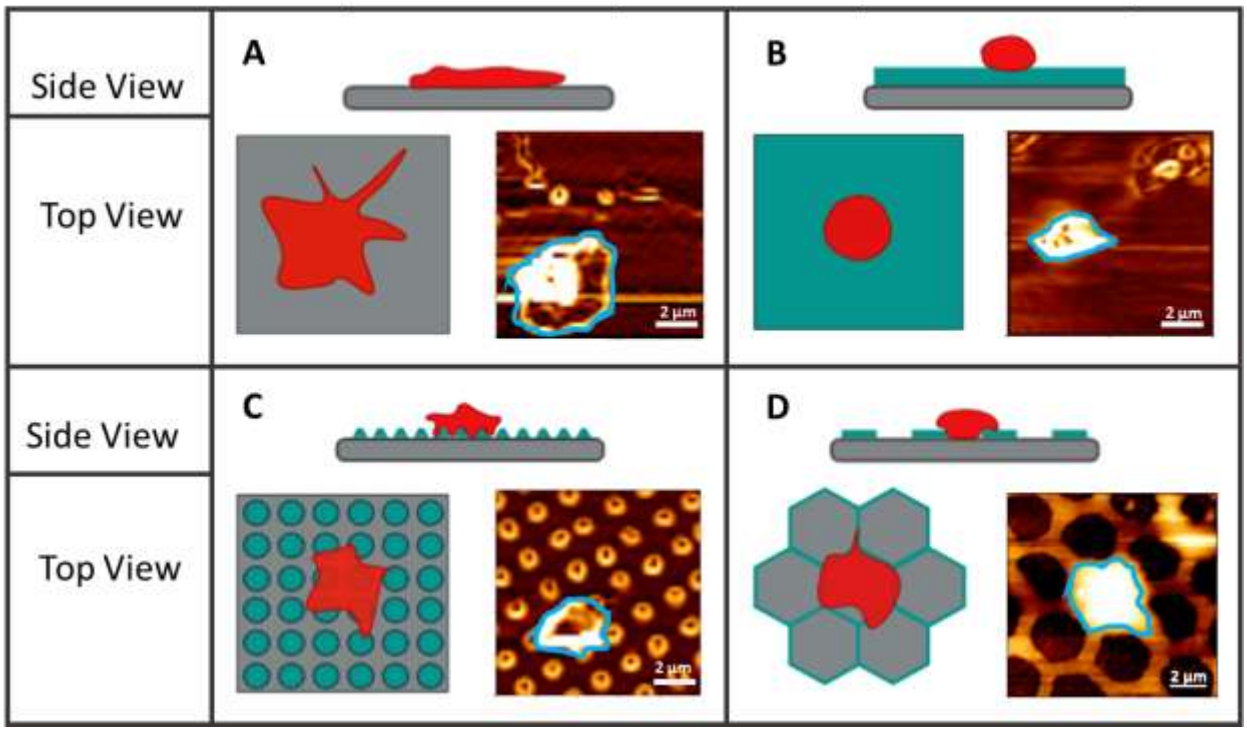

Figure 45: Morphology of platelets on different surfaces represented by schematic models showing top and side views together with AFM images.(A)glass, (B)polymer coating, (C) grid pattern, and (D) hive pattern. Adapted from[126]

On the basis of the obtained results, a schematic depicting the response of platelets on the various surfaces is presented (**Figure 45**). The schematics and corresponding AFM images depict a side view and a top view of the platelets on each surface, revealing how the platelets take topographical cues from the surface to inhibit their activation process. Grid and hive patterns are examples of both continuous and discontinuous topographies. It was hypothesized that the hemispherical structures arranged in a grid can mimic the physiological endothelial cell lining, thereby providing platelets with biophysical cues that inhibit the activation of platelets. In the case of hive patterns, the perimeter of the hexagonal features will help to limit the probing and extension mechanisms displayed by filopodial outgrowths. The "platelet-like shape" of the hexagon may be an advantageous structure for platelets. The symmetrical boundary of the hexagonal feature may generate a homogeneous environment consisting of forces and stiffness that act equally on all contacting components of a platelet body. As platelets activate upon immediate contact with non-physiological surfaces, the inhibition of platelet-surface activation on artificial surfaces, such as platelet storage bags and implants, is highly desired to overcome the limitations of numerous biomedical applications.

The results presented in this chapter were already published in ACS Appl. Mater. Interfaces 2022, 14, 21, 24133–24143

5.4 Limitations

While nanostructures already have a significant impact on much larger biological entities, it would be interesting to investigate the impact of the same structures explored here at greater heights. This is not easily accomplished with the current setup due to technical constraints, but in general, FluidFM with polymer inks is capable of layer-by-layer 3D printing.[157] Although this study focused on the modulation of platelet adhesion and activation by surface topography, other factors such as roughness and wetting behavior are also important in the platelet adhesion process. While the roughness of the patterns is easily accessible via AFM measurements, the wetting properties are much more difficult to access due to the limited patterning area of only 50 × 50 µm. However, by providing contact angles for the accessible substrates (glass and spin-coated polymer), a broad range of expected contact angles on nanopatterns can be estimated. While combining a change in materials with the same patterns would be interesting, the scope of the current work is focused on the patterns as such, limiting us to only one polymer. In the future, nanostructures could be used to improve the platelet storage properties of already optimized and, ideally, regulatory approved materials.

To summarize, there is still a significant knowledge gap to be filled in order to solve the problem of surface-induced platelet activation. Aspect ratio, interspacing, geometry, and topography density should also be considered and optimized in order to achieve an ideal nanostructured surface. In the future, the behavior of platelets on nanostructures made with modified ink in order to incorporate blood-compatible and platelet-repelling chemical motives into the structures can also be explored.

5.5 Conclusion and Outlook

It was concluded that the simple, direct-write patterning technique developed by FluidFM in collaboration with the AFM provides a cost-effective and reliable solution for fabricating nanopatterns of various geometries in a reproducible manner for cell study applications, as demonstrated here for platelet activation. The behavior of human platelets on patterned (grid and hive patterns) and nonpatterned (glass and spin-coated polymer) surfaces was investigated. Platelet behavior is strongly influenced by nanotopography and substrate stiffness. First and foremost, the results showed that the nanostructures could inhibit platelet adhesion and control their spread. The ability of the nanostructures to inhibit platelet activation following the primary steps of platelet adhesion and spreading suggests that they could be a contender in the

The results presented in this chapter were already published in ACS Appl. Mater. Interfaces 2022, 14, 21, 24133–24143

development of nanotextured storage bags for platelets. FluidFM patterning for prototyping structure candidates for platelet activation studies can aid in the identification of promising geometries that can then be transferred into mass production-compatible techniques such as roll-to-roll imprinting or similar pattern replication approaches.

5.6 Experimental section

5.6.1 Printing with FluidFM

The structures were fabricated using a Nanowizard 4 setup (JPK, Berlin, Germany) and a FluidFM add-on (Cytosurge, Opfikon, Switzerland), mounted on an active vibration isolation system (Micro 40, Halcyconics, Germany), and placed under an acoustic hood to reduce the effects of external vibrations. To observe the cantilever and move it to the desired location, an inverted microscope (Axio Observer Zeiss, Jena, Germany) was used.

FluidFM parameter evaluation and optimization for printing: All of the parameters were systematically optimized by modifying only one at a time to evaluate their impact during the printing process. For both force mapping and manipulation printing modes, the setpoint and pressure parameters were optimized. The effect of contact time was investigated using force mapping mode, while the effect of writing velocities was evaluated using manipulation mode.

Printing with force mapping: The AFM was used in force mapping mode to print an array of hemispherical dots on 24 mm round glass coverslips (Plano GmbH, Wetzlar, Germany) that had been pre-cleaned with 80% Ethanol and sonicated for 30 minutes. The reservoir of the micro channeled cantilever was filled with ink (Loctite AA3491, Henkel, Germany), which is a mixture of various methacrylate esters that polymerize when exposed to UV light. Loctite AA3491 is made up of isobornyl acrylate, 2-hydroxyethyl methacrylate, acrylic acid, and hydroxypropyl acrylate monomers. Before each printing cycle, a nanopipette with a 300 nm aperture and a nominal spring constant of 2 N/m (Cytosurge, Opfikon, Switzerland) was calibrated using the contact-free thermal noise method before being approached to the surface with a constant pressure of 150 mbar and a setpoint of 10nN. The nanopipette's contact time with the surface was set to 2.5s. The nanopipette was scanned over a 50 × 50 μm^2 area with a pixel size of 30 × 30 to produce an array of 900 hemispherical features. After printing, the samples were exposed for 5 minutes to a UV lamp at 365 nm for curing.

The results presented in this chapter were already published in ACS Appl. Mater. Interfaces 2022, 14, 21, 24133–24143

Manipulation mode printing: The hexagonal tile structure was printed on a glass coverslip using the AFM in manipulation mode. The structure was pre-designed with the graphic software Inkscape (version 0.17), which allows the user to export the desired pattern as a scalable vector graphic file (svg). This file was then imported into the JPK Nanowizard4 AFM control software. The printing was done on a 50 × 50 μm² area with a continuous positive pressure of 150 mbar, a set point of 10 nN, and a writing speed of 1 μm/s. Following printing, the samples were cured in the manner described above.

5.6.2 Imaging and Roughness Measurements of Nanopatterns

AFM in force modulation mode was used to acquire the topographical scans. The images were captured at a line rate of 0.3 Hz and a resolution of 512 × 512 pixels for all samples. A Mikromasch cantilever (HQ: CSC38/tipless/No AI) with a nominal spring constant value of 0.09 N/m was used. To completely image the 50 × 50 μm printed patterns, a scan size of 80 × 80 μm was used. Using JPK software, line profiles of the features were obtained by selecting the image cross-section option to compute the size of each printed feature. The mean and standard deviation were calculated by measuring the base diameter, interspacing, and height of 10 hemispherical features, as well as the height and diagonal spacing of 10 hive features. The roughness parameters were computed over a 15 × 15 μm² area using the JPKSPM data analysis software to compute the average (Ra) and RMS (Rq) roughness values across all surfaces. Platelets were fixed with PFA, rinsed with PBS, and imaged in force modulation mode in PBS using the same cantilever type as described above at a scan rate of 1 Hz. The images were processed using the JPK Nanowizard4 software.

5.6.3 Wettability Measurements

The static contact angle for the glass and spin-coated samples was measured using the sessile drop method on an OCA 15+ system (Data-Physics Instruments GmbH, Filderstadt, Germany). The dosing volume was set to 3 μl , and the contact angle was calculated using the ellipse fitting method and the OCA15+ software.

5.6.4 Nanoindentation of Patterns

The mechanical properties of the nanopatterns, spin-coated polymer, and glass were measured using AFM nanoindentation. To indent the samples, a cantilever with a 3 μm gold bead (CP-CONT-AU-A, Nanoandmore GmbH, Germany) was used. 2500 pairs of force vs. displacement curves were obtained over the surface from a 20 × 20 μm² area for each sample by subdividing the area into equal-sized pixels and acquiring one pair of curves from the center of each pixel.

The results presented in this chapter were already published in ACS Appl. Mater. Interfaces 2022, 14, 21, 24133–24143

For these measurements, the tip velocities and z-lengths were 3 µm/s and 3µm, respectively. All of the samples were measured in the air with a force of 1000 pN applied. The bulk polymer was measured in liquid, where the entire indentation cycle could be performed. For processing the force curves, the calibrated spring constant of the cantilever was 0.03 N/m in air. Each sample's stiffness was determined by fitting the corresponding extend/approach curve to the Hertz model. During the calculations, the tip geometry was assumed to be a sphere with a tip diameter of 3 µm. The hertz model[212] is given by the formula

$$F = \frac{4E\sqrt{R}\delta^{\frac{3}{2}}}{3(1-v^2)}$$

where F is the applied force, is the indentation depth, R is the radius of the spherical tip, v is the Poisson ratio, and E is the Young's modulus. Sigmaplot 14(Syssat Software GmbH Germany) was used to analyze the data.

5.6.5 Imaging Platelets on Surfaces

Platelets were isolated from the whole blood as mentioned in section **4.6.6 Isolation of Platelets**. Platelets at 30,000/µl concentration were added to the samples and incubated for 1 hour. Unbound platelets were washed away with Phosphate buffer solution (PBS), and the platelets were fixed for 30 minutes in 4% Paraformaldehyde (PFA). The number of platelets adherent to the samples was counted using confocal reflection microscopy. Four samples from three independent donors were quantified for each condition, with an area of 50×50 µm² to make statistics for platelet adhesion and spreading. To quantify platelet spreading on the surface, post-fixation platelets were stained for 1 hour with anti-CD42a FITC antibody (Dianova GmbH, Hamburg, Germany) at a final concentration of 0.1 µg/ml platelet solution. The unbound dye was then washed off the sample twice with PBS. After that, samples were incubated for 10 minutes in permeable buffer before being incubated for 45 minutes at RT (23 °C) in the dark with Phalloidin DY590 (Mobitec GmbH, Göttingen, Germany) (1:20 dilution). At RT in the dark, samples were examined using a confocal laser scanning microscopy Zeiss LSM710 (Carl Zeiss, Gottingen, Germany). Using a 63x objective, the blue fluorescent signal was acquired using the excitation/emission wavelengths of 488/520 nm and the red fluorescent signal was acquired using the excitation/emission wavelengths of 580/599 nm, respectively. Images were also captured with a T80/R20 beam splitter in order to visualize the patterns using confocal reflection microscopy.[224] ImageJ software was used to further

The results presented in this chapter were already published in ACS Appl. Mater. Interfaces 2022, 14, 21, 24133–24143

process the images and quantify the platelet adhesion and spread on each sample.[225,226] Images from both channels (blue and red) were imported, then contrast and brightness were adjusted. Images were converted to a stack and cropped to a 50 × 50 μm² area before being converted back to individual channel images. The images were then analyzed by using ImageJ's thresholding tool to measure overall platelet spreading, followed by the particle analysis tool to count the number of platelets. Confocal reflection microscopy images were merged with individual images from both channels before being assigned pseudocolors using the Look-up table (LUT) tool to visualize the nanostructures.

5.6.6 Single Platelet Force Spectroscopy

The SPFS measurements were carried out using an AFM (JPK, Berlin, Germany) equipped with a FluidFM (Cytosurge, Glattbrugg, Switzerland) add-on device. A pressure of -800 mbar was applied to a micro-channeled cantilever with a 2 μm aperture and a nominal spring constant of 2 N/m (Cytosurge, Glattbrugg, Switzerland). To avoid sucking the platelet into the microchannel cantilever, the largest visible platelets (which are expected to be larger than the size of the cantilever aperture) were targeted. After picking the platelet, the pressure was reduced to 200 mbar and the cantilever was retracted. Force mapping was then used to generate force-displacement (F-D) curves over glass, fabricated nanopatterns, and spin-coated polymer surfaces. On each surface, platelets were collected and measured independently. A 20 × 20 μm square was subdivided into 20 × 20 equal-sized pixels. The force-distance curves were recorded for all samples at a setpoint of 5 nN, z-length of 5 μm, and a pulling speed of 2 μm/s. The adhesion forces were calculated after the force curves were processed in the JPKSPM data processing software. Using Sigmaplot 14.0, the values were displayed as scatter and box plots .

The results presented in this chapter were already published in ACS Appl. Mater. Interfaces 2022, 14, 21, 24133–24143

Chapter 6: Further Investigations into FluidFM based Nanoprinting

6.1 Chapter Overview

The previous chapter focused on the use of FluidFM to reproducibly fabricate stable nanopatterns in order to inflict inhibition of platelet adhesion and spreading. This chapter delves deeper into the various aspects of the printing process and how changing one or more parameters or processes can open up new avenues of investigation. Even though the experiments or their results carried out in this section were not directly translated to platelet research, the rationale was to explore these corelated domains and develop more efficient nanostructures.

FluidFM with an aperture at the cantilever tip can be used to precisely dispense liquid.[154] Micro- and nanostructures can be printed, depending on the size of the tip aperture. Using the commercially available UV-curable adhesive Loctite, hierarchical structures at multidimensional scales could be created using this technique. As a direct-write method, this approach is extremely versatile in patterning, with excellent resolution down to the tens of nanometers scale. However, little is known about the incorporation of functional groups into printed structures to enable specific biological applications. Further biofunctionalization of such structures is currently lacking. In the last part, it was tested whether biofunctional molecules could be mixed into FluidFM's ink and whether the molecules would still retain functionality after being printed and cured by UV. The feasibility of incorporating specific protein coupling sites into printed microstructures was investigated in this study. This is accomplished by incorporating biotin moiety-bearing amphiphilic molecules into the base acrylate ink, which is then cured and presented on the micro- and nanostructured surfaces. Because no chemical post-functionalization is required, the method is a simple way to introduce highly specific protein binding into polymer structures.

In this chapter, a spiral geometry was selected to further explore different topological parameters. As mentioned earlier, when dealing with nanoprinting, it is important to fix the printing parameters.[160] One such parameter is writing speed; since nanopatterning involves the precise deposition of materials on a small scale, this becomes even more crucial. A too-fast or too-slow speed can compromise the quality of printed features.

As previously discussed in Chapter 5, Section 5.4, the current FluidFM setup had technical limitations and was thus unable to scale the features in the z axis. However, in this chapter, layer-by-layer printing was employed to increase the height of the features. This was performed

Part of the results presented in this chapter were already published in MDPI Polymers 2022, 14(7), 1327

by "overwriting" the printed feature without disturbing either the FluidFM probe assembly or the substrate. Previously, studies have reported that changing the feature height of a nano- or microtopography can effectively alter cells' attachment, spreading, and proliferation on the surface.[227,228] Additionally, the height of features may influence the surface energy and hydrophobicity or hydrophilicity, which can affect the adhesion and wetting properties of the surface and ultimately affect the response of cells, or in this case, platelets.[229]

Further, another topographical parameter of nanotopography that is often modulated to invoke a desired response is termed "interspacing." Just as with the height, even controlling the interspacing between adjacent features on biomaterials is known to have a significant impact on the fate of cells. A study undertaken by Koh et al. revealed that the smaller the interspacings, the higher the platelet adhesion, as it increases the points of contact with the platelet. But it's hard to jump to conclusions without taking other things like aspect ratio or surface chemistry into account. A combined approach would be an interesting way to see the complexity of nanostructures.

6.2 Results

6.2.1 Printing Bio-functionalized Ink

The following studies were carried out as part of the collaboration work to determine whether it was possible to successfully integrate bioactive molecules in the ink prior to the printing and curing processes, and whether the binding molecules remained accessible after curing. Two types of modified inks, with different functional properties, were prepared for the experiments, by admixing functionalized phospholipids. For an easy assessment of miscibility and to be able to observe the printed structure by fluorescence microscopy, a fluorescently labeled phospholipid (Rho-PE) was admixed. For the integration of biofunctional molecules into the adhesive-based patterns, a biotinylated phospholipid (biotin-PE) was admixed. The work was published in ***MDPI Polymers 2022, 14(7), 1327***

Following tasks from the published work were accomplished by me at Institute for Bioprocess and Analysis Measurement Technology (IBA),

1.- Printing different geometric patterns like dots, lines, and squares to demonstrate the successful use of FluidFM, a nano dispensing technique.

2.- Nanoindentation measurements were done to figure out how much the biofunctionalized adhesive changed the mechanical properties of the printed structures.

Part of the results presented in this chapter were already published in MDPI Polymers 2022, 14(7), 1327

Results in following parts of the chapter **Section 6.2.1.1** and the corresponding discussion, conclusion and methods.

The remaining part of the published work was carried out by collaboration partners at Institute of Nanotechnology- Karlsruhe Institute of Technology. Results in following parts of the Chapter **Section 6.2.1.2** and the corresponding discussion, conclusion and methods.

6.2.1.1 Comparison of Mechanical Properties

It has frequently been demonstrated that the mechanical properties of a substrate affect cell behavior.[230] As a result, the impact of the biofunctionalized adhesive on the mechanical properties of the printed structures is evaluated here. Nanoindentation measurements were taken over the dot features of both non-functionalized and functionalized adhesives (**Figure 46A**). The force-distance curves derived from these measurements were then examined using JPK software, and the Young's modulus was calculated after fitting the curves with a Hertz model (**Figure 46B**). **Figure 46C** shows histograms of the E-modulus values obtained on the functionalized and non-functionalized adhesives, as well as the values obtained on the glass surface. For all of the ink samples, two distribution peaks can be seen. The measurement on the plain glass serves as a control, distinguishing the values obtained on the dot features from those obtained on the surrounding glass. The indentation maps show that the polymer structures have a low E-modulus (**Figure 46D**, dark area), whereas the surrounding glass has a much higher value (**Figure 46D**, bright area). The distribution of the E-modulus values in the form of a box plot (**Figure 46E**) for the control glass and the inks (after subtracting the values from the glass) shows that adding the functionality bearing phospholipids had no significant effect on the mechanical properties of the resulting printed features. Despite the fact that the addition of rhodamine or biotinylated lipids results in slightly stiffer materials, the obtained values remained within the expected statistical variations, as shown by the error bars.

Part of the results presented in this chapter were already published in MDPI Polymers 2022, 14(7), 1327

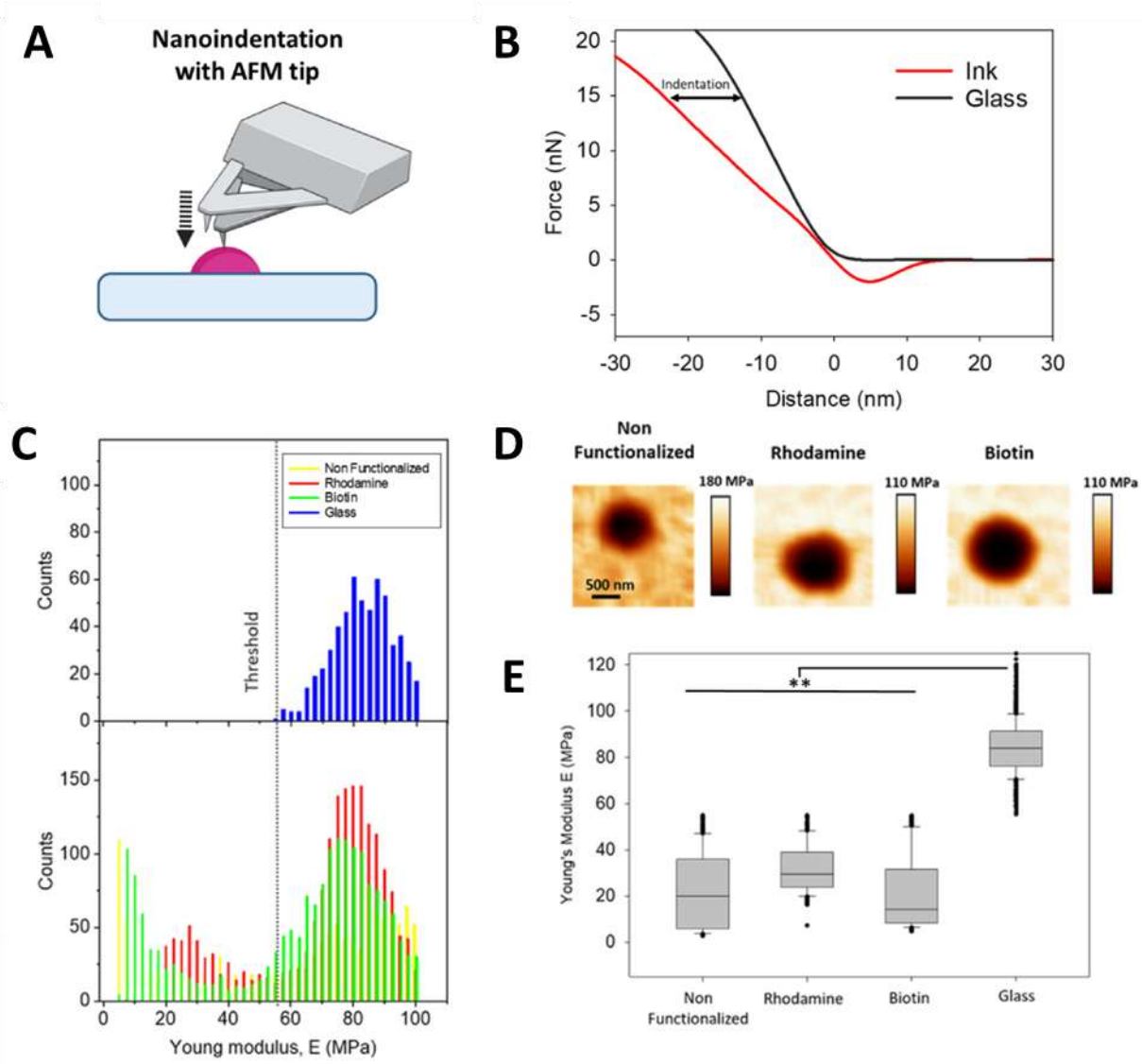

Figure 46: AFM nanoindentation reveals the effect of functional admixing on the mechanical characteristics of printed features. (A) Schematic of the nanoindentation experiments. (B) A typical AFM force-distance curve demonstrates the indentation on hard glass (black) to a compliant ink surface (red). (C) Quantification of Young's modulus of bare glass and samples with modified inks. (D) Indentation map for the different composition nanodots (scale bar equals 500 nm for all images). (E) The Young's modulus of modified nanodots show small variation. Statistically significant difference determined by one-way ANOVA using Dunn's test ** ($p < 0.05$). Adapted from[127]

6.2.1.2 Biofunctionalization of the Ink

Using functionalized phospholipids, two types of modified inks with distinct functional characteristics were created for the studies. A fluorescently labeled phospholipid (Rho-PE) was added so that miscibility could be easily evaluated and the printed structure could be viewed using fluorescence microscopy. Visual inspection revealed that the final mixture was

Part of the results presented in this chapter were already published in MDPI Polymers 2022, 14(7), 1327

homogenous, indicating that the solvents were compatible. This is crucial, as separation of components could clog the FluidFM nanopipette. A biotinylated phospholipid (biotin-PE) was used for the incorporation of biofunctional molecules into adhesive-based patterns. Due to its great binding affinity, the biotin–streptavidin complex [25] is widely utilized in biochemistry research.

To demonstrate that the biotin moieties carried by the mixed phospholipids are accessible, the selective binding of a model protein was established (**Figure 47**). To do this, new samples were created by multiplexing two functionalized adhesive-based inks onto the substrate in the form of distinct micro-/nanostructures. It was ensured that there was no non-specific binding to the bare substrate areas using bovine serum albumin (BSA). In a newly fabricated sample, the molecules were immobilized by curing the adhesive features under UV light for 5 minutes to determine if the biotin moieties remain on the surface and retain their complete functionality after curing. Working with fully cured samples can be crucial for applications, as exposure to ambient light may not be sufficient to fully cure bigger structures, even though small-volume features are frequently already cured. (**Figure 47B,C**) depicts the fluorescent images acquired prior to and following the incubation of fully cured patterns with fluorescently labeled streptavidin. After incubation, the appearance of the second row of patterns in the green channel is unequivocal proof of streptavidin's binding to the biotin moieties.

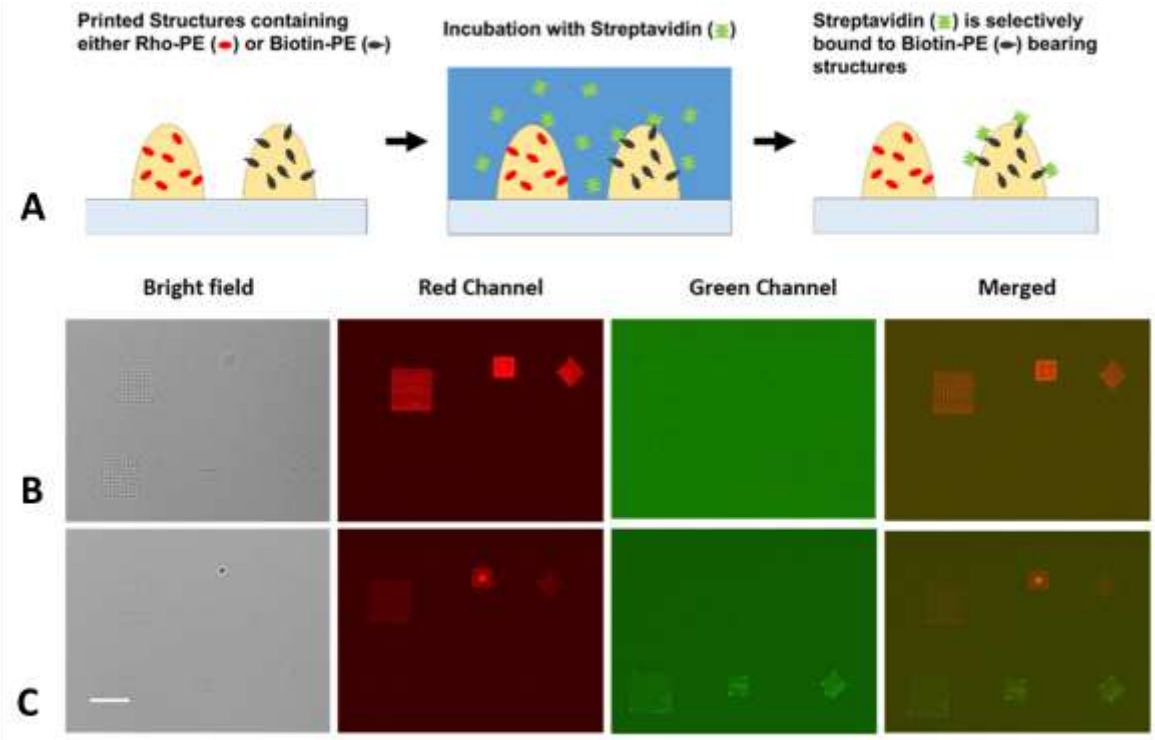

Figure 47: Biofunctionalization of adhesive-based structures by a model protein. (A) Illustration demonstrating the functionalization of the adhesive ink. Microscopy images of (B) adhesive modified with rhodamine-PE (first row) and biotinylated adhesive structures (second row), and (C) the same adhesive structures after incubation with fluorescently labeled streptavidin, demonstrating selective binding. Scale bar equals 40 µm for all images. Adapted from[127].

6.2.2 Screening Effect of Writing speeds

The spiral pattern was selected for further exploration, and hence before modifying different topological parameters, it was important to fix the basic writing parameters. The writing speeds were varied stepwise from 0.1 to 2 µm/s to print spiral structures with outer diameters of 25, 10, 7.5, 5 and 3µm respectively. The smallest spiral, with an outer diameter of 3µm underwent coalescence for all the speeds used. At slower speeds of 0.1 and 0.25 µm/s the spirals, with outer diameters ranging from 10 µm and 7.5 µm respectively, displayed coalescence. The speed, ranging from 0.5 to 1 µm/s displayed satisfactory printing. Printing was not uniform at speeds greater than 1µm/s. **Figure 48** displays the results with the speeds mentioned on top right of each scan.

Part of the results presented in this chapter were already published in MDPI Polymers 2022, 14(7), 1327

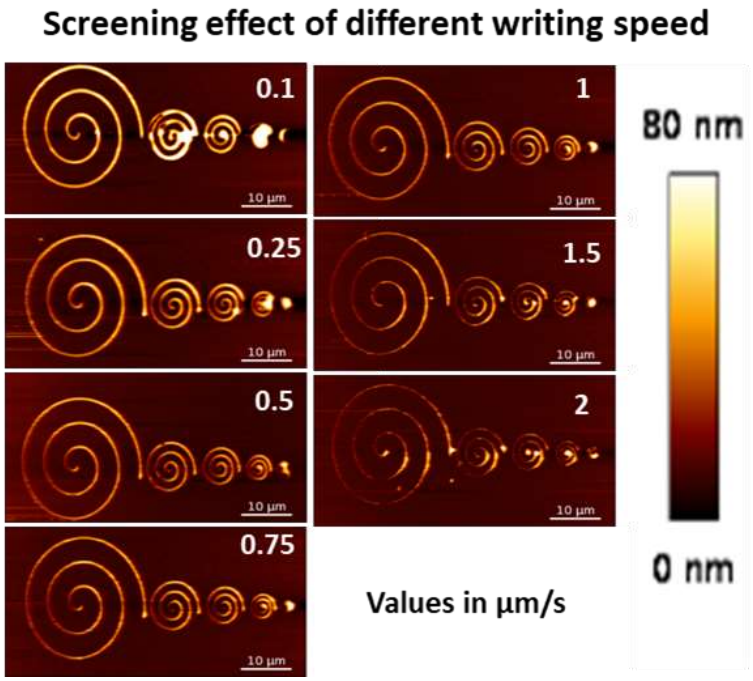

Figure 48: Effect of writing speeds ranging from 0.1 to 2 µm/s on the printed spirals.

6.2.3 Upscaling the Feature Height

The selected spiral pattern was printed by employing the printing parameters. Following the printing of the samples with their respective numbers of layers (1, 5, and 10) they were UV cured for 5mins (**Figure 49**). The features were printed by just changing the number of layers while keeping other printing parameters unchanged. After post-UV curing, the samples were imaged by a miromasch cantilever by using contact mode. The scan size for each sample was 30 × 30, the pixel size 256 × 256 and the line rate was 0.5 Hz. The peak to valley roughness (Rt) parameter calculated by the JPK Nanowizard 4 data processing software showed value of 75.33 nm for 1 layer sample, 155.1 nm for 5 layers, and 199 nm for 10 layers.

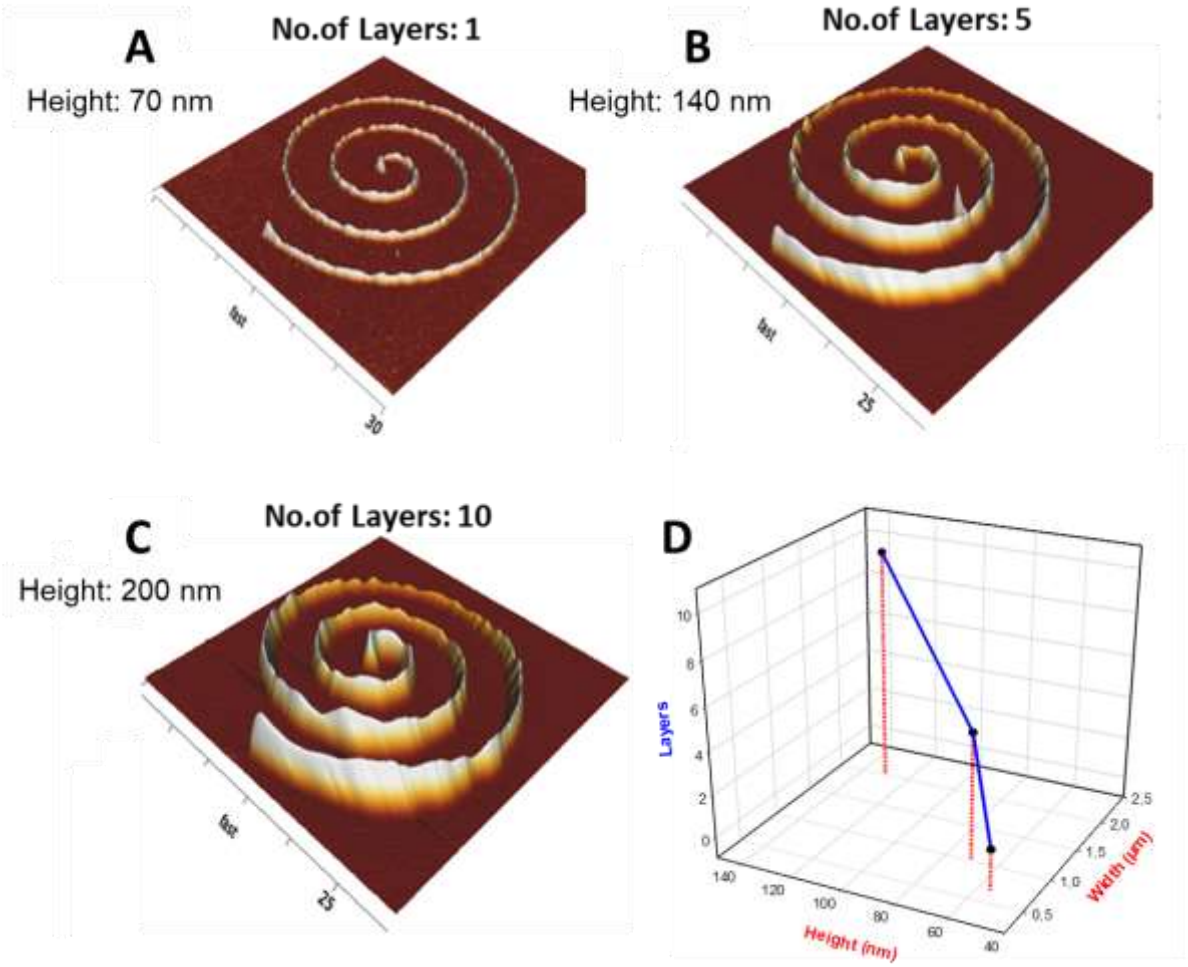

Figure 49: A layer-by-layer printing technique was used to scale up the height of the feature. AFM topographic scans of the printed spirals with no. of layer/s (A)1, (B) 5 and (C)10. A graph (D) depicts the increase in the height and width of the feature as the number of layers increases.

6.2.4 Structures with varied Interspaces

Variation in the interspaces was achieved by resizing the dimensions of the spiral. The geometry was undisturbed so as to only change one parameter at a time. The height for all three samples was similar since the same set of printing parameters were used. **Figure 50A** showed an interspacing of 4.3±0.03µm between adjacent features, which was reduced to 1.81±0.03 µm in **Figure 50B** and further to 1.51±0.01 µm in **Figure 50C**. Having stated earlier that the size of resting platelet is around 3 µm in diameter, it will be interesting to examine their response. The values were manually computed using 'show an image cross section' tool and extracting the line profile with the help of JPK Nanowizard 4 data processing software.

Part of the results presented in this chapter were already published in MDPI Polymers 2022, 14(7), 1327

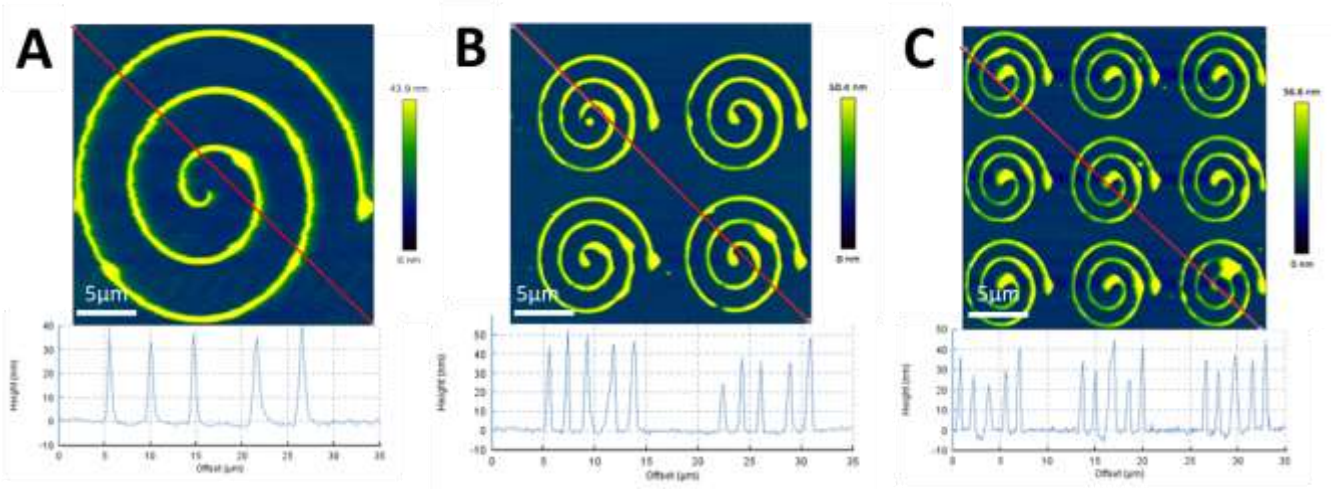

Figure 50: Printing spiral geometries with varied interspacing Printing 1(A), 4(B), and 9(C) spirals within 25 × 25µm.

6.3 Discussion

A potent and incredibly adaptable technique for creating bioactive and functional surfaces for biological research and biomedical applications is three-dimensional nano- and microprinting with UV-curable polymer inks.

The ability to create micro- and nanostructures in arbitrary shapes is one of the requirements for bioapplications. Chemical or biochemical modifications are frequently required to achieve the desired functionality. While conventional approaches are unlikely to achieve specific micro- or nanostructure functionalization, a post-functionalization step can easily achieve a homogeneous chemical modification in bulk. In order to achieve this goal, the inherent functionalization of printed structures is demonstrated by admixing phospholipids with the base adhesive ink. In this study, the resulting structures are functionalized directly, with no additional steps required. Furthermore, multiplexing is possible because structures can be easily written adjacent to one another using different inks. The concept of admixing a fluorescently labeled or biotinylated phospholipid is presented here. Unspecific adhesion is blocked by BSA, and streptavidin is highly selective, binding only to structures formed by the ink containing biotinylated phospholipid. This demonstrates that the biotin moieties remain accessible at the structure-liquid interface, most presumably preferentially oriented outwards of the polymer bulk due to their amphiphilic natures (the hydrophilic head group is modified with the biotin moiety and hydrophobic hydrocarbon chains at the tail end). Surprisingly, the biotin motif provides a broader range of biofunctionalization options because it is one of the

Part of the results presented in this chapter were already published in MDPI Polymers 2022, 14(7), 1327

most common binding tags in biotechnology, with a plethora of compounds available with biotin modifications that could be bound to such structures via a streptavidin linker. The admixing had no effect on the printing or mechanical properties of the printed structures; thus, it is a simple process to incorporate different functionalizations and no interference with, for example, changes in mechanical cues, as stiffness to the cells growing on the structures is to be expected.

Another important consideration when considering bioapplications is the biocompatibility of the materials involved. While methacrylates are problematic in this regard, the material's toxicity is primarily communicated by residual monomers seeping out. Curing will generally be complete for the comparably thin structures produced by FluidFM printing processes, with little monomer remaining, and biocompatibility can be increased further if necessary by additional treatments such as ethanol washing.[231]

While looking at the slow printing speed, it can lead to material spreading, resulting in larger feature sizes and decreased spatial resolution of the pattern. While faster speeds can result in blurring of the features and poor uniformity due to insufficient time for the ink to get deposited on the substrate. Therefore, it's important to find the optimal printing speed, one that allows for precise control of the deposition process while minimizing adverse effects.

Upscaling the height of the nanofeatures has a definite impact on the cell behavior in general.[227] A study by Dai et al. observed that the cells grown on taller nanostructures had reorganized actin stress fibers and vimentin filaments, as well as reduced focal adhesion.[227] On comparing the results for the samples from this experiment, the increase in the height of the features by overwriting the spirals was evident. However, another obvious observation was the growth of the features laterally as the average width of the spirals also increased with the increase in height. It has been observed that the height of the platelets on the surface can be up to a few hundred nanometers (**Figure 43**) which makes this experiment even more relevant. The curvature of the surface of the platelets can be influenced by the height of the features. Previous studies have shown that the behavior of platelets can be varied on the same geometrical structures with different aspect ratios.[81,110,216,232]

The impact of interspacing on cellular adhesion has been reported before by Curtis et al. who report that smaller spacing than 300nm inhibits the formation of focal contacts.[100] In another study relevant to platelet research, it was found that the adhesion of the platelets on the surface decreased as the interspacing between the pillars decreased.[110] The reasoning provided states

Part of the results presented in this chapter were already published in MDPI Polymers 2022, 14(7), 1327

that the contact area of platelets with the surface is smaller, and as a result, the circumstances were unfavorable for the platelets to make stable contact with the surface.[110] Hence, the platelet's shape being constrained by its inability to reach the full surface area, low levels of platelet activation was reported when the interpillar spacing was decreased.[110] In the spirals shown in **Figure 50** the smallest spacing is only about 1.5 µm and hence may need further optimization.

6.4 Conclusion and Outlook

In summary, the results show that polymer ink can be successfully functionalized with model biomolecules and provide proof of principle for how biologically relevant species can be incorporated into direct-patterned nanostructures without significantly altering their global properties. Overall, these findings show that direct printing of functionalized structures using FluidFM or similar dispensing techniques has the potential to create bioactive, protein-presenting micro-/nanostructures for bioapplications. Moving forward integration of anti platelet agents like nitric oxide molecules or dipyridamole can be integrated into nanopatterns fabricated with FluidFM. The successful modulation of different topological parameters like scaling in z-direction and the varying interspacing between adjacent features opens up a lot of possibilities for learning more about platelet surface interaction. The flexibility of the FluidFM can be exploited to develop new prototypes not only to build platelet-compatible structures but also for other cellular applications.

6.5 Experimental section

6.5.1 Biofunctionalization of Ink

6.5.1.1 FluidFM Printing

The following FluidFM systems were used to print the adhesive patterns on glass or silicon substrates: a FlexAFM (Nanosurf, Liestal, Switzerland) system and a BioAFM (JPK, Berlin, Germany) system. FluidFM nanopipettes (Cytosurge, Opfikon, Switzerland) with a nominal cantilever spring constant of 2 N/m and a 300 nm diameter nozzle/aperture at their probe ends were used for the experiments.

After mounting the nanopipette and filling the reservoir with 2 µL of each ink, 1000 mbar of pressure was applied to the reservoir for 1-2 minutes to force the ink through the microchannel

Part of the results presented in this chapter were already published in MDPI Polymers 2022, 14(7), 1327

to the end of the probe aperture. The ink flowed to the substrate without the need for additional pressure once it reached the nozzle. The applied force was typically set between 10 and 20 nN during patterning. To control the feature sizes, the contact time during printing was varied between 0.5 and 5 s for nanodots and between 20 and 60 m/s for print lines.

6.5.1.2 Characterization of Printed Structures

The indentation maps used to calculate Young's modulus were obtained on a JPK BioAFM system (Bruker, Berlin, Germany) with BL-AC40TS probes with a radius of 8 nm (Asylum Research, Santa Barbara, CA, USA), a resonance frequency of 70 Hz, and a nominal force constant of 2 N/m. A total of 625 force curves were analyzed from 2.5 × 2.5 µm2 areas, with the printed feature in the center of the scanning area. The measurements' data were processed by fitting the force curves to the Hertz model, with a pyramidal tip shape and a Poisson's ratio of 0.5. JPKSPM data processing software was used to process the data, and SigmaPlot was used to analyze it (Sysstat Software GmbH, Erkrath, Germany). To obtain control values, measurements were also taken over a plain glass surface.

6.5.1.3 Protein Binding

To avoid nonspecific binding, the samples were first incubated for 30 minutes at room temperature with a 10% BSA solution (Sigma-Aldrich, Darmstadt, Germany). The samples were then biofunctionalized by incubating them in PBS for 30 minutes with a 5 g/mL streptavidin-FITC solution (Thermo Fisher Scientific, Waltham, MA, USA).

6.5.1.4 Optical Microscopy

A Nikon Eclipse Ti2 inverted fluorescence microscope (Nikon, Düsseldorf, Germany) was used for optical microscopy. The light filter was a Texas-red filter (Nikon, Germany), and the biotin-streptavidin bindings were visualized using a green fluorescent protein (GFP)-compatible filter.

6.5.2 Variation in Writing Speeds

The spiral-shaped features were printed using the manipulation mode of the AFM. The spirals with different sizes of outer diameters 25µm, 10µm, 7.5µm, 5µm and 3µm were laterally printed from left to right, respectively. The printing was done at the following writing speeds, 0.1µm/s, 0.25µm/s, 0.5µm/s, 0.75µm/s, 1µm/s, 1.5µm/s and 2µm/s. Post printing and UV curing, the samples were imaged by a Mikromasch cantilever (HQ: CSC38/tipless/No AI) with a nominal spring constant value of 0.09 N/m by using contact mode. The images were captured at 1024 × 1024 pixel resolution and 0.4 Hz line rate.

Part of the results presented in this chapter were already published in MDPI Polymers 2022, 14(7), 1327

6.5.3 Layer by layer Printing

The spiral shaped patterns were designed using the Inkskape software, following which the file was exported as a .svg extension. This format is readable by the JPK software. The AFM was operated in manipulation mode, and the file was imported. The pattern was printed with the respective no. of layers (1,5 and 10) as shown in **Figure 49**. In cases **B** and **C** the cantilever was not moved, and the pattern was printed by so called overwriting layers. A FluidFM cantilever with an aperture of 300 nm was selected to print the spirals. The outermost diameter of the spiral was 25μm. The printing parameters that were selected for printing were as follows, z length =3 μm, writing speed =1 μm/s , set point = 10nN, and a constant pressure of 200 mbar. Post printing and UV curing, the samples were imaged by a Mikromasch cantilever (HQ:CSC38/tipless/No AI) with a nominal spring constant value of 0.09 N/m using contact mode. The scan size for each sample was 30 × 30, the pixel size 256 × 256, and the line rate was 0.5 Hz.

6.5.4 Printing Features with Varied Interspaces

The spiral shape designed in the previous section was used here too, using manipulation mode. The large spiral was resized and arranged so as to have multiple spirals in the equivalent area. Apart from printing one large sized spiral with an outer diameter of 25 μm, two other sizes whee chosen, 4 (2 × 2) spirals with a 15 μm outer diameter and 9 (3 × 3) spirals with a 7.5 μm outer diameter. The printing parameters and the fluidFM probe used were the same as those used in the earlier section. After printing and UV curing, the samples were imaged by AFM. For all samples, the images were captured at a line rate of 0.5 Hz and a resolution of 256 × 256 pixels. A Mikromasch cantilever (HQ: CSC38/tipless/No AI) with a nominal spring constant value of 0.09 N/m was used.

Part of the results presented in this chapter were already published in MDPI Polymers 2022, 14(7), 1327

Chapter 7: Implementing Thermal Nano Imprint Lithography to create Structured Hydrogel Surfaces.

7.1 Chapter Overview

Specific micro- or nanoscale structures, as mentioned in previous chapters, can be used to modulate the response of platelets on the surface. Previous research with agarose hydrogel demonstrated that topographical modulations had promising results in regulating platelet behavior.[117] Furthermore, their surface chemistry and mechanical stability make them ideal candidates for platelet-friendly surfaces. Hydrogel possesses properties like softness, deformability, and the ability to get molded according to the template. Various different types of surface patterning techniques are used in the realm of biomedical research.[233] However, the selection of an appropriate patterning methodology for a particular application is equally important. An innovative technique for nanopatterning called nanoimprint lithography combines high throughput with nanometer-scale resolution. Chou et al. first introduced Nanoimprint lithography (NIL) as a method in which a rigid stamp is pushed into a PMMA layer on a stiff silicon substrate, followed by a little thermal treatment.[234] With resolutions on the order of ten nanometers, a suitable alternative to photolithographic resist patterning could be developed with this technique.[235] The term "NIL" describes the patterning of a polymer layer by pressing a rigid or flexible stamp into a pre-polymer layer coated on a substrate. Various substances, such as monomers, oligomers, polymers, or their solutions, can be used as pre-polymers.[236] After pre-polymer curing, such as UV or thermal curing, and stamp removal, a patterned coating is formed.[236]

Thermal nanoimprint lithography (T-NIL) is a nanofabrication technique used to create high-resolution, large-area nanostructures.[237] T-NIL creates a mold or template by patterning a thin photoresist layer on a substrate. After that, the mold is heated and pressed onto a soft thermoplastic material. Heat melts the material, which cools and solidifies in the mold. The mold is removed, leaving a replica of the original pattern on the substrate. This process is scalable, allowing for the creation of nanostructures with feature sizes ranging from a few nanometers to hundreds of nanometers. T-NIL is a low-cost, high-throughput method for producing large-scale arrays of nanostructures that is widely used in microelectronics, biomedicine, and optoelectronics.[237–239]

When it comes to resolution and aspect ratio, PDMS is a good mold material for T-NIL. Because this elastomer can be wound around cylinders, it enables large-area and high-

throughput processing by incorporating it into efficient roll-to-roll processes.[236] Polydimethylsiloxane (PDMS) is a gas transmittable material that is utilized for flexible molds.[240] PDMS is ideal because it has a distinct combination of properties due to the presence of a siloxane backbone and organic methyl groups attached to silicon atoms.[236] Aside from PDMS's elasticity, the low interfacial surface energy is an advantageous property for soft lithography applications because it results in low adhesion, little chemical interaction, and no swelling due to humidity. Because of its high thermal stability, PDMS can be used for the thermal molding or imprinting of various materials.

In this study, T-NIL was successfully implemented to imprint agarose hydrogels with different topographies, namely dot, chain, pill, and square. Further, the fabricated nanostructures were characterized, and platelet adhesion experiments were performed. In a separate but related extension to the idea discussed in Chapter 4, iron nanoparticles were incorporated into the agarose gel to assess their hypothesized antibacterial effect.

7.2 Results

7.2.1 Fabrication of Imprinted Patterns

The selected geometries were shortlisted with the following rationale: The dot, chain, and pill were the patterns with the smallest dimensions, which were hypothesized to be more effective for platelets. The square geometry with a higher feature dimension was selected to investigate the response a larger micropattern can have. The non-patterned agarose and the plain glass surface served as the controls.

7.2.1.1 Fabrication of Stamps

The geometries exist on the Si master and need to be transferred onto a PDMS stamp, which can then be used to imprint the agarose surface (**Figure 51**). Post-stamp preparation, the stamps were stored in a clean, closed glass container to avoid contamination.

7.2.1.2 Optimization and Selection of Imprinting Parameters for Agarose Substrates

The concentration of agarose used for preparing the film varied from 0.5 g/mL to 3 g/mL. It was observed that the substrate film got disrupted at values below 1 g/mL. At a concentration of between 1 and 2 g/mL, the imprinting was successful, but the features obtained did not have sharply defined structures. At a concentration of 3 g/mL, the imprinted features were found to be satisfactorily stable. Other than the concentration of agarose, the imprinting parameters were finalized after screening over the range of values. The values that produced acceptable results are listed below in **Table 3**.

Table 3 Selected values for imprinting parameters to imprint agarose gels.

Parameter	Description	Value
Temperature of heating	correct temperature depending on the imprint agarose used	70°C
Heat Delay	Heating delay time required to melt the agarose	180s
Pressure P1	Membrane pressure between the contact level and the preposition	117.2kPa
Pressure P2	The membrane pressure when the stamp contacts the surface	135.3kPa
Float Delay	The time for the molten agarose to achieve a complete filling of all cavities	45s
Cooling down	Time needed for the agarose to be back at room temperature	240s

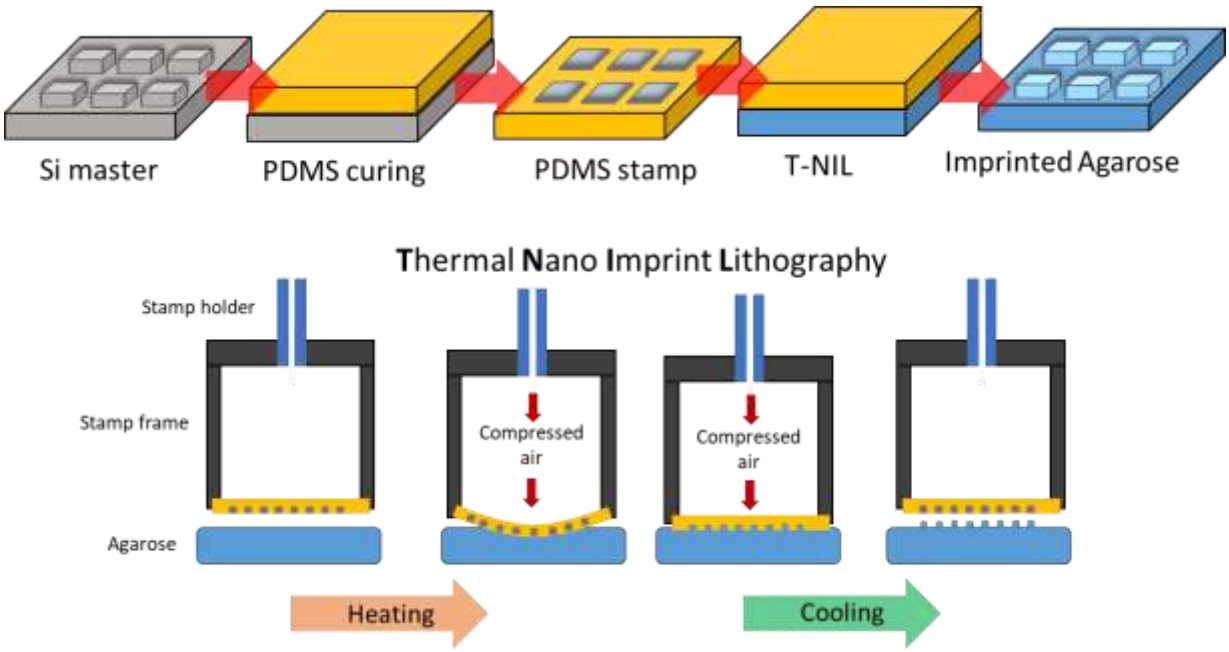

Figure 51: Schematic representation of T-NIL process.

7.2.2 Characterization of Imprinted Agarose Patterns

7.2.2.1 Topographical Characterization of Patterns

The imprinted patterns were imaged using AFM. **Figure 52** shows the respective AFM micrographs for each pattern (top) with their corresponding line profiles (bottom). The diameter of the dot microwell features is 2 µm; the chain pattern has dimensions of 5 µm × 2.5 µm; the pills have a length of 5 µm and a width of 3 µm; and the square features have a length of 10 µm. The AFM data was processed using the JPK Nanowizard4 data processing software.

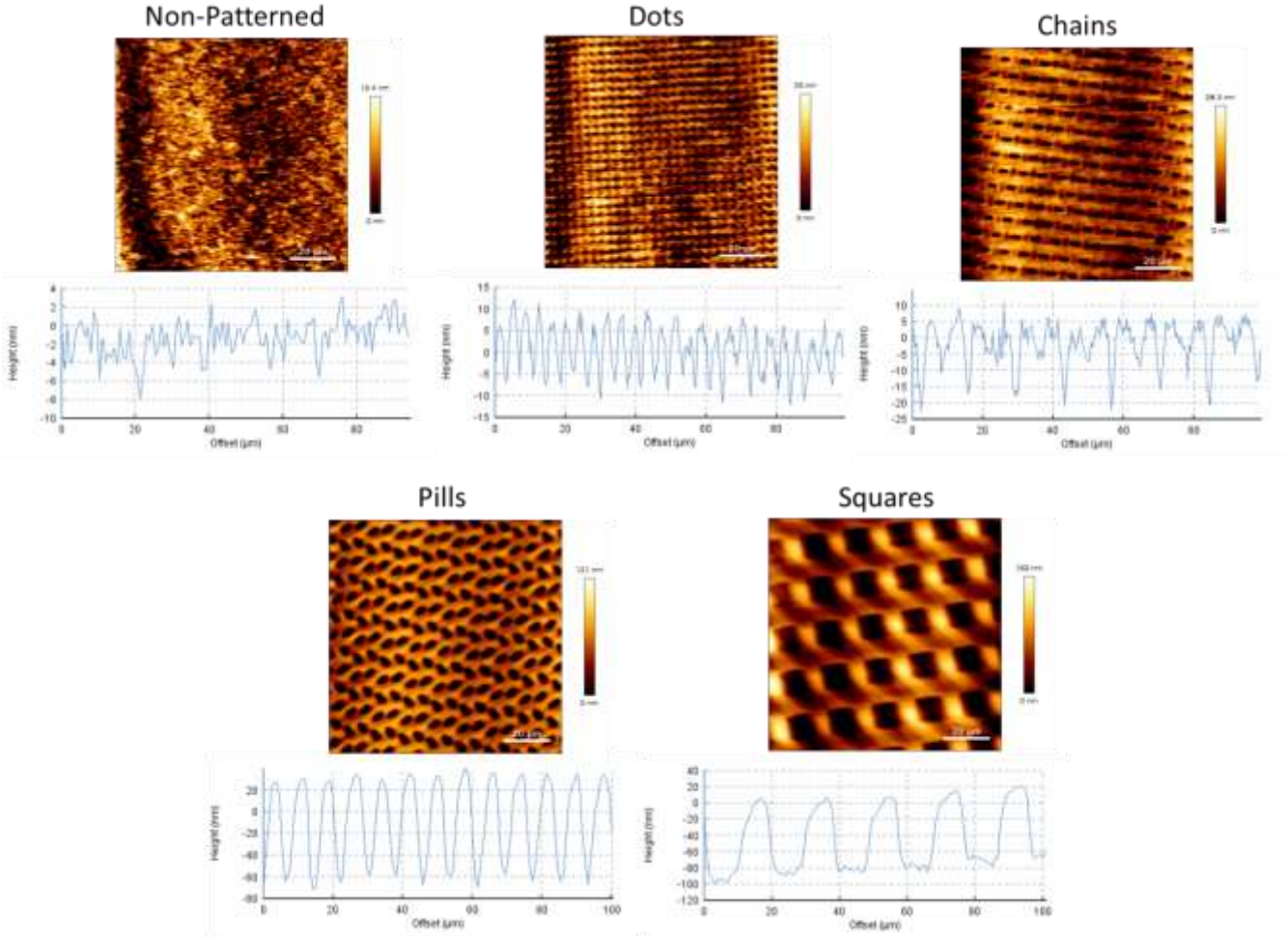

Figure 52: AFM scans of the imprinted and non-imprinted agarose surfaces with their respective line profiles at the bottom.

The following table summarizes the dimensions of the patterns imprinted on the agarose surface. The values for height (Rt) have been calculated after post-processing the image by using a post-processing step of 2nd-degree polynomial line fit.

Table 4 Dimensions of the imprinted pattens on the agarose surface.

Geometry	**Length(µm) L**	**Width(µm) W**	**Diameter(µm) D**	**Height(nm) Rt**
Dot	-	-	2	24.15
Chain	5	2.5	-	33.38
Pill	5	3	-	112.3
Square	10	10	-	118.1
Non-patterned	-	-	-	11.26
Glass	-	-	-	9.9

7.2.2.2 Wettability Measurements

The measurements were carried out using the previously described method for calculating WCA of high-surface-energy surfaces. The measurements indicated that all the agarose-based surfaces, both patterned and non-patterned, were hydrophilic. The contact angle of the glass was computed using the same method as in **Figure 22**. The imprinted and the non-imprinted surfaces did not show any clear trend in the contact angle values. The comparatively small topography compared to the volume of a large air bubble on a surface with similar chemical composition was not enough to induce significant differences amongst the different geometries.

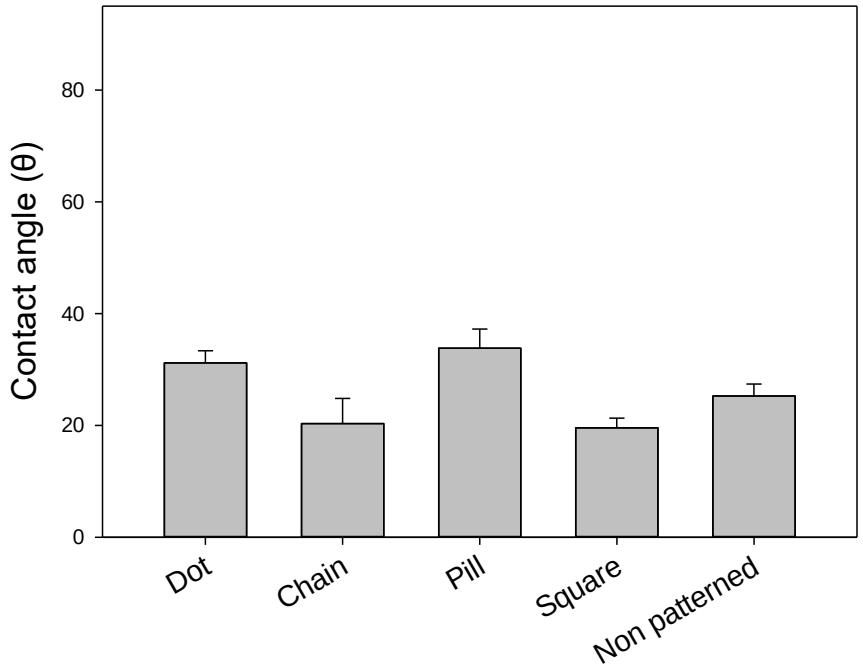

Figure 53: Water contact angles of all the agarose samples, both imprinted and non-imprinted, were measured using the captive bubble method.

7.2.3 Behavior of Platelets

Platelets were pipetted on top of the patterned and nonpatterned surfaces and monitored for 1 hour using the optical microscope. The brightfield **Figure 54 (top)** and CLSM **Figure 54 (bottom)** micrographs were taken on each sample with the respective geometry. It was observed that the staining from anti-CD42a, particularly for the platelets on the agarose surfaces, had a weak signal. The images were processed using ImageJ. The brightfield images do not correspond to the CLSM images.

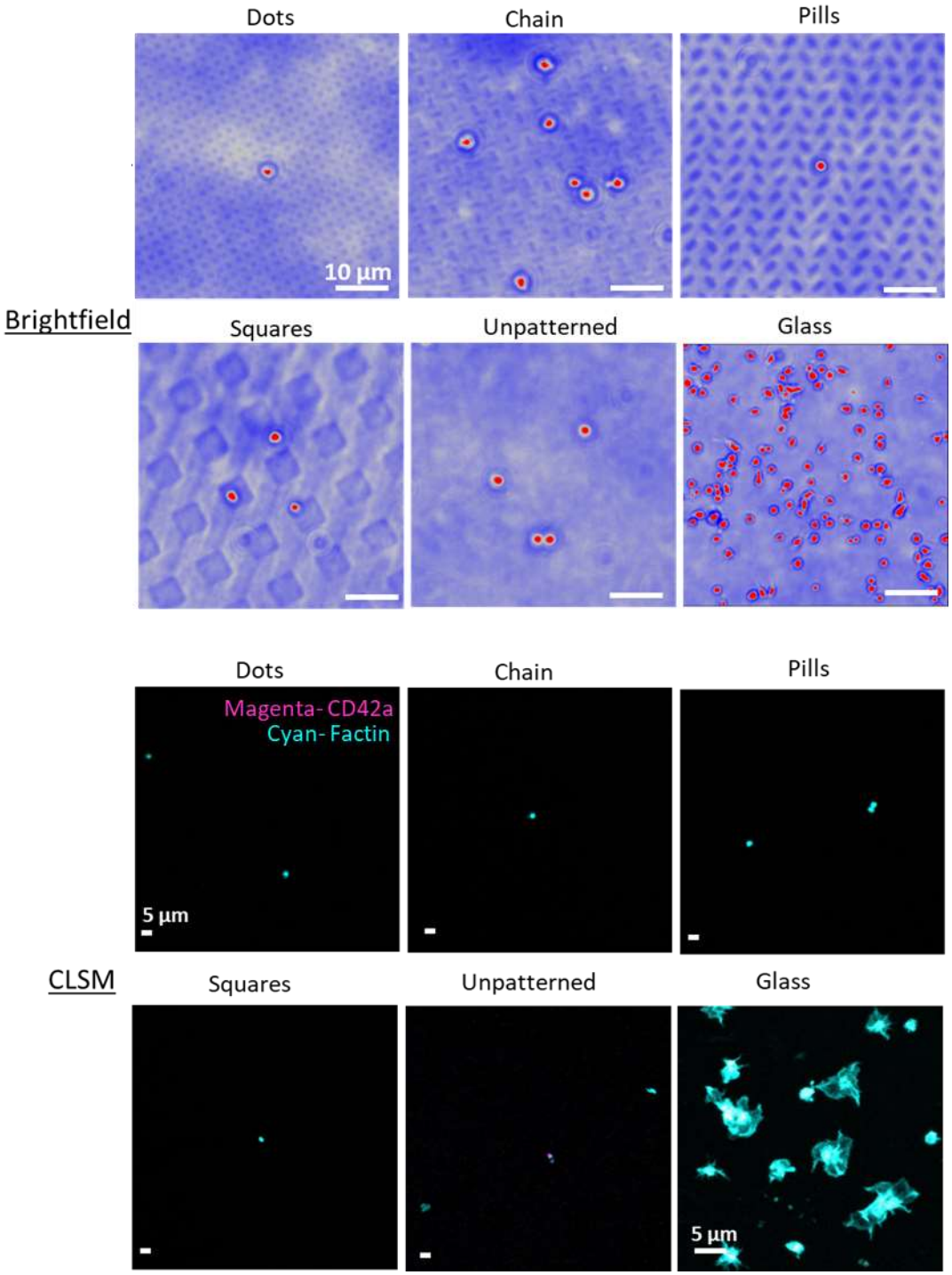

Figure 54: The behavior of platelets on both imprinted and non-imprinted agarose surfaces and on glass, The top panel for each condition shows a bright-field image edited using Image J software, while the bottom panel shows independent CLSM images showing the spreading of platelets.

7.2.3.1 Adhesion of Platelets

The adhesion of platelets was quantified by taking micrographs on samples after 1 hour of incubation. Platelets from three different donors were used to perform three independent repeats. The results revealed that the highest number of platelets adhered to the glass as compared to other agarose-based surfaces (**Figure 55 A**). The CLSM micrographs of the platelets on the glass surface show the activation of platelets and the presence of filopodia and lamellipodia. The number of platelets adhering to the pill-shaped geometry was the lowest of all the experiments performed (**Figure 55 B**).

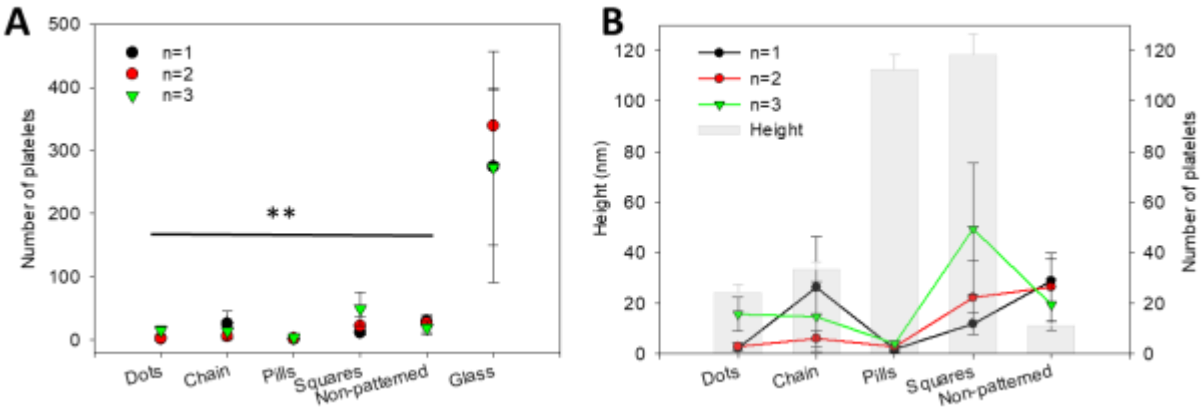

Figure 55: Adhesion of platelets on patterned and non patterned agarose and glass surfaces.(A) Graph represents the number of platelets adhering on respective geometries at 1 hour time point. (B) The rescaled graph indicating the number of platelets adhered on agarose surfaces for all three repetitions together with the height of the features represented by grey bar graph by quantifying roughness using AFM

The influence of time was also examined by taking micrographs at different time points (15 mins,1 hour and 4 hours). The number of platelets was counted on 3 different samples for each geometry for 2 different donors. The results show that at each time point, the number of platelets adhering to the nonpatterned surface was the highest as compared to the patterned surface. Further, an increase in the number of platelets adhering to the nonpatterned and square shaped samples at the 4 hour time point was evident, while the other topographies showed lower adhesion (**Figure 56**). Overall, all the agarose based samples showed a significantly low number of adhered platelets even at the longest time point (4 hours) as compared to the number at the 15 min time point on glass.

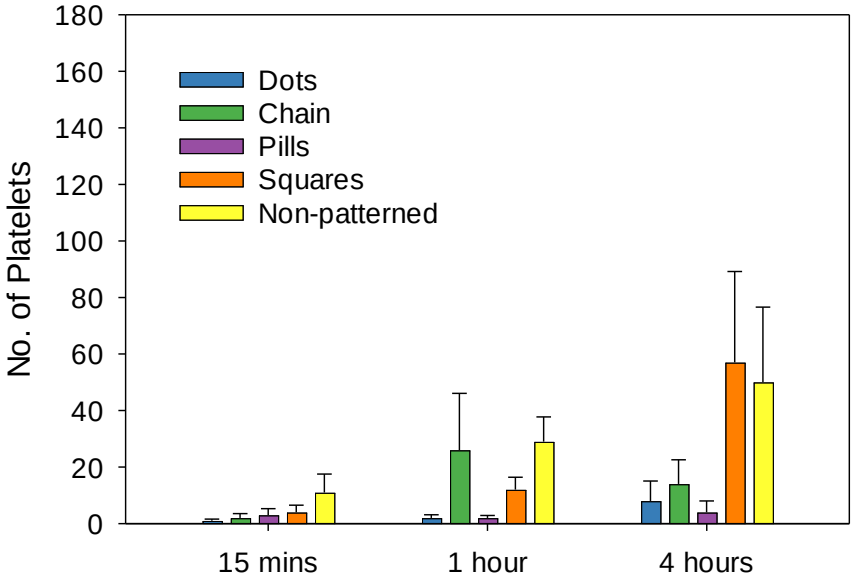

Figure 56: Influence of time on platelet adhesion on the surfaces. The graph represents the adhesion of platelets on different surfaces at three different time points (15mins, 1 hour, 4 hours).

7.2.4 Impact on Bacteria

7.2.4.1 Integration of Nanoparticles

Fe_3O_4 NPs, which were characterized and used earlier in Section 4.2.2, were used for creating nanocomposites with 3% of agarose. The concentration of NPs was selected at 2 mM, as optimized earlier, so that the nanocomposite doesn't lead to platelet activation. The final concentration of nanocomposite was calculated, and accordingly, the stock solution of NPs was added to the heated agarose solution before letting it cool down to room temperature.

7.2.4.1 Bacterial Growth on Modified Surfaces

The micrographs revealed that bacteria adhered to the glass significantly more than they did to agarose and their nanocomposite. The live dead staining revealed the percentage of dead bacteria was higher on the nanocomposite sample as compared to that on glass or the agarose samples (**Figure 57**).

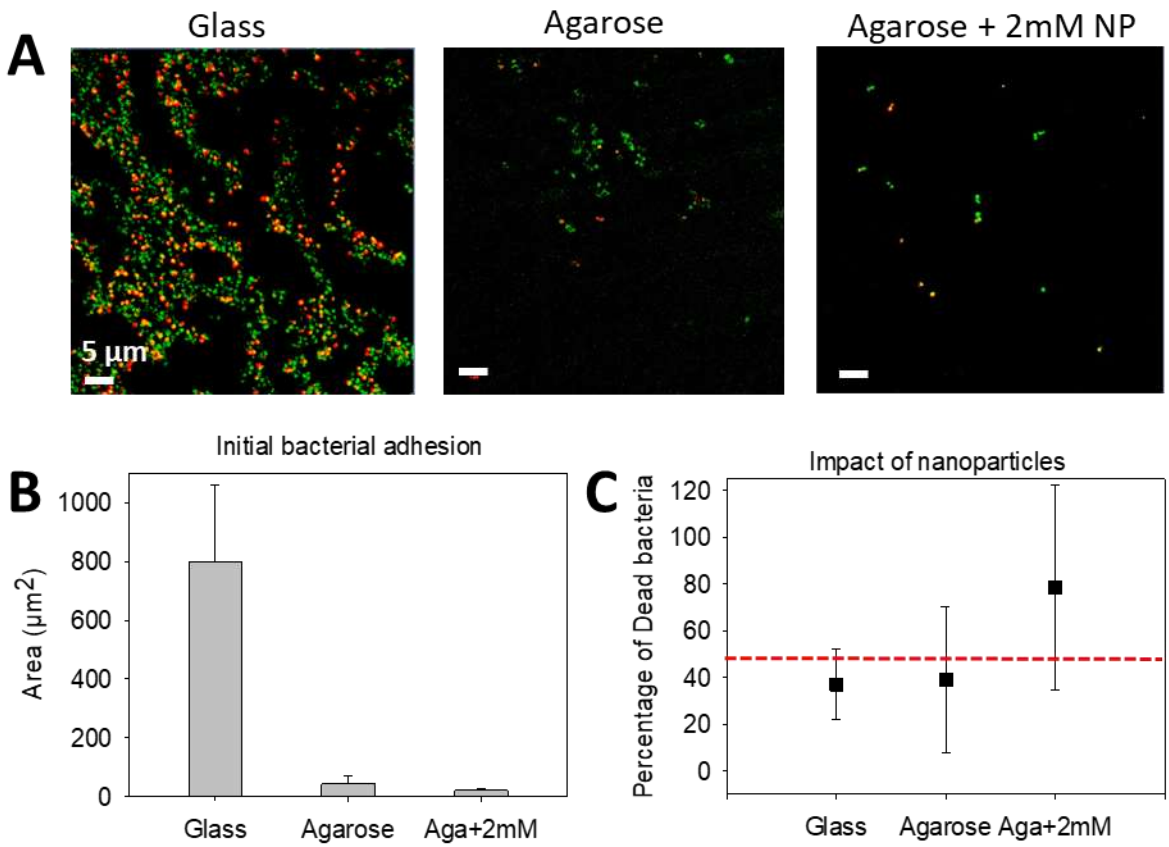

Figure 57: Antibacterial role of nanocomposites in inhibiting bacterial growth. (A) CLSM micrographs showing the bacterial adhesion of different surfaces Cyto-9 is used to stain live bacteria (green), and Propium Iodide (PI) is used to stain dead bacteria (red).(B) Graph displaying the total number of bacteria adhered to all surfaces.(C) The graph represents the percentage of dead bacteria on different surfaces.

7.3 Discussion

The results in Chapter 4 were already very promising, but the study revealed some limitations and the need to include surface patterns. Primarily, this is because fabricated agarose hydrogels can have varying topography on the meso- to macro scale. There may be some uneven domains that cause platelet localization and aggregation. Hence, they either have to be smoothed or should have uniform topography. In the case of choosing the former option, past studies, including the one in Chapter 5, have proved that platelets tend to adhere well and spread more on planar surfaces. On the contrary, patterned surfaces, particularly those at the submicron scale, can make a significant difference in the behavior of platelets.

It was discovered in this study that hydrophilic and stable agarose hydrogels can be successfully patterned using thermal-nano imprint lithography. Four different geometries,

namely dot, chain, pill, and square, were successfully transferred from a silicon wafer onto the agarose hydrogel films. The imprinted agarose films were able to repel platelets. The agarose based films strongly discourage bacterial fouling on their surfaces. Further, the gels, when incorporated with nanoparticles to fabricate nanocomposites, displayed their antibacterial properties. Though preliminary, the results with agarose gels imprinted with pill shaped topography seem promising.

The initial optimization of the agarose concentration from the previously used 1% in Chapter 4 to 3% in this study was crucial to establishing a stable imprinting procedure. Once the correct concentration was identified, other parameters like the heating temperature and the imprinting pressure could be selected. The homogeneous imprint visible in the AFM micrographs and line profiles could only be achieved through precise control of the imprint process. An equal volume of molten agarose gel was pipetted onto the surface of the glass substrate without creating air bubbles, which can interfere with the imprinting process. Consequently, sufficient time was given for the gel to cool down and harden so as not to destroy the imprinted structures. The results from water contact angle measurements were rather inconclusive. The contact angle measurements performed in Chapter 4 revealed the WCA for agarose films to be 10.6±6.8°; however, much higher values were reported during this study. The reason for this can be the higher concentration of agarose used in the films' formation. The submicron topologies did not seem to significantly alter the trends in the spreading of an air bubble used for the measurements in this captive bubble method of computing the WCA. Having said that, the values of patterned and nonpatterned agarose films still remain within the range of hydrophilic surfaces.

The platelet studies once again emphasize the previous findings from Chapter 4 that the agarose-based materials have a low level of platelet adhesion and activation as compared to other biomaterials. Agarose based materials have previously been shown to be non-thrombogenic in vivo, as they refrain from promoting clotting in animal models or when used in medical devices.[183] The number of platelets adhering was strikingly low on all the agarose based gels as compared to that on the glass surface. Not only were the results promising at the 1 hour time point, but even after 4 hours of incubation, the number of platelets adhering to the soft gels was consistently low. This demonstrates the excellent thrombocompatibilty of the agarose hydrogels. The CLSM images showed no signs of platelet activation on the agarose surfaces, unlike those of the glass surface, where the spiky filopodia and the planar lamellopdia

were clearly evident. Though these observations are preliminary and require further exploration, they are promising.

In the final phase of the study, the presumption put forward in the previous chapters was tested. The Fe_3O_4 nanoparticles, at a concentration of 2 mM as stated in Chapter 3, were incorporated in the agarose hydrogel to form a nanocomposite. The quantification of the bacterial adhesion on the surfaces revealed that the bacterial adhesion on agarose-based films was negligible in comparison to the glass surface, which exhibited the highest fouling. Furthermore, the nanocomposite was found to kill the highest number of bacteria as compared to the surfaces without nanoparticles. The antibacterial properties of iron nanoparticles integrated with hydrogels have been previously reported.[198,199] The physicochemical properties of materials are well known to influence bacterial adhesion.[241] The behavior of the bacteria on the hydrogels can also be attributed to their wetting properties. The wettability represented by the water contact angle at material surfaces is primarily determined in order to evaluate non-covalent surface interactions.[242] Thus the water contact angle is an important parameter for estimating the acting forces or energies between a substrate surface and bacteria, particularly during the early stages of an adhesion process.[241] The biofilm accumulation sequence is strongly associated with non-covalent forces acting between microorganisms and the corresponding substratum surface.[243]

The current work, in combination with the previous results from chapter 4, offers agarose as a strong candidate as a substitute for platelet storage material. Undoubtedly, additional elements must also be considered, but this is a solid starting point for accomplishing a broader objective.

7.4 Limitations

The quantification of platelets on glass becomes challenging since platelets activate rapidly after their initial contact. It has been previously reported that as little as a 15-minute time period is needed for the platelets to spread their cytoskeleton across the glass surface. Hence, in cases where the incubation of platelets is done for more than an hour, it will result in the formation of aggregates at some sites, which can be a challenge when quantifying the number of platelets. The challenges of CLSM-based imaging platelets on hydrogel surfaces have already been mentioned in Section 4.6.

The T-NIL technique was consistent and showed great reproducibility in imprinting the features toward the central region of the sample. However, as the periphery of the imprinted sample was screened, a few inhomogeneous and misaligned features partially overlapping with the adjacent ones were observed. In some cases, an outward drag was observed towards the features on the edges of the stamp. This could have been due to insufficient pressure during the imprinting process or polymer chain relaxation. In any case, it is important to control and improve the nanoimprinting process so that these problems are less likely to happen and high-quality imprinted patterns can be produced.

The scope of this study was limited to studying the impact of the nanoparticles on the inhibition of S. aureus bacteria. In practicality, there are more known strains that are known to infiltrate the platelet concentrates during their storage, with the majority of them being the ones found on the skin at the site of the puncture. Other pathogens include coagulase-negative Staphylococci, *viridans group Streptococci*, *Bacillus spp*., *Corynebacteria* as well as anaerobic diphteroid gram-positive bacilli such as *Propionibacterium acnes*.[71]

7.5 Conclusion and Outlook

The highly hydrophilic and platelet-friendly agarose hydrogels demonstrated a strong ability to undergo nanoimprinting and mold themselves into different shapes. The nanoimprinting technique is a fast, high-throughput technique that was optimized to fabricate agarose-based patterned samples. The antibacterial effect of iron nanoparticles integrated within agarose hydrogels to make nanocomposites was tested by their ability to inhibit the fouling of Staphylococcus aureus. Further quantification of dead bacteria revealed that nanocomposites showed a higher ability to kill the bacteria as compared to glass or agarose hydrogel. Agarose-based nanocomposites can be further explored for their potential applications in the area of platelet storage.

7.6 Experimental Section

7.6.1 Fabrication of Imprinted Nanopatterns

7.6.1.1 Master

The term "master" refers to the structure etched on the silicon (Si) wafer from which the stamp is derived. Masters can be fabricated using different techniques that can produce well-defined

structures on a surface. Here are the masters with different features and shapes, printed using e-beam lithography on Si substrate and obtained from GeSiM GmbH. The masters with four topographies, namely dot, chain, pill, and square, were selected for fabrication of agarose imprints using T-NIL. In principle, multiple stamps can be generated from a single master, and each such stamp can be used many times in the process of patterning or imprinting.

7.6.1.2 Stamp

PDMS (polydimethylsiloxane) is a colorless and transparent soft polymer that is used in the T-NIL process. The two components of the silicone elastomer Sylgard 184 (Dow Corning, Midland, USA) were used: 10 parts base and one part curing agent. In a glass container, 5 mL of the elastomer base and 0.5 mL of curing agent were added. The viscous mixture was thoroughly stirred for two minutes. The glass container was placed in an exsiccator and degassed at room temperature under a low vacuum. The degassed PDMS was then sucked into a syringe and prepared for use. The degassed PDMS was then sucked into a syringe and prepared for use. Meanwhile, the Si master was placed in the central cavity of the aluminum block (**Figure 58A,C**). A teflon spacer was added **Figure 58B**. The PDMS was then filled in the groove of the polycarbonate stamp holder **Figure 58D**. The PMMA plug is then pushed into the polycarbonate cylinder **Figure 58E**, and both are placed in the casting station over the existing master and spacer assemblies **Figure 58F**. The screw of the casting station was then fastened. PDMS was then injected into the inlet port until the liquid came out from the opposite side. The set-up is then placed in an oven at 65 °C for 4 hours for PDMS to crosslink. With the help of a scalpel, leaked PDMS was scraped. The demolding process was completed by carefully detaching the master from the stamp surface. The PMMA plug is then gently pulled out of the stamp body such that the newly fabricated PDMS diaphragm remains intact.

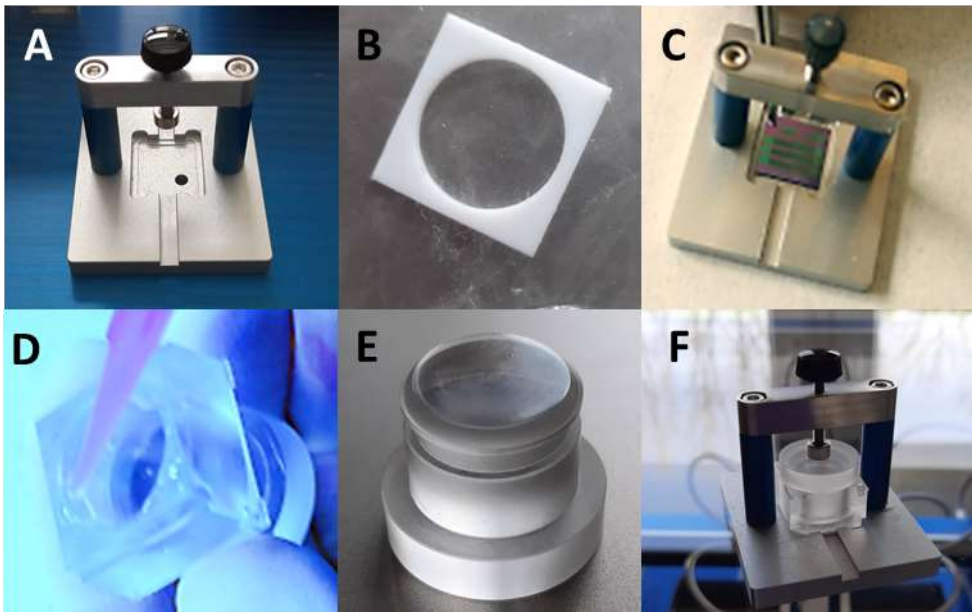

Figure 58: Components involved in imprinting procedure.

7.6.1.3 Resist

Resists are crucial components in the thermal nanoimprint lithography process (T-NIL). They act as a guide for transferring patterned features from the mold onto the substrate. In T-NIL, the resist is heated and pressed against the mold to form the pattern, and then removed to reveal the patterned substrate. In this study, 3% agarose in PBS was prepared. 1 mL of microwaved agarose solution was pipetted on a glass substrate and allowed to cool down for 15 min before starting the imprinting process.

7.6.1.4 Imprinting

The imprinting process was carried out using a GeSiM GmbH Microcontact-Printing System (µCP 3.0). The PDMS stamps fabricated earlier were picked up by the stamp holder. The substrates were placed on substrate holders, and the imprinting activity was conducted with the µ-CP control software (**Figure 59A**). The T-NIL process is then defined in the software by entering parameters like heater temperature, delay, cool down time, initial and final stamping pressure, etc. The set of parameters shown in **Figure 59A** was used for imprinting the agarose in this case. To summarize, the stamp was pressed onto the heated agarose films in order to imprint the material into the space between the features of the stamp. The agarose films were cut in a square shape along the periphery of the imprinted structures with the help of a laboratory spatula (**Figure 59B-C**).

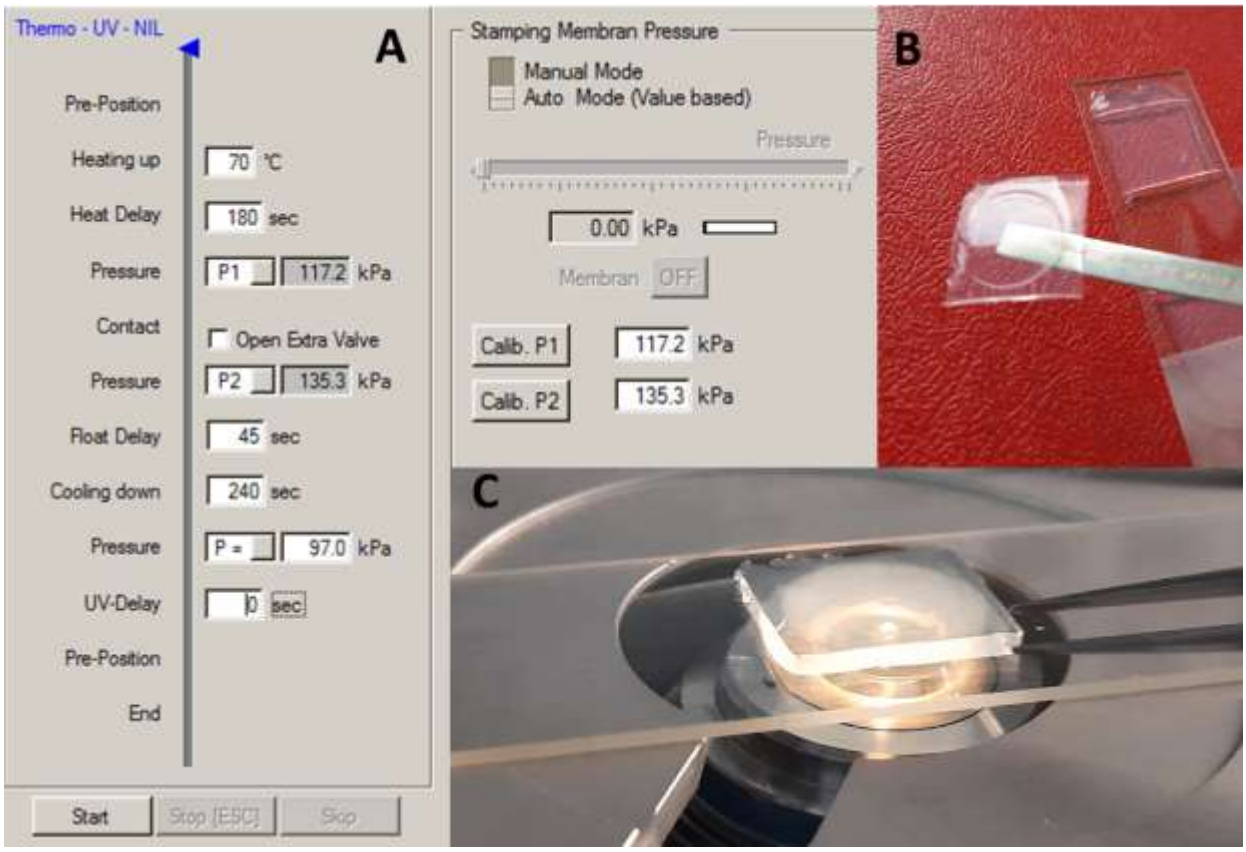

Figure 59: Parameters as viewed on the software interface along with the imprinted agarose film

7.6.2 Imaging by Atomic Force Microscopy

The imprinted patterns were imaged using AFM. AFM was used in force modulation mode to acquire the topographical scans. The images were captured at a line rate of 2 Hz and a resolution of 128 × 128 pixels for all samples. A Mikromasch cantilever (HQ: CSC38/tipless/No AI) with a nominal spring constant value of 0.09 N/m was used. A scan size of 100 × 100 µm² was used to scan each sample at 5 different regions. Using JPK Nanowizard4 software, line profiles of the features were obtained by selecting the image cross-section option to compute the size of each printed feature (**Figure 52**).

7.6.3 Water Contact Angle

The water contact angle of the glass surface and agarose films (patterned and nonpatterned) was measured using the OCA 15+ system (DataPhysics Instruments GmbH, Filderstadt, Germany) by using the captive bubble method. As previously stated, this method is particularly advantageous when dealing with surfaces with high surface free energy, especially to avoid the drying of hydrogels during measurement. A small air bubble with a volume of 3 µl was injected

beneath the sample, which was placed facing downward, at a dosing rate of 1 µl/s. The contact angle was calculated using the ellipse fitting method. All samples with different geometries were probed with three air bubbles at different positions. The calculation of contact angles was done by OCA 15+ software.

7.6.4 Platelet Studies

Platelets were isolated from the whole blood as mentioned in section **4.6.6 Isolation of Platelets**. Platelets were pipetted onto the samples at a concentration of 30,000/µL to the samples, and incubated for 1 h. Unbound platelets were removed by rinsing with phosphate buffered saline (PBS), and the platelets were fixed using 4% paraformaldehyde (PFA) for 30 min. To obtain CLSM micrographs, the fixed platelets were stained for 1 hour with anti-CD42a FITC antibodies (Dianova GmbH, Hamburg, Germany) at a final concentration of 0.1µg/ml platelet solution. The unbound dye was then washed off the sample twice with PBS. After that, samples were incubated for 10 minutes in permeable buffer before being incubated for 45 minutes at RT (23 °C) in the dark with phalloidin DY590 (Mobitec GmbH, Göttingen, Germany) (1:20 dilution). At RT in the dark, samples were examined using a confocal laser scanning microscope, the Zeiss LSM710 (Carl Zeiss, Gottingen, Germany). Using a 20× and 63× objective, the magenta fluorescent signal was acquired using the excitation/emission wavelengths = 488/520 nm and the cyan fluorescent signal was acquired using the excitation/emission wavelengths = 580/599 nm, respectively.

The samples were then imaged under a brightfield microscope with 40x magnification. The images were then processed by ImageJ. The processing was done by importing the image and then adjusting the contrast. Quantification involved measuring particles by filtering the area of platelets between 1 to 10 µm. The quantification on glass was approximate in the case of platelet aggregates. The influence of time was examined by quantifying the number of platelets adhered to the patterned and nonpatterned surfaces at different time points, 15 minutes, 1 hour, and 4 hours. The samples were then imaged under a brightfield microscope with 40x magnification. The platelets from two donors were used for independent experiments.

7.6.5 Bacterial Studies

Preparation for Staphylococcus aureus

The preculture was made by thawing 4 cryopearls of Staphylococcus aureus DSM 20231 (DSMZ-German Collection of Microorganisms and Cell Cultures GmbH, Braunschweig,

Germany) in 50 mL Tryptic Soy Broth, Medium 92 (TSB) (Sigma-Aldrich, Schnelldorf, Germany) to inoculate growth media. For the experiments, the culture was incubated overnight in a flask under sterile conditions by adding 20 µl of an existing preculture to TSB under continuous shaking. The bacteria concentration was measured on the following day using the LIVE/DEAD™ BacLight™ Bakterien-Viabilitäts-Kit, für die Mikroskopie und quantitative Assays (Thermo Fisher Scientific, Dreieich, Germany), which was used to stain the bacteria in the Thomas chamber by making a dilution of 1:1000. The suspension was prepared such that the final concentration was adjusted to 50000 bacteria in 2 mL of medium/ well. Each film sample was added to the well of a 12 well plate, followed by adding the bacteria together with the medium. The well plates were incubated overnight at 37°C on a shaker. The next day, discard the contents of each well. Rinse each well twice with PBS. To quantify bacterial adhesion on the surface of each sample, 0.3 µl Syto 9 for living bacteria and 0.15 µl propidium iodide for the dead was added in 500 µl of PBS. Bacteria were stained for 15 mins, following which the samples were then fixed. Syto 9 and propidium iodide (PI) are two different dyes that were used to differentiate between live and dead bacteria. Syto 9 is a green fluorescent nucleic acid stain that is able to penetrate the cell membrane of both live and dead cells and stain the DNA. PI is a fluorescent red nucleic acid stain that can only penetrate the cell membrane of dead cells and stain their DNA. At RT in the dark, samples were examined using a confocal laser scanning microscope, the Zeiss LSM710 (Carl Zeiss, Gottingen, Germany). Using a 20× objective, the green fluorescent signal was acquired using the excitation/emission wavelengths of 485/498 nm and the red fluorescent signal was acquired using the excitation/emission wavelengths of 535/617 nm, respectively.

Chapter 8: General Summary and Outlook

The global demand for platelet transfusions is rapidly shifting due to a combination of factors, including a growing population and advancements in medical treatments. Cancer patients, individuals with blood disorders, auto-immune disease, those undergoing organ transplant surgery, or those who have suffered trauma are frequently in dire need of platelets. The fact that platelets have a short shelf life complicates matters even more. The low shelf life of platelets can be attributed to surface-induced platelet activation and the risk of bacterial contamination. Add to that the threat of plasticizers leaching into the stored platelets and causing a risk of toxicity, and the overall problem just keeps aggravating. This work tried to address the problems in platelet storage on various levels.

In the initial part of the work, as an alternative to the artificial plastic material, agarose and gelatin based hydrogel films together with their nanocomposites obtained by admixing the iron nanoparticles were fabricated. Given their biocompatibility and ability to mimic the mechanical and physical properties of soft tissues, they were examined for their potential to inhibit platelet adhesion and spreading. The fabricated films were physically characterized, followed by platelet experiments that involved quantification of platelet spreading and measurement of the adhesive force experienced by the platelets when in contact with each surface. The agarose based films displayed overall better physicochemical and biological properties. The incorporation of iron nanoparticles was not only to improve the mechanical properties of the materials but also to impart antibacterial properties to the surface. The results obtained from analyzing the percentage of dead bacteria revealed that the antibacterial effect of the particles was evident.

However, the primary goal of the work was to develop a nanotopology for the surface because commercial platelet storage bags available on the market have impactless microtopography. This was achieved by implementing techniques like FluidFM, a direct writing method, and T- NIL, an embossing method. In the first technique, acrylate-based commercial ink was used to print 3D nanostructures. After optimizing various printing parameters, the pattern of a honeycomb hive and hemispherical grids were printed to minimize platelet activation and spreading. The printed patterns were physically characterized, and the behavior of platelets adhering to the patterns was studied. Following the achievement of statistically significant

results that indicated containment in platelet lamellopodial formation on the grid and the hive patterns, which were observed by accessing the platelet spread using microscopic imaging, further research into incorporating biofunctional molecules within the ink was carried out with the goal of developing platelet inhibitors that could be incorporated into platelet-friendly nanostructures. The capability of FluidFM was further explored by its ability to print structures by modifying topographical parameters like the height of the structure and the interspacing within adjoining structures, thus exhibiting the versatility of the technique. T-NIL was used to imprint selected geometrical shapes like dots, chains, pills, and squares by first transferring the patterns etched on the Si wafer onto the PDMS stamp and then by imprinting them onto the agarose resist. The imprinting parameters were optimized, following which the topography of the imprinted structures was examined. Platelet adhesion experiments revealed that the imprinted surfaces had few bound platelets, with pills-shaped geometry having the fewest bound platelets consistently.

The whole course of the study tried to not only address the problem of surface induced platelet activation but also address the associated problems in platelet storage. The following schematic in **Figure 60** shows the problems in the domain of platelet storage, the state-of-the art approaches to address these challenges, their unintended consequences, emphasizes the key contributions towards the topic, and highlights the implications of the findings.

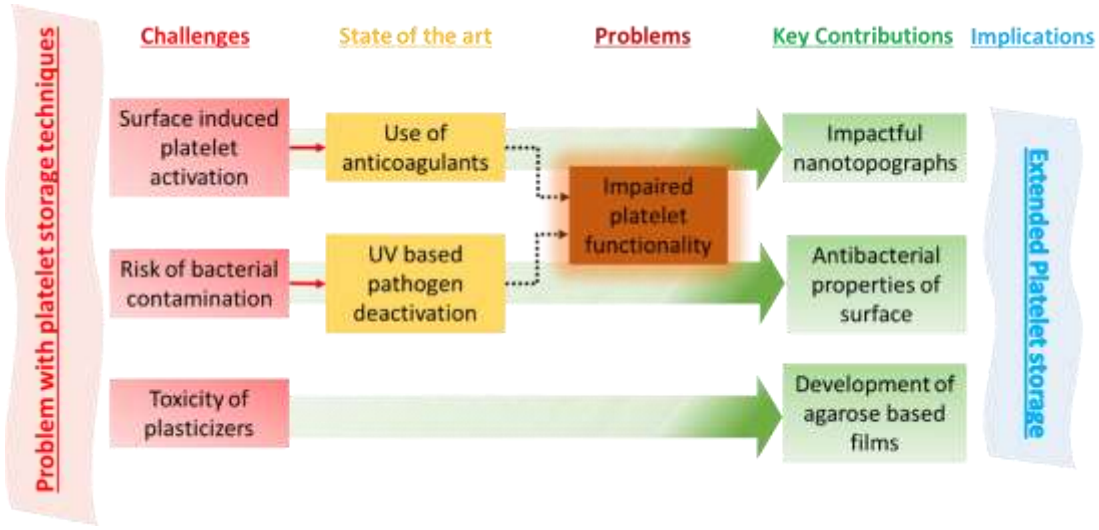

Figure 60: Schematic outlining the summary of the project

Though the results obtained during the course of the work have made significant headway in the field of platelet storage, there are still plenty of questions and open ends that can be

investigated in order to develop a novel platelet storage technique. To begin, a thorough investigation must be conducted to determine the ideal geometrical design by using methods such as modeling or finite element analysis to determine shape and dimensions for maximum platelet compatibility. The techniques used here by FluidFM can be implemented for developing a prototype, whereas the T-NIL can be employed for roll-to-roll pattern manufacturing because of its ability to produce high-quality patterns at high speeds and with low costs. As far as substituting the platelet bag material is concerned, agarose based hydrogels or nanocomposites can be applied in the form of coatings. However, other factors responsible for extending the shelf life of platelets like pH, temperature, and gas permeability should also be considered. The antibacterial properties of the iron nanoparticles are encouraging; however, a wide screening of other nanoparticles can be done in the future to obtain an even better outcome.

References

1. Ramaiah, L., Bounous, D. I. & Elmore, S. A. Hematopoietic System. *Haschek Rousseaux's Handb. Toxicol. Pathol.* 1863–1933 (2013).

2. Mcdonald, T. P. The regulation of megakaryocyte and platelet production. *Int. J. Cell Cloning* **7**, 139–155 (1989).

3. Boyle, R. *The Secret Life of the Sun*. *Scientific American* vol. 318 (Octopus, 2018).

4. Shin, E. K., Park, H., Noh, J. Y., Lim, K. M. & Chung, J. H. Platelet shape changes and cytoskeleton dynamics as novel therapeutic targets for anti-thrombotic drugs. *Biomol. Ther.* **25**, 223–230 (2017).

5. Blanco, A. & Blanco, G. Hemostasis. in *Medical Biochemistry* 781–789 (Academic Press, 2017).

6. French, D. L. & Seligsohn, U. Platelet Glycoprotein IIb/IIIa Receptors and Glanzmann's Thrombasthenia. *Arterioscler. Thromb. Vasc. Biol.* **20**, 607–610 (2000).

7. Selvadurai, M. V. & Hamilton, J. R. Structure and function of the open canalicular system – the platelet's specialized internal membrane network. **29**, 319–325 (2018).

8. Ebbeling, L., Robertson, C., McNicol, A. & Gerrard, J. M. Rapid Ultrastructural Changes in the Dense Tubular System Following Platelet Activation. *Blood* **80**, 718–723 (1992).

9. Ostrowska, M. *et al.* Stratified Approaches to Antiplatelet Therapies Based on Platelet Reactivity Testing. *Front. Cardiovasc. Med.* **6**, 176 (2019).

10. Gremmel, T., Frelinger, A. L. & Michelson, A. D. Platelet Physiology. (2016).

11. Blair, P. & Flaumenhaft, R. Platelet α–granules: Basic biology and clinical correlates. *Blood Rev.* **23**, 177 (2009).

12. Bergstrand, J. *et al.* Super-resolution microscopy can identify specific protein distribution patterns in platelets incubated with cancer cells. *Nanoscale* **11**, 10023–10033 (2019).

13. Reed, G. L. Platelet Secretion. in *Platelets* 309–318 (Academic Press, 2007).

14. Flaumenhaft, R. & Sharda, A. The life cycle of platelet granules. *F1000Research* **7**, (2018).

15. Wicki, A. N. *et al.* Isolation and characterization of human blood platelet mRNA and construction of a cDNA library in lambda gt11. Confirmation of the platelet derivation by identification of GPIb coding mRNA and cloning of a GPIb coding cDNA insert. *undefined* **61**, 448–453 (1989).

16. Denis, M. M. *et al.* Escaping the Nuclear Confines: Signal-Dependent Pre-mRNA Splicing in Anucleate Platelets. *Cell* **122**, 379 (2005).

17. Clemetson, K. J. & Clemetson, J. M. Platelet Receptors. *Platelets* 169–194 (2013).

18. Geraldo, R. B. *et al.* Platelets: Still a Therapeutical Target for Haemostatic Disorders. *Int. J. Mol. Sci.* **15**, 17901 (2014).

19. Bearer, E. L., Prakash, J. M. & Li, Z. Actin Dynamics in Platelets. *Int. Rev. Cytol.* **217**, 137 (2002).

20. Stalker, T. J., Newman, D. K., Ma, P., Wannemacher, K. M. & Brass, L. F. Platelet Signaling. *Handb. Exp. Pharmacol.* **210**, 59 (2012).

21. Periayah, M. H., Halim, A. S. & Saad, A. Z. M. Mechanism Action of Platelets and Crucial Blood Coagulation Pathways in Hemostasis. *Int. J. Hematol. Stem Cell Res.* **11**, 319 (2017).

22. Ham, H. O., Park, S. H., Kurutz, J. W., Szleifer, I. G. & Messersmith, P. B. Antifouling glycocalyx-mimetic peptoids. *J. Am. Chem. Soc.* **135**, 13015–13022 (2013).

23. Yau, J. W., Teoh, H. & Verma, S. Endothelial cell control of thrombosis. *BMC Cardiovasc. Disord.* **15**, 130 (2015).

24. Esmon, C. T. & Esmon, N. L. The link between vascular features and thrombosis. *Annu. Rev. Physiol.* **73**, 503–514 (2011).

25. Rivera, J., Lozano, M. L., Navarro-Núñez, L. & Vicente García, V. Platelet receptors and signaling in the dynamics of thrombus formation. *Haematologica* **94**, 700–711 (2009).

26. Jackson, S. P. The growing complexity of platelet aggregation. *Blood* **109**, 5087–5095 (2007).

27. Golebiewska, E. M. & Poole, A. W. Platelet secretion: From haemostasis to wound healing and beyond. *Blood Rev.* **29**, 153–162 (2015).

28. Fritz, M., Radmacher, M. & Gaub, H. E. Granula motion and membrane spreading during activation of human platelets imaged by atomic force microscopy. *Biophys. J.* **66**, 1328–1334 (1994).

29. Waples, L. M., Olorundare, O. E., Goodman, S. L., Lai, Q. J. & Albrecht, R. M. Platelet-polymer interactions: Morphologic and intracellular free calcium studies of individual human platelets. *J. Biomed. Mater. Res.* **32**, 65–76 (1996).

30. Fatisson, J., Mansouri, S., Yacoub, D., Merhi, Y. & Tabrizian, M. Determination of surface-induced platelet activation by applying time-dependency dissipation factor versus frequency using quartz crystal microbalance with dissipation.

31. Baumgartner HR, Muggli R, Tschopp TB, T. V. Platelet adhesion, release and aggregation in flowing blood: effects of surface properties and platelet function. *Thromb Haemost.* **35**, 124–138 (1976).

32. Park, K., Mao, F. W. & Park, H. Morphological characterization of surface-induced platelet activation. *Biomaterials* **11**, 24–31 (1990).

33. Escolar, G. & White, J. G. Combined use of immunocytochemical techniques and ligand-gold complexes for investigation of platelet membrane responses to surface

activation. *Microsc. Res. Tech.* **28**, 308–326 (1994).

34. Yoshimoto, Y. *et al.* Ultrastructural characterization of surface-induced platelet activation on artificial materials by transmission electron microscopy. *Microsc. Res. Tech.* **76**, 342–349 (2013).

35. Cerecedo, D., Cisneros, B., Mondragón, R., González, S. & Galván, I. J. Actin filaments and microtubule dual-granule transport in human adhered platelets: The role of α-dystrobrevins. *Br. J. Haematol.* **149**, 124–136 (2010).

36. Escolar, G., Leistikow, E. & White, J. G. The Fate of the Open Canalicular System in Surface and Suspension-Activated Platelets. *Blood* **74**, 1983–1988 (1989).

37. Cerecedo, D., Stock, R., González, S., Reyes, E. & Mondragón, R. Modification of actin, myosin and tubulin distribution during cytoplasmic granule movements associated with platelet adhesion. *Haematologica* **87**, 1165–1176 (2002).

38. Blumberg, N., Heal, J. M. & Phillips, G. L. Platelet transfusions: Trigger, dose, benefits, and risks. *F1000 Med. Rep.* **2**, 5 (2010).

39. Doherty, T. M. & Kelley, A. Bleeding Disorders. *Gynakologische Endokrinol.* **17**, 25–38 (2022).

40. Bielski, M., Yomtovian, R., Lazarus, H. M. & Rosenthal, N. Prolonged isolated thrombocytopenia after hematopoietic stem cell transplantation: Morphologic correlation. *Bone Marrow Transplant.* **22**, 1071–1076 (1998).

41. Wandt, H., Schäfer-Eckart, K. & Greinacher, A. Platelet transfusion in hematology, oncology and surgery. *Dtsch. Arztebl. Int.* **111**, 809–815 (2014).

42. Hamada, S. R. *et al.* Impact of platelet transfusion on outcomes in trauma patients. *Crit. Care* **26**, 1–10 (2022).

43. *Guidance for FDA Reviewers Premarket Notification Submissions for Empty Containers for the Collection and Processing of Blood and Blood Components*. http://www.fda.gov/cber/guidelines.htm (2001).

44. Kreuger, A. L. *et al.* Effect of storage time of platelet products on clinical outcomes after transfusion: a systematic review and meta-analyses. *Vox Sang.* **112**, 291–300 (2017).

45. Aubron, C., Flint, A. W. J., Ozier, Y. & McQuilten, Z. Platelet storage duration and its clinical and transfusion outcomes: A systematic review. *Crit. Care* **22**, 185 (2018).

46. Kilkson, H., Holme, S. & Murphy, S. Platelet Metabolism During Storage of Platelet Concentrates at 22 °C. *Blood* **64**, 406–414 (1984).

47. Sugimoto, A., Ohnoki, S., Yamaguchi, H. & Okubo, Y. Oxygen permeability of the container necessary for storage of platelet concentrate. *J. Japan Soc. Blood Transfus.* **35**, 26–31 (1989).

48. Sahler, J. *et al.* Platelet storage and transfusions: New concerns associated with an old therapy. *Drug Discov. Today Dis. Mech.* **8**, e9–e14 (2011).

49. Estcourt, L. J. Why has demand for platelet components increased? A review. *Transfus. Med.* **24**, 260–268 (2014).

50. Veihola, M., Aroviita, P., Linna, M., Sintonen, H. & Kekomäki, R. Variation of platelet production and discard rates in 17 blood centers representing 10 European countries from 2000 to 2002. *Transfusion* **46**, 991–995 (2006).

51. Ning, S. *et al.* Platelet Transfusion Practices in the ICU: Data From a Large Transfusion Registry. *Chest* **150**, 516–523 (2016).

52. Vlaar, A. P. J. *et al.* Supernatant of aged erythrocytes causes lung inflammation and coagulopathy in a two-hit in vivo syngeneic transfusion model. *Anesthesiology* **113**, 92–103 (2010).

53. Prowse, C. V., de Korte, D., Hess, J. R. & van der Meer, P. F. Commercially available blood storage containers. *Vox Sang.* **106**, 1–13 (2014).

54. Yuasa, T. *et al.* Improved extension of platelet storage in a polyolefin container with higher oxygen permeability. *Br. J. Haematol.* **126**, 153–159 (2004).

55. Vit, G., Klüter, H. & Wuchter, P. Platelet storage and functional integrity. *J. Lab. Med.* **44**, 285–293 (2020).

56. Etulain, J. *et al.* Hyperthermia inhibits platelet haemostatic functions and selectively regulates the release of alpha-granule proteins. *J. Thromb. Haemost.* **9**, 1562 (2011).

57. Handin, R. I. & Valeri, C. R. Improved Viability of Previously Frozen Platelets. *Blood* **40**, 509–513 (1972).

58. Alving, B. M., Reid, T. J., Fratantoni, J. C. & Finlayson, J. S. Frozen platelets and platelet substitutes in transfusion medicine. *Transfusion* **37**, 866–876 (1997).

59. Raynel, S., Padula, M. P., Marks, D. C. & Johnson, L. Cryopreservation alters the membrane and cytoskeletal protein profile of platelet microparticles. *Transfusion* **55**, 2422–2432 (2015).

60. Johnson, L., Coorey, C. P. & Marks, D. C. The hemostatic activity of cryopreserved platelets is mediated by phosphatidylserine-expressing platelets and platelet microparticles. *Transfusion* **54**, 1917–1926 (2014).

61. Eker, İ. *et al.* Generation of Platelet Microparticles after Cryopreservation of Apheresis Platelet Concentrates Contributes to Hemostatic Activity. *Turkish J. Hematol.* **34**, 64 (2017).

62. Slichter, S. J. *et al.* Review of in vivo studies of dimethyl sulfoxide cryopreserved platelets. *Transfus. Med. Rev.* **28**, 212–225 (2014).

63. Lozano, M. & Cid, J. Cryopreserved platelets: a narrative review of its current role in transfusion therapy. *Ann. Blood* **0**, 0–0 (2021).

64. Zhao, H. & Devine, D. V. The Missing Pieces to the Cold-Stored Platelet Puzzle. *Int. J. Mol. Sci.* **23**, (2022).

65. For bleeding patients, can cold storage of platelets improve blood clotting? –

Washington University School of Medicine in St. Louis. https://medicine.wustl.edu/news/for-bleeding-patients-can-cold-storage-of-platelets-improve-blood-clotting/.

66. Holme, S., Heaton, W. A. & Courtright, M. Platelet Storage Lesion in Second-Generation Containers: Correlation with Platelet ATP Levels. *Vox Sang.* **53**, 214–220 (1987).

67. Dekkers, D. W. C., De Cuyper, I. M., Van Der Meer, P. F., Verhoeven, A. J. & De Korte, D. Influence of pH on stored human platelets. *Transfusion* **47**, 1889–1895 (2007).

68. Van Der Meer, P. F. *et al.* In vitro comparison of platelet storage in plasma and in four platelet additive solutions, and the effect of pathogen reduction: a proposal for an in vitro rating system. *Vox Sang.* **98**, 517–524 (2010).

69. Simon, T. L., Nelson, E. J. & Murphy, S. Extension of platelet concentrate storage to 7 days in second-generation bags. *Transfusion* **27**, 6–9 (1987).

70. Van der Meer, P. F. & Korte, D. de. Platelet preservation: Agitation and containers. *Transfus. Apher. Sci.* **44**, 297–304 (2011).

71. Védy, D. *et al.* Bacterial contamination of platelet concentrates: pathogen detection and inactivation methods. *Hematol. Rep.* **1**, 5 (2009).

72. Hamzeh-Cognasse, H. *et al.* Platelets and infections - Complex interactions with bacteria. *Front. Immunol.* **6**, 82 (2015).

73. Portier, I. & Campbell, R. A. Role of platelets in detection and regulation of infection. *Arterioscler. Thromb. Vasc. Biol.* **41**, 70 (2021).

74. Pamphilon, D. H. *et al.* Platelet concentrates irradiated with ultraviolet light retain satisfactory in vitro storage characteristics and in vivo survival. *Br. J. Haematol.* **75**, 240–244 (1990).

75. HUSTON, B. M., Brecher, M. D. & BANDARENKO, N. Lack of Efficacy for Conventional Gamma Irradiation of Platelet Concentrates to Abrogate Bacterial Growth. *Coagul. Transfus. Med.* **109**, 743–747 (1998).

76. Nodeh, F. K., Hosseini, E. & Ghasemzadeh, M. The effect of gamma irradiation on platelet redox state during storage. *Transfusion* **61**, 579–593 (2021).

77. Qanash, H. The Possibility to Expand Platelets' Storage Time Beyond Five Days. *Hail J. Heal. Sci.* **3**, 1 (2021).

78. Bruun-Rasmussen, P., Kragh Andersen, P., Banasik, K., Brunak, S. & Johansson, P. I. Intervening on the storage time of RBC units and its effects on adverse recipient outcomes using real-world data. *Blood* **139**, 3647–3654 (2022).

79. Stubbs, J. R., Shaz, B. H., Vassallo, R. R. & Roback, J. D. Expanding the platelet inventory to mitigate the impact of severe shortages. *Hematol. Am. Soc. Hematol. Educ. Progr.* **2022**, 424 (2022).

80. Apte, G. *et al.* Modulation of Platelet-Surface Activation: Current State and Future

Perspectives. *ACS Appl. Bio Mater.* **3**, 5574–5589 (2020).

81. Bui, V. C. *et al.* Response of Human Blood Platelets on Nanoscale Groove Patterns: Implications for Platelet Storage. *ACS Appl. Nano Mater.* **3**, 6996–7004 (2020).

82. Kämmerer, P. W. *et al.* Early implant healing: Promotion of platelet activation and cytokine release by topographical, chemical and biomimetical titanium surface modifications in vitro. *Clin. Oral Implants Res.* **23**, 504–510 (2012).

83. Vogler, E. A. Water and the acute biological response to surfaces. *J. Biomater. Sci. Polym. Ed.* **10**, 1015–1045 (1999).

84. Ishihara, K. Bioinspired phospholipid polymer biomaterials for making high performance artificial organs. *Sci. Technol. Adv. Mater.* **1**, 131–138 (2000).

85. Holmlin, R. E., Chen, X., Chapman, R. G., Takayama, S. & Whitesides, G. M. Zwitterionic SAMs that resist nonspecific adsorption of protein from aqueous buffer. *Langmuir* **17**, 2841–2850 (2001).

86. Ostuni, E., Chapman, R. G., Holmlin, R. E., Takayama, S. & Whitesides, G. M. A survey of structure-property relationships of surfaces that resist the adsorption of protein. *Langmuir* **17**, 5605–5620 (2001).

87. Tanaka, M. *et al.* Blood compatible aspects of poly(2-methoxyethylacrylate) (PMEA)-relationship between protein adsorption and platelet adhesion on PMEA surface. *Biomaterials* **21**, 1471–1481 (2000).

88. Milleret, V. *et al.* Protein adsorption steers blood contact activation on engineered cobalt chromium alloy oxide layers. *Acta Biomater.* **24**, 343–351 (2015).

89. Hylton, D. M., Shalaby, S. W. & Latour, R. A. Direct correlation between adsorption-induced changes in protein structure and platelet adhesion. *J. Biomed. Mater. Res. - Part A* **73**, 349–358 (2005).

90. Yang, M. C. *et al.* Electrochemical polymerization of PEDOT-graphene oxide-heparin composite coating for anti-fouling and anti-clotting of cardiovascular stents. *Polymers (Basel).* **11**, 1520 (2019).

91. Tanaka, M., Sawaguchi, T., Sato, Y., Yoshioka, K. & Niwa, O. Synthesis of phosphorylcholine-oligoethylene glycol-alkane thiols and their suppressive effect on non-specific adsorption of proteins. *Tetrahedron Lett.* **50**, 4092–4095 (2009).

92. Corum, L. E. & Hlady, V. Screening platelet–surface interactions using negative surface charge gradients. *Biomaterials* **31**, 3148–3155 (2010).

93. Park, K. D. *et al.* Platelet adhesion and activation on polyethylene glycol modified polyurethane surfaces. Measurement of cytoplasmic calcium. *ASAIO J.* **42**, (1996).

94. Kim, M. H., Sawada, Y., Taya, M. & Kino-oka, M. Influence of surface topography on the human epithelial cell response to micropatterned substrates with convex and concave architectures. *J. Biol. Eng.* **8**, 13 (2014).

95. Park, S. *et al.* Nanopatterned Scaffolds for Neural Tissue Engineering and Regenerative Medicine. *Adv. Exp. Med. Biol.* **1078**, 421–443 (2018).

96. Shekaran, A. & Garcia, A. J. Nanoscale engineering of extracellular matrix-mimetic bioadhesive surfaces and implants for tissue engineering. *Biochim. Biophys. Acta - Gen. Subj.* **1810**, 350–360 (2011).

97. Firkowska-Boden, I., Zhang, X. & Jandt, K. D. Controlling Protein Adsorption through Nanostructured Polymeric Surfaces. *Adv. Healthc. Mater.* **7**, 1700995 (2018).

98. Wang, J., Hu, H., Yang, Z., Wei, J. & Li, J. IPN hydrogel nanocomposites based on agarose and ZnO with antifouling and bactericidal properties. *Mater. Sci. Eng. C* **61**, 376–386 (2016).

99. Wang, Y. *et al.* Research of protein adsorption on the different surface topography of the zinc oxide. *Surf. Interface Anal.* **47**, 245–252 (2015).

100. Curtis, A. & Wilkinson, C. Topographical control of cells. *Biomaterials* **18**, 1573–1583 (1997).

101. Curtis, A. S. G., Dolby, M. & Gadegaand, N. Cell signaling arising from nanotopography: Implications for nanomedical devices. *Nanomedicine* **1**, 67–72 (2006).

102. Hasirci, V. & Kenar, H. Novel surface patterning approaches for tissue engineering and their effect on cell behavior. *Nanomedicine* **1**, 73–90 (2006).

103. Kulangara, K. & Leong, K. W. Substrate topography shapes cell function. *Soft Matter* **5**, 4072–4076 (2009).

104. Ermis, M., Antmen, E. & Hasirci, V. Micro and Nanofabrication methods to control cell-substrate interactions and cell behavior: A review from the tissue engineering perspective. *Bioact. Mater.* **3**, 355–369 (2018).

105. Webster, T. J. & Ahn, E. S. Nanostructured biomaterials for tissue engineering bone. *Adv. Biochem. Eng. Biotechnol.* **103**, 275–308 (2006).

106. Valencia, S., Gretzer, C. & Cooper, L. F. Surface nanofeature effects on titanium-adherent human mesenchymal stem cells. *J. Prosthet. Dent.* **102**, 164 (2009).

107. Milner, K. R., Snyder, A. J. & Siedlecki, C. A. Sub-micron texturing for reducing platelet adhesion to polyurethane biomaterials. *J. Biomed. Mater. Res. - Part A* **76**, 561–570 (2006).

108. Mao, C. *et al.* Preparation of lotus-leaf-like polystyrene micro- and nanostructure films and its blood compatibility. *J. Mater. Chem.* **19**, 9025–9029 (2009).

109. Simon-Walker, R. *et al.* Glycocalyx-inspired nitric oxide-releasing surfaces reduce platelet adhesion and activation on titanium. *ACS Biomater. Sci. Eng.* **3**, 68–77 (2017).

110. Koh, L. B., Rodriguez, I. & Venkatraman, S. S. The effect of topography of polymer surfaces on platelet adhesion. *Biomaterials* **31**, 1533–1545 (2010).

111. Hulander, M. *et al.* Gradients in surface nanotopography used to study platelet adhesion and activation. *Colloids Surfaces B Biointerfaces* **110**, 261–269 (2013).

112. Sheppeck, R., Bentz, M., Dickson, C., Hribar, S. & White, J. Examination of the roles

of glycoprotein Ib and glycoprotein IIb/IIIa in platelet deposition on an artificial surface using clinical antiplatelet agents and monoclonal. (1991).

113. Tsai, W. B., Grunkemeier, J. M., McFarland, C. D. & Horbett, T. A. Platelet adhesion to polystyrene-based surfaces preadsorbed with plasmas selectively depleted in fibrinogen, fibronectin, vitronectin, or von Willebrand's factor. *J. Biomed. Mater. Res.* **60**, 348–359 (2002).

114. Qiu, Y. *et al.* Platelet mechanosensing of substrate stiffness during clot formation mediates adhesion, spreading, and activation. *Proc. Natl. Acad. Sci. U. S. A.* **111**, 14430–14435 (2014).

115. Kaneva, V. N., Martyanov, A. A., Morozova, D. S., Panteleev, M. A. & Sveshnikova, A. N. Platelet Integrin αIIbβ3: Mechanisms of Activation and Clustering; Involvement into the Formation of the Thrombus Heterogeneous Structure. *Biochem. Suppl. Ser. A Membr. Cell Biol.* **13**, 97–110 (2019).

116. Kee, M. F., Myers, D. R., Sakurai, Y., Lam, W. A. & Qiu, Y. Platelet mechanosensing of collagen matrices. *PLoS One* **10**, e0126624 (2015).

117. Apte, G., Lindenbauer, A., Schemberg, J., Rothe, H. & Nguyen, T. H. Controlling Surface-Induced Platelet Activation by Agarose and Gelatin-Based Hydrogel Films. *ACS Omega* **6**, 10963–10974 (2021).

118. Biran, R. & Pond, D. Heparin coatings for improving blood compatibility of medical devices. *Adv. Drug Deliv. Rev.* **112**, 12–23 (2017).

119. Follmann, H. D. M. *et al.* Advanced fibroblast proliferation inhibition for biocompatible coating by electrostatic layer-by-layer assemblies of heparin and chitosan derivatives. *J. Colloid Interface Sci.* **474**, 9–17 (2016).

120. Sabino, R. M. *et al.* Enhanced hemocompatibility and antibacterial activity on titania nanotubes with tanfloc/heparin polyelectrolyte multilayers. *J. Biomed. Mater. Res. - Part A* **108**, 992–1005 (2020).

121. Li, G. *et al.* The effect of coimmobilizing heparin and fibronectin on titanium on hemocompatibility and endothelialization. *Biomaterials* **32**, 4691–4703 (2011).

122. Yang, Y. *et al.* Polydopamine Modified TiO2 Nanotube Arrays for Long-Term Controlled Elution of Bivalirudin and Improved Hemocompatibility. *ACS Appl. Mater. Interfaces* **10**, 7649–7660 (2018).

123. Yang, T. *et al.* From surface to bulk modification: Plasma polymerization of amine-bearing coating by synergic strategy of biomolecule grafting and nitric oxide loading. *Bioact. Mater.* **5**, 17–25 (2020).

124. Luo, R. *et al.* Multifunctional coatings that mimic the endothelium: surface bound active heparin nanoparticles with in situ generation of nitric oxide from nitrosothiols. *J. Mater. Chem. B* **6**, 5582–5595 (2018).

125. Chug, M. K. & Brisbois, E. J. Recent Developments in Multifunctional Antimicrobial Surfaces and Applications toward Advanced Nitric Oxide-Based Biomaterials. *ACS Mater. Au* **2**, 525–551 (2022).

126. Apte, G., Hirtz, M. & Nguyen, T.-H. FluidFM-Based Fabrication of Nanopatterns: Promising Surfaces for Platelet Storage Application. *ACS Appl. Mater. Interfaces* **14**, 24133–24143 (2022).

127. Berganza, E., Apte, G., Vasantham, S. K., Nguyen, T.-H. H. & Hirtz, M. Integration of Biofunctional Molecules into 3D-Printed Polymeric Micro-/Nanostructures. *Polymers (Basel).* **14**, 1327 (2022).

128. Gustavsson, P. E. & Son, P. O. L. Monolithic Polysaccharide Materials. *J. Chromatogr. Libr.* **67**, 121–141 (2003).

129. Arnott, S. *et al.* The agarose double helix and its function in agarose gel structure. *J. Mol. Biol.* **90**, 269–284 (1974).

130. Araki, C. Structure of the Agarose Constituent of Agar-agar. *Bull. Chem. Soc. Jpn.* **29**, 543–544 (1956).

131. Zhang, Y., Fu, X., Duan, D., Xu, J. & Gao, X. Preparation and characterization of agar, agarose, and agaropectin from the red alga Ahnfeltia plicata. *J. Oceanol. Limnol.* **37**, 815–824 (2019).

132. Zarrintaj, P. *et al.* Agarose-based biomaterials for tissue engineering. *Carbohydr. Polym.* **187**, 66–84 (2018).

133. Tako, M., Tamaki, Y., Teruya, T. & Takeda, Y. The Principles of Starch Gelatinization and Retrogradation. *Food Nutr. Sci.* **05**, 280–291 (2014).

134. Geckil, H., Xu, F., Zhang, X., Moon, S. & Demirci, U. Engineering hydrogels as extracellular matrix mimics. *Nanomedicine* **5**, 469–484 (2010).

135. Salati, M. A. *et al.* Agarose-Based Biomaterials: Opportunities and Challenges in Cartilage Tissue Engineering. *Polym. 2020, Vol. 12, Page 1150* **12**, 1150 (2020).

136. Tako, M. & Nakamura, S. Gelation mechanism of agarose. *Carbohydr. Res.* **180**, 277–284 (1988).

137. Tako, M. Structural Principles of Polysaccharide Gels. *J. Appl. Glycosci.* **47**, 49–53 (2000).

138. Campos, F. *et al.* Evaluation of Fibrin-Agarose Tissue-Like Hydrogels Biocompatibility for Tissue Engineering Applications. *Front. Bioeng. Biotechnol.* **8**, 596 (2020).

139. Khodadadi Yazdi, M. *et al.* Agarose-based biomaterials for advanced drug delivery. *J. Control. Release* **326**, 523–543 (2020).

140. Haessler, U., Kalinin, Y., Swartz, M. A. & Wu, M. An agarose-based microfluidic platform with a gradient buffer for 3D chemotaxis studies. *Biomed. Microdevices* **11**, 827–835 (2009).

141. Soffe, R., Altenhuber, N., Bernach, M., Remus-Emsermann, M. N. P. & Nock, V. Comparison of replica leaf surface materials for phyllosphere microbiology. *PLoS One* **14**, e0218102 (2019).

142. Moore, M. J. *et al.* The dance of the nanobubbles: detecting acoustic backscatter from sub-micron bubbles using ultra-high frequency acoustic microscopy. *Nanoscale* **12**, 21420–21428 (2020).

143. Vahabi, S., Nazemi Salman, B. & Javanmard, A. Atomic Force Microscopy Application in Biological Research: A Review Study. *Iran. J. Med. Sci.* **38**, 76 (2013).

144. Meister, A. *et al.* FluidFM: Combining atomic force microscopy and nanofluidics in a universal liquid delivery system for single cell applications and beyond. *Nano Lett.* **9**, 2501–2507 (2009).

145. Guillaume-Gentil, O., Zambelli, T. & Vorholt, J. A. Isolation of single mammalian cells from adherent cultures by fluidic force microscopy. *Lab Chip* **14**, 402–414 (2014).

146. Potthoff, E., Ossola, D., Zambelli, T. & Vorholt, J. A. Bacterial adhesion force quantification by fluidic force microscopy. *Nanoscale* **7**, 4070–4079 (2015).

147. Potthoff, E. *et al.* Rapid and Serial Quantification of Adhesion Forces of Yeast and Mammalian Cells. *PLoS One* **7**, e52712 (2012).

148. Guillaume-Gentil, O., Mittelviefhaus, M., Dorwling-Carter, L., Zambelli, T. & Vorholt, J. A. FluidFM Applications in Single-Cell Biology. *Open-sp. Microfluid. Concepts, Implementations, Appl.* 325–354 (2018).

149. Patrick, F., Paul, W. & Dalia, Y. FluidFM: Precise fluidic positioning and delivery platform with applications in cell biology and soft matter - 2018 - Wiley Analytical Science. *Wiley analytical science* (2018).

150. Hirt, L. *et al.* Template-Free 3D Microprinting of Metals Using a Force-Controlled Nanopipette for Layer-by-Layer Electrodeposition. *Adv. Mater.* **28**, 2311–2315 (2016).

151. Khalili, A. A. & Ahmad, M. R. A Review of Cell Adhesion Studies for Biomedical and Biological Applications. *Int. J. Mol. Sci.* **16**, 18149 (2015).

152. Cohen, N., Sarkar, S., Hondroulis, E., Sabhachandani, P. & Konry, T. Quantification of intercellular adhesion forces measured by fluid force microscopy. *Talanta* **174**, 409–413 (2017).

153. Amarouch, M. Y., El Hilaly, J. & Mazouzi, D. AFM and FluidFM Technologies: Recent Applications in Molecular and Cellular Biology. *Scanning* **2018**, (2018).

154. Zambelli, T. *et al.* FluidFM: Development of the Instrument as well as Its Applications for 2D and 3D Lithography. *Open-sp. Microfluid. Concepts, Implementations, Appl.* 295–323 (2018).

155. Grüter, R. R., Vörös, J. & Zambelli, T. FluidFM as a lithography tool in liquid: spatially controlled deposition of fluorescent nanoparticles. *Nanoscale* **5**, 1097–1104 (2013).

156. Berganza, E. & Hirtz, M. Direct-Write Patterning of Biomimetic Lipid Membranes in Situ with FluidFM. *ACS Appl. Mater. Interfaces* **13**, 50774–50784 (2021).

157. Ventrici De Souza, J. *et al.* Three-Dimensional Nanoprinting via Direct Delivery. *J.*

Phys. Chem. B **122**, 956–962 (2018).

158. Deng, W. N., Wang, S., Ventrici de Souza, J., Kuhl, T. L. & Liu, G. New Algorithm to Enable Construction and Display of 3D Structures from Scanning Probe Microscopy Images Acquired Layer-by-Layer. *J. Phys. Chem. A* **122**, 5756–5763 (2018).

159. LOCTITE AA 3491 - Light-cure, acrylic-based instant adhesive - Henkel Adhesives. https://www.henkel-adhesives.com/de/en/product/uv-curing-adhesives/loctite_aa_3491.html.

160. Pattison, T. G., Wang, S., Miller, R. D., Liu, G. & Qiao, G. G. 3D nanoprinting via spatially controlled assembly and polymerization. *Nat. Commun.* **13**, 1941 (2022).

161. Lee, A. *et al.* 3D bioprinting of collagen to rebuild components of the human heart. *Science (80-.).* **365**, 482–487 (2019).

162. Wang, D., Xu, Y., Li, Q. & Turng, L. S. Artificial small-diameter blood vessels: Materials, fabrication, surface modification, mechanical properties, and bioactive functionalities. *J. Mater. Chem. B* **8**, 1801–1822 (2020).

163. Ma, K., Khan, M. A. & Hussain, A. Haemodialysis Membranes: A Review. *J Membr Sci Technol* **9**, 199 (2019).

164. Rebelo, R., Fernandes, M. & Fangueiro, R. Biopolymers in Medical Implants: A Brief Review. *Procedia Eng.* **200**, 236–243 (2017).

165. Stamatialis, D. F. *et al.* Medical applications of membranes: Drug delivery, artificial organs and tissue engineering. *J. Memb. Sci.* **308**, 1–34 (2008).

166. Zhu, J. & Marchant, R. E. Dendritic saccharide surfactant polymers as antifouling interface materials to reduce platelet adhesion. *Biomacromolecules* **7**, 1036–1041 (2006).

167. Sin, D. C., Kei, H. L. & Miao, X. Surface coatings for ventricular assist devices. *Expert Rev. Med. Devices* **6**, 51–60 (2009).

168. Nguyen, T. H. *et al.* Rupture Forces among Human Blood Platelets at different Degrees of Activation. *Sci. Rep.* **6**, 25402 (2016).

169. Smyth, S. S. & Parise, L. V. Regulation of ligand binding to glycoprotein IIb-IIIa (integrin α(IIb)β3) in isolated platelet membranes. *Biochem. J.* **292**, 749–758 (1993).

170. Jaffer, I. H., Fredenburgh, J. C., Hirsh, J. & Weitz, J. I. Medical device-induced thrombosis: What causes it and how can we prevent it? *J. Thromb. Haemost.* **13**, S72–S81 (2015).

171. Smith, S. A., Travers, R. J. & Morrissey, J. H. How it all starts: Initiation of the clotting cascade. *Crit. Rev. Biochem. Mol. Biol.* **50**, 326–336 (2015).

172. Peng, M., Kurokawa, T., Gong, J. P., Osada, Y. & Zheng, Q. Effect of surface roughness of hydrophobic substrate on heterogeneous polymerization of hydrogels. *J. Phys. Chem. B* **106**, 3073–3081 (2002).

173. Murosaki, T., Ahmed, N. & Ping Gong, J. Antifouling properties of hydrogels. *Sci.*

Technol. Adv. Mater. **12**, 064706 (2011).

174. Itagaki, N. *et al.* Surface Characterization and Platelet Adhesion on Thin Hydrogel Films of Poly(vinyl ether). *Langmuir* **33**, 14332–14339 (2017).

175. Lee, K. Y. & Mooney, D. J. Hydrogels for tissue engineering. *Chem. Rev.* **101**, 1869–1879 (2001).

176. Slaughter, B. V., Khurshid, S. S., Fisher, O. Z., Khademhosseini, A. & Peppas, N. A. Hydrogels in regenerative medicine. *Adv. Mater.* **21**, 3307–3329 (2009).

177. Gaharwar, A. K., Peppas, N. A. & Khademhosseini, A. Nanocomposite hydrogels for biomedical applications. *Biotechnol. Bioeng.* **111**, 441–453 (2014).

178. Sperling, C., Fischer, M., Maitz, M. F. & Werner, C. Blood coagulation on biomaterials requires the combination of distinct activation processes. *Biomaterials* **30**, 4447–4456 (2009).

179. Awad, H. A., Wickham, M. Q., Leddy, H. A., Gimble, J. M. & Guilak, F. Chondrogenic differentiation of adipose-derived adult stem cells in agarose, alginate, and gelatin scaffolds. *Biomaterials* **25**, 3211–3222 (2004).

180. Ahearne, M., Liu, Y. & Kelly, D. J. Combining freshly isolated chondroprogenitor cells from the infrapatellar fat pad with a growth factor delivery hydrogel as a putative single stage therapy for articular cartilage repair. *Tissue Eng. - Part A* **20**, 930–939 (2014).

181. Stokols, S. & Tuszynski, M. H. Freeze-dried agarose scaffolds with uniaxial channels stimulate and guide linear axonal growth following spinal cord injury. *Biomaterials* **27**, 443–451 (2006).

182. Rashid, T. U. *et al.* Gelatin-Based Hydrogels. in *Cellulose-Based Superabsorbent Hydrogels* 1601–1641 (Springer, Cham, 2019).

183. van Oss, C. J., Zingg, W., Hum, O. S. & Neumann, A. W. Platelet activation on agar/agarose gel surfaces: Variation correlated with casting technique and hydrophobic/hydrophilic balance as reflected in contact angle measurements. *Thromb. Res.* **11**, 183–191 (1977).

184. Dannert, C., Stokke, B. T. & Dias, R. S. Nanoparticle-hydrogel composites: From molecular interactions to macroscopic behavior. *Polymers (Basel).* **11**, 275 (2019).

185. Gao, W., Zhang, Y., Zhang, Q. & Zhang, L. Nanoparticle-Hydrogel: A Hybrid Biomaterial System for Localized Drug Delivery. *Ann. Biomed. Eng.* **44**, 2049–2061 (2016).

186. Rafieian, S., Mirzadeh, H., Mahdavi, H. & Masoumi, M. E. A review on nanocomposite hydrogels and their biomedical applications. *IEEE J. Sel. Top. Quantum Electron.* **26**, 154–174 (2019).

187. Ayala, V., Herrera, A. P., Latorre-Esteves, M., Torres-Lugo, M. & Rinaldi, C. Effect of surface charge on the colloidal stability and in vitro uptake of carboxymethyl dextran-coated iron oxide nanoparticles. *J. Nanoparticle Res.* **15**, 1874 (2013).

188. Allia, P. *et al.* Fe3O4nanoparticles and nanocomposites with potential application in biomedicine and in communication technologies: Nanoparticle aggregation, interaction, and effective magnetic anisotropy. *J. Appl. Phys.* **116**, 113903 (2014).

189. Anastasova, E. I. *et al.* A pure magnetite hydrogel: Synthesis, properties and possible applications. *Soft Matter* **13**, 8651–8660 (2017).

190. Gabrielyan, L., Hovhannisyan, A., Gevorgyan, V., Ananyan, M. & Trchounian, A. Antibacterial effects of iron oxide (Fe 3 O 4) nanoparticles: distinguishing concentration-dependent effects with different bacterial cells growth and membrane-associated mechanisms. *Appl. Microbiol. Biotechnol.* **103**, 2773–2782 (2019).

191. Gabrielyan, L., Badalyan, H., Gevorgyan, V. & Trchounian, A. Comparable antibacterial effects and action mechanisms of silver and iron oxide nanoparticles on Escherichia coli and Salmonella typhimurium. *Sci. Rep.* **10**, 13145 (2020).

192. Gornall, J. L. & Terentjev, E. M. Helix-coil transition of gelatin: Helical morphology and stability. *Soft Matter* **4**, 544–549 (2008).

193. Milton, J. G. Dependence of platelet volume measurements on heterogeneity of platelet morphology. *Biophys. J.* **35**, 257–261 (1981).

194. Wan, G. J. *et al.* Platelet activation behavior on nitrogen plasma-implanted silicon. *Mater. Sci. Eng. C* **27**, 928–932 (2007).

195. Yang, P. *et al.* Wettability and biocompatibility of nitrogen-doped hydrogenated amorphous carbon films: Effect of nitrogen. *Nucl. Instruments Methods Phys. Res. Sect. B Beam Interact. with Mater. Atoms* **242**, 22–25 (2006).

196. Xu, L. C., Bauer, J. W. & Siedlecki, C. A. Proteins, platelets, and blood coagulation at biomaterial interfaces. *Colloids Surfaces B Biointerfaces* **124**, 49–68 (2014).

197. Slepickova Kasalkova, N., Slepicka, P., Kolska, Z. & Svorcik, V. Wettability and Other Surface Properties of Modified Polymers. *Wetting and Wettability* 323–355 (2015).

198. Tran, N. *et al.* Bactericidal effect of iron oxide nanoparticles on Staphylococcus aureus. *Int. J. Nanomedicine* **5**, 277–283 (2010).

199. Bhushan, M., Kumar, Y., Periyasamy, L. & Viswanath, A. K. Antibacterial applications of α-Fe2O3/Co3O4 nanocomposites and study of their structural, optical, magnetic and cytotoxic characteristics. *Appl. Nanosci.* **8**, 137–153 (2018).

200. Mohan, P. & Mala, R. Comparative antibacterial activity of magnetic iron oxide nanoparticles synthesized by biological and chemical methods against poultry feed pathogens. *Mater. Res. Express* **6**, 115077 (2019).

201. Handigund, M. & Cho, Y. G. Review: Insights into platelet storage and the need for multiple approaches. *Ann. Clin. Lab. Sci.* **45**, 713–719 (2015).

202. Pandiyarajan, C. K., Prucker, O., Zieger, B. & Rühe, J. Influence of the Molecular Structure of Surface-Attached Poly(N-alkyl Acrylamide) Coatings on the Interaction of Surfaces with Proteins, Cells and Blood Platelets. *Macromol. Biosci.* **13**, 873–884 (2013).

203. Claus, J. *et al.* Swelling characteristics and biocompatibility of ionic liquid based hydrogels for biomedical applications. *PLoS One* **15**, e0231421 (2020).

204. Oliveira, J. T. & Reis, R. L. Hydrogels from polysaccharide-based materials: Fundamentals and applications in regenerative medicine. *Nat. Polym. Biomed. Appl.* 485–514 (2008).

205. Ren, K., Crouzier, T., Roy, C. & Picart, C. Polyelectrolyte multilayer films of controlled stiffness modulate myoblast cell differentiation. *Adv. Funct. Mater.* **18**, 1378–1389 (2008).

206. Grohmann, S., Rothe, H. & Liefeith, K. Investigations on the secondary structure of polypeptide chains in polyelectrolyte multilayers and their effect on the adhesion and spreading of osteoblasts. *Biointerphases* **7**, 1–13 (2012).

207. Ruggeri, Z. M. & Mendolicchio, G. L. Adhesion mechanisms in platelet function. *Circ. Res.* **100**, 1673–1685 (2007).

208. Hofherr, L., Müller-Renno, C. & Ziegler, C. FluidFM as a tool to study adhesion forces of bacteria - Optimization of parameters and comparison to conventional bacterial probe Scanning Force Spectroscopy. *PLoS One* **15**, e0227395 (2020).

209. Nguyen, T. H., Schuster, N., Greinacher, A. & Aurich, K. Uptake Pathways of Protein-Coated Magnetic Nanoparticles in Platelets. *ACS Appl. Mater. Interfaces* **10**, 28314–28321 (2018).

210. Poldervaart, M. T. *et al.* 3D bioprinting of methacrylated hyaluronic acid (MeHA) hydrogel with intrinsic osteogenicity. *PLoS One* **12**, e0177628 (2017).

211. Vishal Gupta, N. & Shivakumar, H. G. Investigation of Swelling Behavior and Mechanical Properties of a pH-Sensitive Superporous Hydrogel Composite. *Iran. J. Pharm. Res.* **11**, 481–493 (2012).

212. Hertz, H. Ueber die Berührung fester elastischer Körper. *J. fur die Reine und Angew. Math.* **1882**, 156–171 (1882).

213. Shadden, S. C. & Hendabadi, S. Potential fluid mechanic pathways of platelet activation. *Biomech. Model. Mechanobiol.* **12**, 467–474 (2013).

214. Farrugia, B. L. *et al.* Perspectives on the use of biomaterials to store platelets for transfusion. *Biointerphases* **11**, 029701 (2016).

215. Ventre, M., Natale, C. F., Rianna, C. & Netti, P. A. Topographic cell instructive patterns to control cell adhesion, polarization and migration. *J. R. Soc. Interface* **11**, (2014).

216. Ding, Y. *et al.* Effects of microtopographic patterns on platelet adhesion and activation on titanium oxide surfaces. *J. Biomed. Mater. Res. - Part A* **101 A**, 622–632 (2013).

217. Kita, A. *et al.* Microenvironmental geometry guides platelet adhesion and spreading: A quantitative analysis at the single cell level. *PLoS One* **6**, e26437 (2011).

218. Pham, T. T. *et al.* Hemodynamic aspects of reduced platelet adhesion on bioinspired microstructured surfaces. *Colloids Surfaces B Biointerfaces* **145**, 502–509 (2016).

219. Nandakumar, D. *et al.* Fabrication of Semiordered Nanopatterned Diamond-like Carbon and Titania Films for Blood Contacting Applications. *ACS Appl. Mater. Interfaces* **8**, 6802–6810 (2016).

220. Hansen, C. E., Qiu, Y., McCarty, O. J. T. & Lam, W. A. Platelet Mechanotransduction. *Annu. Rev. Biomed. Eng.* **20**, 253–275 (2018).

221. Elbert, D. L. & Hubbell, J. A. Surface treatments of polymers for biocompatibility. *Annu. Rev. Mater. Sci.* **26**, 365–394 (1996).

222. Majhy, B., Priyadarshini, P. & Sen, A. K. Effect of surface energy and roughness on cell adhesion and growth-facile surface modification for enhanced cell culture. *RSC Adv.* **11**, 15467–15476 (2021).

223. Firkowska-Boden, I., Jandt, K. D., Helbing, C., Dauben, T. J. & Pieper, M. How nanotopography-induced conformational changes of fibrinogen affect platelet adhesion and activation. *Langmuir* **36**, 11573–11580 (2020).

224. Paddock, S. Confocal reflection microscopy: The 'other' confocal mode. *Biotechniques* **32**, 274–278 (2002).

225. Schneider, C. A., Rasband, W. S. & Eliceiri, K. W. NIH Image to ImageJ: 25 years of image analysis. *Nat. Methods* **9**, 671–675 (2012).

226. Abràmoff, M. D., Magalhães, P. J. & Ram, S. J. Image processing with imageJ. *Biophotonics Int.* **11**, 36–41 (2004).

227. Dai, J., Gong, J., Kong, N. & Yao, Y. Cellular architecture response to aspect ratio tunable nanoarrays. *Nanoscale* **12**, 12395–12404 (2020).

228. Emmert, M. *et al.* Modulation of Mammalian Cell Behavior by Nanoporous Glass. *Adv. Biol.* **5**, (2021).

229. Min, S. *et al.* Gradient wettability induced by deterministically patterned nanostructures. *Microsystems Nanoeng. 2020 61* **6**, 1–9 (2020).

230. Breuls, R. G. M., Jiya, T. U. & Smit, T. H. Scaffold Stiffness Influences Cell Behavior: Opportunities for Skeletal Tissue Engineering. *Open Orthop. J.* **2**, 103–109 (2008).

231. Alifui-Segbaya, F. & George, R. Biocompatibility of 3D-Printed Methacrylate for Hearing Devices. *Invent. 2018, Vol. 3, Page 52* **3**, 52 (2018).

232. Fallon, M. E. *et al.* Hemocompatibility of micropatterned biomaterial surfaces is dependent on topographical feature size. *Front. Physiol.* **13**, 1883 (2022).

233. Lee, J. S., Hill, R. T., Chilkoti, A. & Murphy, W. L. Surface Patterning. in *Biomaterials Science* 553–573 (Academic Press, 2020).

234. Chou, S. Y., Krauss, P. R. & Renstrom, P. J. Imprint of sub-25 nm vias and trenches in polymers. *Appl. Phys. Lett.* **67**, 3114 (1998).

235. Chou, S. Y. & Krauss, P. R. Imprint lithography with sub-10 nm feature size and high throughput. *Microelectron. Eng.* **35**, 237–240 (1997).

236. Wisser, F. M., Schumm, B., Mondin, G., Grothe, J. & Kaskel, S. Precursor strategies for metallic nano-and micropatterns using soft lithography †. *J. Mater. Chem. C* **3**, 2717 (2015).

237. Wiley, B. J., Qin, D. & Xia, Y. Nanofabrication at high throughput and low cost. *ACS Nano* **4**, 3554–3559 (2010).

238. Preetam, S. *et al.* Emergence of microfluidics for next generation biomedical devices. *Biosens. Bioelectron. X* **10**, 100106 (2022).

239. Cleveland, N. & Sun, H. Simulation of mold deformation and pattern interaction in nanoimprint lithography. *MRS Proc.* **1626**, 1–10 (2014).

240. Suzuki, K., Youn, S. W. & Hiroshima, H. Filling behavior and mold release force in UV nanoimprinting using PDMS mold in different atmosphere. *2017 IEEE 12th Nanotechnol. Mater. Devices Conf. NMDC 2017* **2018-January**, 167–168 (2018).

241. Montag, D., Frant, M., Horn, H. & Liefeith, K. Dependence of the initial adhesion of biofilm forming Pseudomonas putida mt2 on physico-chemical material properties. *Biofouling* **28**, 315–327 (2012).

242. Pringle, J. H. & Fletcher, M. Influence of Substratum Wettability on Attachment of Freshwater Bacteria to Solid Surfaces. *Appl. Environ. Microbiol.* **45**, 811–817 (1983).

243. Kreve, S. & Reis, A. C. D. Bacterial adhesion to biomaterials: What regulates this attachment? A review. *Jpn. Dent. Sci. Rev.* **57**, 85 (2021).

Appendix

List of Abbreviations

ACD-A- Anticoagulant Citrate Dextrose-A

ADP- Adenosine diphosphate

AFM- Atomic force microscopy

ATP- Adenosine triphosphate

BTHC- butyryl-tri-n-hexyl citrate

CLSM- confocal laser scanning microscopy

CMD- carboxymethyl dextran

DEHP- di(2-ethylhexyl) phthalate

DINCH- diisononyl ester of 1,2-cyclohexane-dicarboxylic acid

DLS- dynamic light scattering

DMSO- Dimethyl sulfoxide

DNA- Deoxyribonucleic acid

DTS- Dense tubular system

FDA- Food and Drug Administration

FGF- Fibroblast growth factor

GAG- Glycosaminoglycan

ITP- Immune thrombocytopenia

LbL- Layer by Layer

NP- Nanoparticle

OCS- Open canalicular system

PBS- Phosphate-buffered saline

PC- Phosphorylcholine

PDMS- Polydimethylsiloxane

PEG- Poly ethylene glycol

PEI- Polyethylenimine

PEM- Polyelectrolyte multilayers

PFA- Parafomaldehyde

PI- Propidium iodide

PMMA-Poly methyl methacrylate

PRP- Platelet rich plasma

PU- Polyurethane

PVC- Polyvinyl Chloride

RNA- Ribonucleic acid

RT- Room Temprature

SEM- Scanning electron microscopy

SIPA- Surface-induced platelet activation

SPFS- Single platelet force spectroscopy

T-NIL- Thermal nanoimprint lithography

TOTM- trioctyltrimellitate

TSB- Tryptic Soy Broth

UV- Ultra voilet

VEGF- vascular endothelial growth factor

vWF -von Willebrand factor

WCA- Water contact angle

List of Figures

List of Tables

List of publications

Journal papers

(1) **Apte, G**.; Bö, J.; Rothe, H.; Liefeith, K.; Nguyen, T.-H. H.; Börke, J.; Rothe, H.; Liefeith, K.; Nguyen, T.-H. H. Modulation of Platelet-Surface Activation: Current State and Future Perspectives. *ACS Appl. Bio Mater.* **2020**, *3* (9), 5574–5589.

(2) Bui, V. C.; Medvedev, N.; **Apte, G**.; Chen, L. Y.; Denker, C.; Greinacher, A.; Nguyen, T. H. Response of Human Blood Platelets on Nanoscale Groove Patterns: Implications for Platelet Storage. *ACS Appl. Nano Mater.* **2020**, *3* (7), 6996–7004.

(3) **Apte, G**.; Lindenbauer, A.; Schemberg, J.; Rothe, H.; Nguyen, T. H. Controlling Surface-Induced Platelet Activation by Agarose and Gelatin-Based Hydrogel Films. *ACS Omega* **2021**, *6* (16), 10963–10974.

(4) Chen, L.Y.†; **Apte, G**.†; Lindenbauer, A.; Frant, M.; Nguyen, T. H. Effect of Hit Components on the Development of Breast Cancer Cells. *Life* **2021**, *11* (8), 1–13.

(5) Berganza, E.†; **Apte, G**.†; Vasantham, S. K.; Nguyen, T.-H.; Hirtz, M. Integration of Biofunctional Molecules into 3D-Printed Polymeric Micro-/Nanostructures. *Polymers (Basel).* **2022**, *14* (7), 1327.

(6) **Apte, G**.; Hirtz, M.; Nguyen, T.-H. FluidFM-Based Fabrication of Nanopatterns: Promising Surfaces for Platelet Storage Application. *ACS Appl. Mater. Interfaces* **2022**, *14* (21), 24133–24143.

(7) Schemberg, J.; Abbassi, A. El; Lindenbauer, A.; Chen, L. Y.; Grodrian, A.; Nakos, X.; **Apte, G**.; Khan, N.; Kraupner, A.; Nguyen, T. H.; Gastrock, G. Synthesis of Biocompatible Superparamagnetic Iron Oxide Nanoparticles (SPION) under Different Microfluidic Regimes. *ACS Appl. Mater. Interfaces* **2022**, *14* (42), 48011–48028.

Conference contributions

(1) **Apte, G**.; Chen, L. Y.; Lindenbauer, A.; Gruel Y.; Rollin J.; Greinacher A.; Nguyen, T. H. HIT Antibodies as Mediators between Platelets and Breast Cancer Cells. Conference: XXII. Annual Linz Winter Workshop 2020 - Advances in Single-Molecule Research for Biology & Nanoscience. (**Talk)**

(2) **Apte, G**.; Lindenbauer, A.; Schemberg, J.; Rothe, H.; Nguyen, T. H. Inhibition of Surface-induced Platelet Activation on Hydrogel Films. Conference: The XXIX Congress of the International Society on Thrombosis and Haemostasis July 17-21, 2021(**Poster**)

Patent application

(1) Nguyen, T. H.; Chen, L. Y.; **Apte, G**. EP4109103A1 METHOD FOR DETECTION OF HEPARIN-INDUCED THROMBOCYTOPENIA ANTIBODIES

Acknowledgements

This thesis wouldn’t have been possible without the support of so many people. I would like to offer my heartfelt thanks to my supervisor, Dr.Dr.Thi Huong-Nguyen, who is one of the most enthusiastic people I have ever met. I owe her my profound gratitude for her constant guidance and support throughout my research journey and also for introducing me to the AFM technique. I further thank her for giving me this opportunity to work at NanoTI on this project. I am grateful for the amount of freedom she gave me to explore ideas and the time spent discussing the path of this thesis on a regular basis. In the academic world of "publish or perish," I appreciate her constant encouragement in motivating me to write manuscripts. I would like to express my gratitude to PD Dr. Dr. Michael Hirtz for giving me the opportunity to do my PhD as an external student at KIT under his guidance and for being supportive all the time. I appreciate the time he spent discussing my project and providing feedback and an outlook, especially for the nanoprinting and imprinting work. Furthermore, I thank him for his valuable inputs on structuring this thesis and his role in a smooth and successful collaboration with his group at INT. I would also like to take this opportunity to acknowledge Prof. Dr. Annie Powell for the time she spent reading and providing feedback on my work. I am much obliged to her for agreeing to be one of the referees for my thesis.

During my last three years in Heiligenstadt, I came across so many people who have made valuable contributions to my journey. To begin with, I am indebted to IBA for hiring me for this position and helping me to pursue my doctoral dream. Next, I would like to thank the Nieren- und Dialysezentrum Eichsfeld and their staff for their help in extracting the blood, without which none of the platelet experiments in this work would have been possible. They always did so, taking time out from their busy schedules with a smile on their faces. I'd like to thank Annerose Lindenbauer for her assistance with the lab activities, like helping during platelet isolation, buffer preparation, zeta potential measurements, and, of course, several non-laboratory-related things like sharing the fresh vegetables from her garden every summer. Furthermore, thanks to Holger Rothe for his valuable insights on AFM and for providing his perspective on my work. I wish to acknowledge the contribution of Dr. Jörg Schemberg in providing me with the synthesized iron nanoparticles. I really appreciate the help I received from Robert Römer for introducing me to T-NIL. I also thank Dr. Uwe Schirmer for introducing me to CLSM and sharing his expertise from time to time.

I am also thankful to my collaborator at INT, Dr. Eider Berganza, for the joint execution of a successful project. I appreciate the exchange of ideas and all the discussions we had about the project as well as about my PhD work. Next, I'd like to thank GeSIM Gmbh and Cytosurge AG for their prompt technical assistance in helping me resolve the problems I encountered while executing some experiments, as well as for generously gifting some of the consumables.

I would like to express my gratitude to all the colleagues from the BW, BPT, and AMT departments at IBA for their feedback and constructive criticism during the biannual PhD seminars, which led me to improve my skills and develop new approaches. I also extend my thanks to the colleagues in the administration department for their logistical support throughout my time at IBA. I am also thankful to all the students from the DAAD exchange program and the ones doing their master's theses at our group for helping broaden my research mindset.

I would like to express my special thanks to two of my fellow labmates turned friends with whom I have enjoyed this PhD journey: Franziska Oberhaus and LiYu Chen. The space is too small to accommodate all our adventures, from our hiking trips around the year to multicuisine cooking sessions. All those lunchtime talks that ranged from brainstorming scientific ideas to helping each other encounter workplace challenges—I am sure we discussed absolutely any and every topic under the sun. I consider myself extremely lucky to have had you guys and have enjoyed sharing all of our successes and failures together during our PhD stint. I really cherish this friendship we had in this otherwise very lonely town.

I can't finish the acknowledgement section without thanking the people who have always been there for me in my personal life. A special thanks is due to my friends, who are spread across different countries and timezones, for those countless hours spent on calls; they provided me with much-needed distractions from the work-related stress. I am grateful for the affection I have always received from my grandmothers, and I am truly blessed to have loving parents who have been my unwavering supporters and my emotional support system throughout my life. None of this would have been possible without their constant encouragement and their countless sacrifices. I am forever indebted to you guys.

Finally, but certainly not least, to my beloved wife, Rutuja, whose love, encouragement, and belief in me have been the backbone of my master's and doctoral journeys. I will always be grateful for her constant motivation and understanding, especially during the writing phase of this thesis. Thanks for everything and, most importantly, for always being there.